Holographic Gauge/Gravity Duality and Symmetry Breaking in Semimetals

by

Namshik Kim

M.Sc., The University of British Columbia, 2011

A THESIS SUBMITTED IN PARTIAL FULFILLMENT OF
THE REQUIREMENTS FOR THE DEGREE OF

DOCTOR OF PHILOSOPHY

in

The Faculty of Graduate and Postdoctoral Studies

(Physics)

THE UNIVERSITY OF BRITISH COLUMBIA

(Vancouver)

February 2017

Abstract

We use the AdS/CFT correspondence (the holographic duality of gauge/gravity theory) to study exciton driven dynamical symmetry breaking in certain (2+1)-dimensional defect quantum field theories. These models can be argued to be analogs of the electrons with Coulomb interactions which occur in Dirac semimetals and the results our study of these model systems are indicative of behaviours that might be expected in semimetal systems such as monolayer and double monolayer graphene. The field theory models have simple holographic duals, the D3-probe-D5 brane system and the D3-probe-D7 brane system. Analysis of those systems yields information about the strong coupling planar limits of the defect quantum field theories. We study the possible occurrence of exciton condensates in the strong coupling limit of single-defect theories as well as double monolayer theories where we find a rich and interesting phase diagram. The phenomena which we study include the magnetic catalysis of chiral symmetry breaking in monolayers and inter-layer exciton condensation in double monolayers. In the latter case, we find a solvable model where the current-current correlations functions in the planar strongly coupled field theory can be computed explicitly and exhibit interesting behavior. Although the models that we analyze differ in detail from real condensed matter systems, we identify some phenomena which can occur at strong coupling in a generic system and which could well be relevant to the ongoing experiments on multi-monolayer Dirac semimetals. An example is the spontaneous nesting of Fermi surfaces in double monolayers. In particular, we suggest an easy to observe experimental signature of this phenomenon.

Preface

This thesis contains achievements published by the author and appeared in the Journal of High Energy Physics, and Physics Letter B. All the papers are based on the one big project, finding a dual gravity model for double monolayer semimetals.

A version of chapter 2 has been published : Gianluca Grignani, Namshik Kim and Gordon W. Semenoff, *D3- D5 Holography with Flux*, Phys. Lett. B **715**, 225 (2012). The thesis author was responsible for solving the equation of the motion of the systems and double-checking and refining the numerical results which my collaborators obtained.

A version of chapter 3 has been published : Namshik Kim and Joshua L. Davis, *Flavor-symmetry Breaking with Charged Probes*, JHEP 1206 **064** (2012) [54]. The thesis author contrived the critical idea to stabilize the joined embedding, and was mainly responsible for numerical calculations and its visualization.

A version of chapter 4 has been published : Gianluca Grignani, Namshik Kim and Gordon W. Semenoff, *D7-anti-D7 bilayer: holographic dynamical symmetry breaking,* Phys. Lett. B **722**, 360 (2013) [91]. The thesis author contributed to all the main computations of correlation functions and writing a first draft for published paper. It was modified by Gianluca Grignani, and Gordon Semenoff rewrote it compactly after the first draft.

A version of chapter 5 and 6 are based on the same project. The version of the chapter 5 has been published : Gianluca Grignani, Namshik Kim, Andrea Marini and Gordon W. Semenoff, *D7-anti-D7 bilayer: holographic dynamical symmetry breaking,* JHEP **1412**, 091 (2014) [100]. The version of the chapter 6 has been accepted for publication in Phys. Lett. B. The thesis author studied the corresponding field theory model for both gravity dual systems, and contributed obtaining D7-branes dual gravity model and numerically investigating it.

Table of Contents

List of Tables

List of Figures

Glossary

JHEP Journal of High Energy Physics

PRL Physics Review Letter

PLB Physics Letter B

QFT Quantum field theory

QCD Quantum Chromodynamics

QED Quantum Electrodynamics

AdS Anti de Sitter space-time

CFT Conformal field theory

dCFT Defect conformal field theory

CMT Condensed matter theory

SYM Supersymmetric Yang-Mills theory

EC Exciton condensate

N The number of colors or D3-branes

$\mathcal{N}$ The number of super charges

Acknowledgements

My supervisor Gordon Semenoff is the first one should be appreciated for this thesis. His passion, keen intuition and broad knowledge of physics have been always very impressive to me. I could be here as following the sight of his back. I like his jokes and laughs, too.

I would like to thank Gianluca Grignani, professor at Università degli Studi di Perugia, Perugia. He is a true gentleman. I was so pleased at co-working with him. I also thank to Josh Davis, and Andrea Marini I worked together.

At last, I express my gratitude to Ariel Zhitnisky, Joanna Karczmarek, Moshe Rozali, Fei Zhou, Janis McKenna, Seungjoon Hyun, and all the physicists and students that I was affected by.

For my personal life, I appreciate the support and love of my girl friend, May Tang. I specially thank my parents, Tagil Kim and Jaeok Lee. Without their unbelievable support and devotion, I could not reach this point. I love you.

To my parents.

Chapter 1

Introduction and Summary of Results

VLADIMIR :
We'll hang ourselves tomorrow. Unless Godot comes.
ESTRAGON :
And if he comes?
VLADIMIR :
We will be saved.

- Waiting for Godot by Samuel Beckett

1.1 Why AdS/CMT

Quantum field theory (QFT) is an important tool for understanding the behavior of condensed matter systems. Interacting quantum field theories are notoriously difficult to solve. In fact, there are very few if any exactly solvable field theories which describe systems where the interactions between particles are important. There are two main approaches to understanding an interacting quantum field theory. One is numerical where the idea is simply to solve the equations of motion by numerical means. This approach has proven quite useful in many cases, however, it has severe limitations. Because the complexity of many condensed matter problems requires prohibitive amounts of computer power, there are also specific problems such as descriptions of Fermi surface and finite density where the more powerful techniques (e.g, Monte-Carlo simulations) cannot be used.

The other main approach is perturbative. It assumes that interactions are small, and systematically takes them into account using time-dependent perturbation theory. Of course, this can yield accurate results for many systems where the interactions are indeed small. However, there are some condensed matter systems where the interactions are much larger. Moreover,

perturbation theory is not a reliable technique. These systems are said to be strongly coupled.

A couple of intrinsically non-perturbative approaches to quantum field theory using time dependent perturbation theory have been developed over time. Perhaps the most exciting one is AdS/CMT. This approach uses the duality between certain strongly interacting quantum field theories and certain solutions of superstring theory to study the quantum field theory in the strongly coupled regime. It holds the promise of providing us with a way of solving interesting quantum field theories in the limit where their interactions are very large. It also, in principle, gives a way of systematically correcting this strong coupling limit.

There are two common approaches to AdS/CMT. Currently, the most common one is bottom-up. It searches for phenomena occurring in strongly coupled field theories which are so universal that they should be exhibited by practically any strongly coupled systems with similar environmental factors. The ultimate goal of this approach is to develop paradigms which enable understanding and classification of strongly coupled systems.

The top-down approach, on the other hand, seeks quantum field theories which have a resemblance to specific condensed matter systems, and which, simultaneously, have a string theory dual. It, then, uses the techniques of string theory to study the behavior of the field theory in the parametric regime where the string theory is tractable. This is usually the strong coupling regime of field theory. The top-down approach is the main one which will be used in this thesis.

1.2 D-brane and statement of AdS/CFT conjecture

The key to understanding AdS/CFT are D-branes, which are extended objects in string theory. Let us start from the dynamics of a string ,which are governed by Polyakov action. Polyakov action is classically equivalent to Nambu-Goto action, the action of a relativistic string which has length and tension.

$$S = -\frac{1}{4\pi\alpha'} \int d^2\sigma \; \partial_\alpha X \cdot \partial^\alpha X \tag{1.1}$$

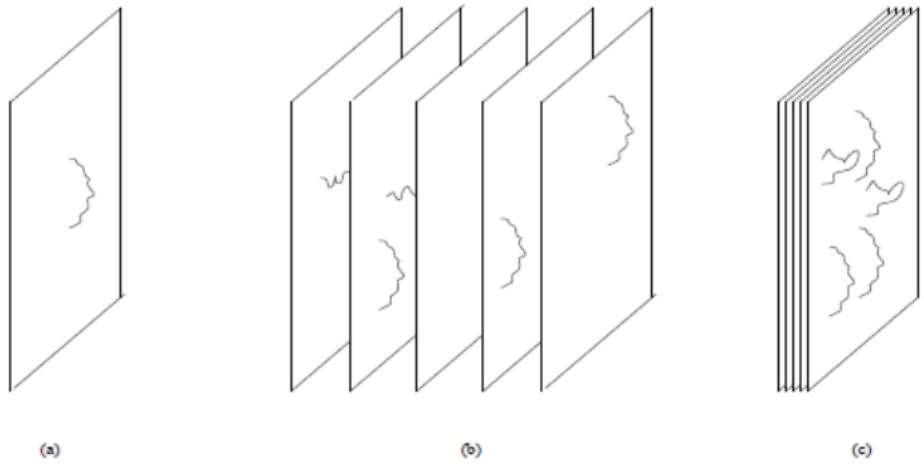

Figure 1.1: The picture is obtained from [8] which is also a good reference for AdS/CFT correspondence. (a) A single D-brane and a strings on it transforms in $U(1)$ representation. The length of the open string should be very short because of the tension of it, so it is massless. (b)A stack of D-branes constitute $U(1) \times U(1) \times U(1) \cdots$ gauge group. (c)The distance between D-branes is proportional to the mass of the open strings between D-branes. For the coincident N D-branes, we obtain non-Abelian $SU(N)$ gauge theory. The index of the gauge field in the adjoint representation is obtained from labeling N D-branes on which open strings end.

$X^\mu(\sigma, \tau)$[1] We derive the equation of motion from the extrema of the action. Let us consider the variation of the action from τ_i to τ_f.

$$\delta S = -\frac{1}{2\pi\alpha'} \int_{\tau_i}^{\tau_f} d\tau \int_0^\pi d\sigma \ \partial_\alpha X \cdot \partial^\alpha \delta X \tag{1.2}$$

The total derivative term becomes as follows from an integration by part.

$$\int_0^\pi \ d\sigma \ \dot{X} \cdot \delta X|_{\tau_i}^{\tau_f} - \int_{\tau_i}^{\tau_f} \ d\tau \ X' \cdot \delta X|_0^\pi \tag{1.3}$$

To satisfy the equation of the motion, this total derivative term should

[1] σ, τ are worldsheet coordinates where a string sweeps out. For a periodic $\sigma \in [0, 2\pi)$, we have a closed string, and for $\sigma \in [0, \pi]$ we have an open string.

all vanish. The first term is destroyed by requiring $\delta X^\mu = 0$ at $\tau = \tau_i,\ \tau_f$. To eliminate the second term of (1.3), we demand as follows :

$$\partial_\sigma X^\mu \delta X_\mu = 0 \quad at \ \ \sigma = 0,\ \pi \tag{1.4}$$

There are various boundary conditions which satisfy the above equation. For example, Dirichlet boundary conditions, X^μ, fix end points of the open string to lie on some hypersurface called a Dp-brane. Moreover, the condition breaks Lorentz and translation symmetry. The 'p' in Dp-branes indicates the number of spatial dimensions. Thus, Dp-branes are simply p+1 dimensional hypersurfaces on which open strings are attached to begin and end. When quantum fluctuation of an open string is taken into account, the D-brane becomes a dynamical object.

In Fig. 1.1, we have used the terminology, *representation*. we want to briefly introduce about it and others which will be useful in this thesis. A representation of G (group) is a mapping, D of the element of G onto a set of linear operator preserve the structure of group multiplications. If we assume the group element depends on the continuous parameter, we can expand the linear operator of the representation, and can define the generator, T_a, $D(d\alpha) = 1 + i\ d\alpha_a T_a + \ldots$, where $d\alpha$ is an infinitesimal change of the continuous parameter. The generators can have some commutation relations and if the structure constants from commutators themselves generate a representation, then we call it an *adjoint representation*. The *fundamental representation* can be understood as the representation for a spin. We can define raising and lowering operators (or creation and annihilation oprerators) from generators, and can define the highest spin eigenvalues. If we want to interpret some quantum excitation as a spin or a gauge field. They should transform in the proper representations. [2]

Some readers would have been wondering what AdS is. Instead of describing AdS, here we will introduce its interesting properties. The curvature of the space-time is constant and negative, so it exerts a repulsive force against the boundary. In Minkowski space-time, the Hawking thermal radiation from a black hole causes it to gradually evaporate. However, if you put a black hole at Poincaré killing horizon of AdS space-time, the Hawking radiation comes back to the black hole. For example, AdS_3 space-time has a Poincaré killing horizon at $r = 0$ since it cannot cover all AdS with the Poincaré patch, $ds^2 = r^2(-dt^2 + dx^2) + \frac{dr^2}{r^2}$[14]. There is no temperature associated with it. However, if use AdS-Schwarzshild space-time, the

[2]For the better and more deeper understanding, see the book written by Howard Georgi. It is not too abstract and easier to read for the physics majored.[7].

temperature is associated. By this mechanism, we can stabilize the embedding. As a result, if we allow for the thermodynamic property of the black hole, we can utilize the AdS space-time as a perfect box for thermodynamic experiments.

A dual description of D-branes for AdS/CFT is one of the most successful achievements in string theory. It is also a black brane solution of supergravity or type II superstring theory. D3 branes are the most interesting D-branes because the solution of gauge theory is more precise. D3 branes provide $\mathcal{N} = 4$ SYM in four dimensions. D3 branes extend in time and three spatial dimensional directions. D3 branes have a mass per unit volume, and they have a charge associated to a self-dual 5-form field strength. Its world-brane has 3+1 dimensional Poincaré invariance, and has constant axion and dilation fields, Dilaton fields Φ and axion C are solutions of Type II string theory here. The dilaton-axion field $\tau \equiv C + i\ e^{-i\Phi}$ changes under a Moebius transformation. $\tau \to \frac{a\tau+b}{c\tau+d},\ ad - bc = 1,\ a, b, c, d \in \mathbf{R}$. This property will be important in AdS/CFT as the reflection of duality in $\mathcal{N} = 4$ SYM theory. See references [3–5] for more details. This means that D3-branes are regarded as solutions of the ten-dimensional Einstein equations coupled to the 5-form. When we consider a stack of N D3-branes, a factor of the string coupling g from the genus and a factor of N from the Chan-Paton trace, in string perturbation theory, are considered. Thus, perturbation theory is good as $gN \ll 1$ and bad as $gN \gg 1$. $g \equiv g_{string} = g^2_{YM}$. The black branes and D-branes source the same Ramond-Ramond fluxes [13]. The near horizon geometrical solution of a black 3-brane is $AdS_5 \times S^5$:

$$ds^2_{D3} = \frac{r^2}{L^2}(-dt^2 + dx^2 + dy^2 + dz^2) + \frac{L^2 dr^2}{r^2} + L^2 d\Omega^2_{S^5}{}^3. \tag{1.5}$$

L is the curvature radius of AdS_5 and S^5, and $L^4 = 4\pi g_s N \alpha'^2$ obtained from the black brane solution. As $gN \gg 1$, L is large in string units, so the low energy supergravity is nicely described, but as $gN \ll 1$, that is no more effective. Therefore, these two perturbative prescriptions are complementary in each limit.

D-branes have definite charges, and when a large number of D-branes are put, they become massive and the black hole is expected. This gives two approaches to the dynamics of the theory at the low energy limit. At this limit, both $gN \gg 1$ and $gN \ll 1$ descriptions consist of massless strings (open and closed). As $gN \ll 1$, only open strings remain interacting, and closed strings are irrelevant and decoupled. The lowest energy excitations

[3] $S^n \equiv \{x \in R^{n+1} : ||x|| = 1\}$.

of the open strings are described by gauge fields. These provide a supersymmetric Yang-Mills gauge theory, which lives on the world-volume of the branes. As $gN \gg 1$, there are massive energy states in the curved geometry. The low energy dynamics is supergravity in the $AdS_5 \times S^5$, which is the low energy limit of closed string theory. The degrees of freedom are fluctuations of the supergravity fields about the black brane background and they live in the bulk of ten dimensional space-time. There are some situations where these two descriptions have an overlapping domain of validity. In those cases, the same physical system is described by two different theories which must therefore be dual to each other. Because the degrees of freedom in these theories live on spaces of different dimensions (bulk and its boundary), it is a holographic principle – a property of string theories and a supposed property of quantum gravity that describe the physics of a bulk and can be encoded on a boundary.

The original conjectured statement of AdS/CFT [12] is that there is an exact duality between $\mathcal{N} = 4$ supersymmetric SU(N) Yang-Mills (SYM) theory in flat 4D space-time (boundary of the AdS_5) and the full quantum type IIB string theory on $AdS_5 \times S^5$. For the strongest conjecture, there is an exact equivalence of the physical spectra at any value of the parameters between two theories, including operator observables, states, correlation functions and full dynamics, Wilson loop, thermal states, and so on, which are also translated into the languages of strong theory in AdS. The weaker form of a conjecture is that $\mathcal{N} = 4$ supersymmetric $SU(N)$ Yang-Mills theory in flat 4D for t'Hooft limit, large fixed $\lambda = g^2_{YM}N$ and classical type IIB supergravity on $AdS_5 \times S^5$. Moreover, the $\lambda^{-1/2}$ expansion on the gauge theory corresponds to α' expansion on gravity side. There are many good reviews and original papers to introduce AdS/CFT correspondences. We found [8]-[14] useful. More basic knowledge on string theory is available in textbooks [3–5]. In addition, many videos and lectures on the personal websites of physicists are useful study tools for beginners to quickly grasp the whole picture.[6]

There is an equivalence of the physical spectra at any value of the parameters between two theories, including operator observables, states, correlation functions and full dynamics, Wilson loop, thermal states, and so on, which are also translated into the languages of string theory in AdS. Thus, we can utilize the dictionary to convert the physical quantities from one theory to the other [8].

1.3 AdS/CFT dictionary

In this section, we will briefly review the application of AdS/CFT correspondence : the mapping between contents of two corresponding theories. We will introduce some mapping which will be used in the thesis. The gravitational partition function is as follows :

$$Z_{AdS} = \int_{\phi_0} \mathcal{D}\phi e^{-S(\phi,\, g_{\mu\nu})}$$

$$\phi(t,\, x^i,\, ; r = \infty) = r^{\Delta - d}\phi_0(t,\, x^i) + \frac{\langle \mathcal{O} \rangle}{2\Delta - 4} r^{-\Delta} + \cdots \tag{1.6}$$

ϕ_0 is the boundary value of the field in the gravity side. Δ is a conformal dimension. The concerned field is a scalar field in the equation, but we can generalize it to have indices. Z_{AdS} is simply a classical action of supergravity. It is not difficult to obtain using perturbation.

These partition functions are exactly the same as

$$Z_{CFT} = \langle e^{\int_{\partial M} \phi_0\, \mathcal{O}} \rangle$$

Thus, $\mathcal{O}$ is the corresponding operator of the source ϕ_0 lives on the asymptotic boundary. Because $Z_{AdS} = Z_{CFT}$, the one point function is obtained as follows :

$$\langle \mathcal{O} \rangle = \frac{\delta\, log\, Z_{AdS}[\phi]}{\delta \phi_0} \tag{1.7}$$

Similarly, the two point function can be acquired. We present one example we will use in later chapters. Remember that the separation between D-branes is proportional to the mass of the string connected between the branes. For a D3-probe-D5 system, the model has $SO(3) \times SO(3)$ symmetry and the non-zero separation breaks either of the $SO(3)$ symmetries. That corresponds to chiral symmetry breaking [76]. It occurs with an external magnetic field. We will go through this subject thoroughly in later chapters. In this section, let us accept this correspondence, and see how to utilize the holographic duality.

For example, let us consider our probe D5 branes. The induced metric of probe D5 branes without an external field provides the near horizon geometry, $AdS_4 \times S^2$.

$$ds^2_{D5} \sim r^2(-dt^2 + dx^2 + dy^2) + \frac{dr^2}{r^2} + d\Omega^2_{S^2} \tag{1.8}$$

We expect Dirac fermionic fields and consider the action of the fields. The relevant coordinate along the separation is ψ of S^2 of S^5 in 1.5. If ψ is non-zero, the rotational $U(1)$ symmetry perpendicular to D5 branes is broken, and it is dual to $U(1)$ chiral symmetry in the gauge theory side. Here is the asymptotic expansion,

$$\psi(r) = \frac{\pi}{2} + \frac{m}{r} + \frac{c}{r^2} + \cdots, \qquad r \to \infty \tag{1.9}$$

The length of the separations is $r\cos(\psi)$ which is asymptotically m. $m \propto m_q$. m_q is the mass of the corresponding quark. By the equation 1.6, c is the expectation value of the corresponding dual field operator and is linear to chiral condensation, $c \propto \langle \bar{q}q \rangle$. $\mathcal{O}$ should be $\bar{q}q$ from the mass term of Dirac Hamiltonian, $m\bar{q}q$. $\Delta = 1$, 2 by $\Delta_\pm = \frac{1}{2}\left(d + \sqrt{d^2 + 4m^2L^2}\right)$. $d = 3$ for this defect field theory. As expected, the source m and $\langle \bar{q}q \rangle$ are encoded in the asymptotic expansion of the scalar field.

1.4 Motivation

Graphene is a single 2+1 dimensional layer of carbon, packed in a hexagonal lattice. Carbon hybridization forms three sp^2 orbitals, one P_z orbital. Thus, the sp^2 orbitals arrange themselves in a plane at 120 angles, and the lattice thus formed is the honeycomb lattice. It has been a subject of great interest as a 2+1 dimensional material and the origin of several fascinating predictions [98] since many decades ago. Recently, it has captured attentions in condensed matter physics and even in other theoretical physics since Geim and his collaborators acquired the material in laboratory [15]. A carbon atom has four valence electrons. Three of these electrons form strong covalent σ-bonds with neighboring atoms. The fourth, π-orbital is un-paired. This property of orbital bonding enables a honeycomb lattice structure in 2+1 D. The Hamiltonian is

$$H = \sum_{\vec{A},i} (t\ b^\dagger_{\vec{A}+\vec{s}_i} a_{\vec{A}} + t^* a^\dagger_{\vec{A}} b_{\vec{A}+\vec{s}_i}), \qquad t \sim 2.7ev, \quad |\vec{s}_i| \sim 1.4\mathring{A} \tag{1.10}$$

It is easy to find the energy dispersion of a single layer of graphene using tight binding approximation. For the wave function of graphene, we take a linear combination of Bloch functions for sublattices A and B.

$$a_{\vec{A}} = e^{iEt/\hbar + i\vec{k}\cdot\vec{A}} a_0, \qquad\qquad b_{\vec{B}} = e^{iEt/\hbar + i\vec{k}\cdot\vec{B}} b_0 \tag{1.11}$$

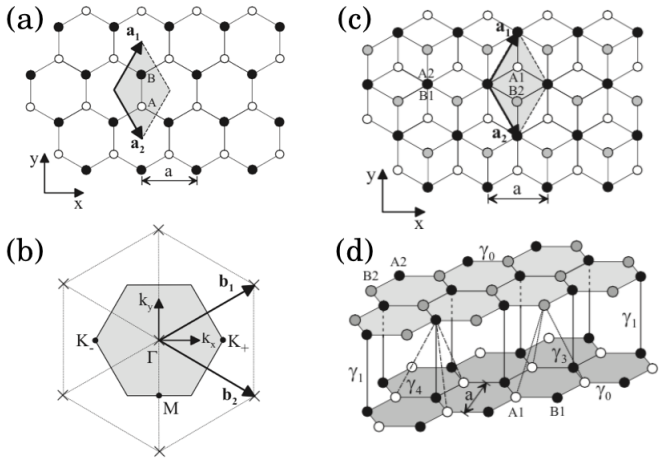

Figure 1.2: This figure and captions are taken from [17]. (a) Crystal structure of monolayer graphene with A (B) atoms shown as white (black) circles. The shaded area is the conventional unit cell, a_1 and a_2 are primitive lattice vectors. (b) Reciprocal lattice of monolayer and double-layer graphene with lattice points indicated as crosses, b_1 and b_2 are primitive reciprocal lattice vectors. The shaded hexagon is the first Brillouin zone with Γ indicating the center, and K_+ and K_- showing two non-equivalent corners. (c) Above and (d) side view of the crystal structure of double-layer graphene. Atoms $A1$ and $B1$ on the lower layer are shown as white and black circles, $A2$, $B2$ on the upper layer are black and grey, respectively. The shaded area in (c) indicates the conventional unit cell.

As a result, we obtain two energy bands.

$$E(k) = \pm t\sqrt{(1 + 2\cos(\frac{3k_y s}{2})\cos(\frac{\sqrt{3}k_x s}{2}))^2 + \sin^2(\frac{3k_y s}{2})}\ , \tag{1.12}$$

where s is the distance of between sites. It is plotted in Fig. 1.3. We obtain two bands which are degenerated at the K_+ and K_- points.

Graphene has unique properties that derive from its honeycomb-like lattice structure such as the Dirac-like spectrum around the tip of the Dirac cone. In other words, in the case of graphene, the low energy properties near the Fermi energy can be described by Dirac equation by expanding the energy dispersion around the K_+ and K_- points, and it is a direct consequence of graphene's crystal symmetry. Let us consider a wave vector for valley K as $\mathbf{q} = \mathbf{K} - \mathbf{k}$, and expand with $|k| \ll 1$. The Hamiltonian with

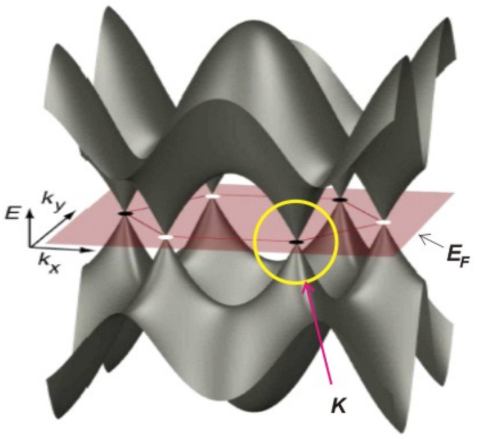

Figure 1.3: Energy dispersion with two bands for the p_z electrons; red plane indicates the Fermi level [18].

Fermi velocity, $v_g \equiv \frac{3s|t|}{2\hbar} \sim 10^6 m/s$[4] is as following :

$$H\Psi = v_g \begin{pmatrix} -\vec{\sigma}^* \cdot \mathbf{p} & 0 \\ 0 & \vec{\sigma} \cdot \mathbf{p} \end{pmatrix} \Psi, \tag{1.13}$$

where the $\vec{\sigma} = (\sigma_x, \sigma_y)$ is a vector of Pauli matrices, and Ψ is a bi-spinor of K-points of the first Brillouin zone. The corners of the Brillouin zone form two inequivalent groups of K-points. Thus, $\Psi = (\Psi^{K+}, \Psi^{K-})^T$.

$$H\Psi = c \begin{pmatrix} -\vec{\sigma}^* \cdot \mathbf{p} & 0 \\ 0 & \vec{\sigma} \cdot \mathbf{p} \end{pmatrix} \Psi \tag{1.14}$$

From the comparison with Dirac equation, (1.14), we can see that Fermi velocity of the graphene, v_g, behaves like the speed of light. This spinor is called a pseudospin. QED phenomena inversely proportional to the speed of light should be, in graphene, enhanced by a factor of $c/v_g \sim 300$[5]. This relativistic behaviour of electrons in graphene in low energy could lead to new possibilities for testing relativistic phenomena (e.g. Some QED effects cannot be tested in particle physics such as perfect tunnelling of relativistic electrons). The energy level is half-filled in the neutral graphene. The

[4] v_g is obtained from understanding of the Fig. 1.3. The yellow circle around the valley, K-point, provides Dirac-like spectrum around the tip of the Dirac cone, and we read the velocity from comparison of the slope with Dirac cone.

[5] Fine structure constant with Gauss' unit is $\frac{e^2}{\hbar c}$. Since v_g behaves like speed of light, the effective fine structure constant of our model should be $\frac{e^2}{\hbar}$.

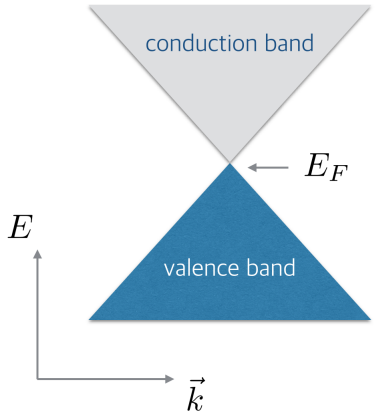

$$E = \hbar c\, \vec{k}$$

$$E = \hbar v_g \vec{k}$$

$$\alpha = \frac{1}{4\pi\epsilon_0}\frac{e^2}{\hbar c}$$

$$\alpha_g = \frac{1}{4\pi\epsilon_0}\frac{e^2}{\hbar v_g} = \frac{c}{v_g}\alpha \sim 300\alpha$$

Figure 1.4: As we look into the $\vec{K}$ point of Fig. 1.3, we find out the interactions of electrons in graphenes are very strong. We will discuss about the energy band and Fermi energy, E_F, later in this section.

conduction band and valence band meet at he Dirac chemical point, and graphene is a zero gap semimetal, which is a material with a small overlap between the conduction band and the valence band. A semimetal or semiconductor is an insulator at 0 K. Since the energy gap is almost none, the valence band is slightly populated at room temperature. In other words, there can be small electrical conductivity in the semimetal at some finite temperature.

Because of the strength and specificity of its covalent bonds, graphene is one of the strongest materials in nature, with literally no extrinsic substitutional impurities, yielding the highest electronic mobilities among metals and semiconductors [15] [16]. Therefore, graphene is being considered for many applications that range from conducting paints and flexible displays to high speed electronics.

We model the 2+1 dimensional defect dual field theory in graphene double monolayers separated by a dielectric barrier which controls the strength of interactions between an electron on one layer and a hole on the other layer. The double monolayer semimetal means two monolayers of semimetals, each of them would be a Dirac semimetal in isolation, and they are separated by an insulator, so we ignore direct transfer of electric charge between the layers. A double monolayer should be distinguished from bi-

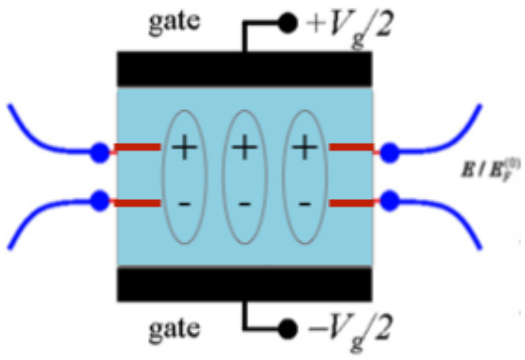

Figure 1.5: Schematic illustration of a graphene double monolayers exciton condensate channel in which two single-layer graphene sheets are separated by a dielectric (SiO_2 in this illustration) barrier. We predict that electron and hole carriers induced by external gates will form a high temperature exciton condensate. This figure and captions are modified from the figure and caption in [66]

layer by whether allows hop or not between each monolayers, and hopping is controlled by dielectric materials between double layers. Then, the system has two conserved charges, the electric charge in each layer. The Coulomb interaction between an electron in one layer and a hole in the other layer is attractive. A bound state of an electron and a hole forms is called an exciton. Exciton is a boson and, at low temperatures they can condense to form a charge-neutral superfluid. We will call this an inter-layer exciton condensate. To distinguish the condensate can occur on the same layer, we will call it an intra-layer condensate.

Electric external gates on each layer adjust the chemical potentials of each layer. For the weakly coupled system (Fig. 1.5), when biased by external gates, the perfect nesting of the electron and hole Fermi surfaces in each layer tend to form inter-layer exciton condensates[6](EC) [65, 66]. In condensed matter physics, Fermi energy is an internal chemical potential at zero temperature. This is also the maximum kinetic energy of particles in Fermi gas. Fermi-Dirac distribution is as follows :

$$\langle n_i \rangle = \frac{1}{e^{(\epsilon_i - \mu)/k_B T} + 1} \ ,$$

where $\langle n_i \rangle$ is the mean occupation number, and μ is the Fermi energy. At

[6]The quantum coherent bound states of an electron on one layer and a hole on the other layer. The bound states from the same monolayer form intra-layer EC.

$T = 0$,

$$\langle n_i \rangle \approx \begin{cases} 1 & (\epsilon_i < \mu) \\ 0 & (\epsilon_i > \mu) \end{cases}$$

By Pauli exclusion principle, the number of the states below μ is exactly the same as that of the energy level below μ. In momentum space, these particles fill up a sphere of radius μ. The surface of the sphere is equivalent to Fermi surface. In condensed matter physics, we can consider a Fermi surface as a boundary in reciprocal space. It is very useful for predicting the thermal, electrical, magnetic, and optical properties of metals, semimetals, and doped semiconductors. The shape of the Fermi surface is derived from the periodicity and symmetry of the crystalline lattice and from the occupation of electronic energy bands. The energy band shows the possible energy range of electrons in the material. The presence of free electrons tells us if the material is a metal, a semiconductor or an insulator.

because of the Pauli exclusive principle, electrons pack into the lowest available energy states and build up a *Fermi sea* of electron energy states. Fermi level is the highest energy of the electrons at zero temperatures. The conduction band is the lowest range of vacant electronic states, and the valence band is the lower band below the conduction band and the band gap. Chemical potential is the required energy to add an electron in the system, and it is same as the Fermi energy at zero temperature. Due to Pauli exclusion principle, the adding electron should have a new highest energy.

In conductors, electrons only partially fill the valence band and the valence and conduction bands are very close or overlap, thus electrons become conductive easily. On the other hand, insulators and semiconductors have Fermi levels lying in the forbidden band gap and have full valence bands, therefore insulators have electrons with nowhere to go or jump and semiconductors become conductive only at certain temperatures since for $T > 0$, thermal excitation allow the particles to be found in the higher energy states. The nesting condition with $\vec{k} = 0$ requires only that the Fermi surfaces be identical in area and shape. It does not require the two layers to have aligned honeycomb lattices and hence aligned Brillouin-zones. At weak coupling, a binding energy is maximized when the momenta are as $\vec{p_1} = -\vec{p_2}$, which means the Fermi energies are nested, $\epsilon_1 = \epsilon_2 = \frac{\vec{p}_{1,2}^2}{2m}$. Similarly, it is observed that a Cooper pair is destroyed when an external magnetic field is exerted in the system since the Fermi energies are split by Zeeman effect.

These studies of inter-layer EC are very interesting for understanding

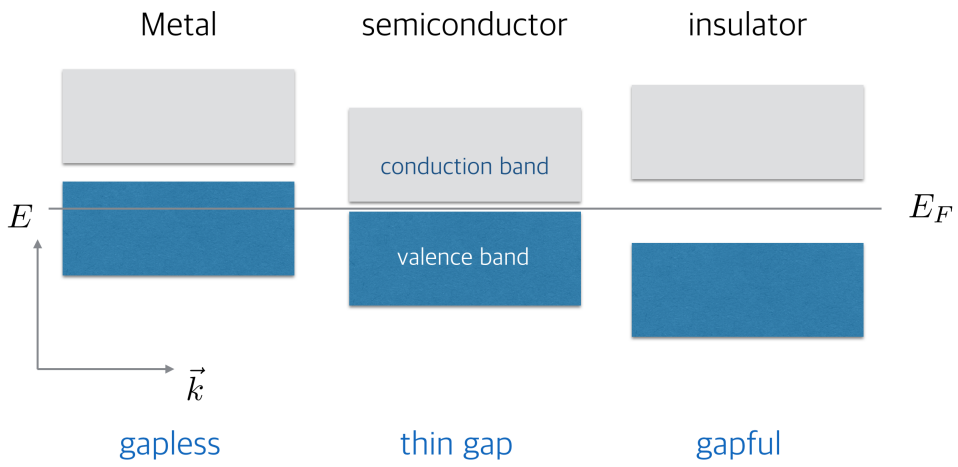

Figure 1.6: The energy band and Fermi level are very useful to see the physical properties of solids. We can classify solids from the size of the gap and where the gap and Fermi level are. These are related to the presence of the free electrons in solids.

fundamental issues with quantum coherence over mesoscopic distance scales and dynamical symmetry breaking. Moreover, the study accompanies numerous interesting applications in electronic devices because the result of mean field theory calculations expects a room temperature superfluid [66]. As a quantum phenomenon, the room temperature superfluid is intriguing. It is known that superfluidity occurs at very low temperature and weak coupling [2]. Let us consider a finite density ρ of non-relativistic bosons interacting with a short ranged repulsive Mexican well potential. Then, a spontaneous symmetry breaking occurs; and a gapless mode in the fluid of bosons with linear dispersion, $(\omega \propto \vec{k})$ yields superfluidity. A fluid flowing down with a velocity v and mass m could lose its momentum by creating a momentum excitation : $mv = mv' + \hbar k$. The energy becomes $\frac{1}{2}mv^2 \geq \frac{1}{2}mv'^2 + \hbar\omega$. By eliminating v', we obtain the relation, $v \geq \omega/k$. In other words, if the fluid is slower than that critical velocity $v_c = \omega/k$, it cannot lose its momentum, and so it gains superfluidity. It can be understood easily by comparing to a Fermi liquid having a continuum of gapless excitations. Thus, we should lower the temperature of the weakly coupled system to gain the superfluidity. If the interaction is strong enough, we could expect the energy gap between the lowest state and an excited state to become bigger and might gain superfluidity with higher temperature. Therefore, it is

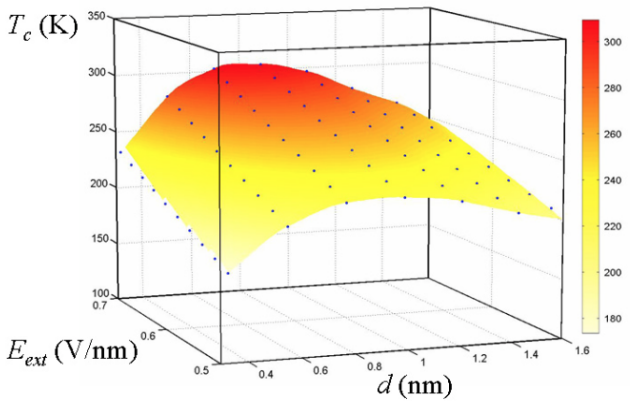

Figure 1.7: Normal to superfluid phase diagram at weak coupling and caption taken from [66]. The critical temperature T_c in Kelvin on distance is around room temperature with nanoscale distances. It is obtained using a coupling constant appropriate for a SiO_2 dielectric.

important to check if the system has an energy gap, which results in exciton condensates and superfluidity (and superconductivity). We can investigate the superfluidity by checking the gap and correlation functions in strong interacting systems.

In the model the temperature should be higher than that of usual Bose-Einstein condensates or typical superconductors because condensation is driven by Coulomb interactions over the fill band width, rather than by phonon-mediated interactions among quasiparticles in a narrow shell around the Fermi surface. In this sense, exciton condensation is more similar to ferromagnetism, which is also driven by Coulomb interactions and appears to be at high temperatures [66]. Besides, with an external gate, the model has more carriers, and graphene layers are so thin that the Coulomb interaction is not screened as much as in semiconductor quantum well bilayers. The numerical estimation is shown in Fig. 1.7.

In fact, the potential applications of superfluids are not as exciting and wide as those of superconductors. However, it is still useful for various areas. The most interesting application from this model might be bilayer (or possibly double monolayers) pseudo spin field-effect transistor (BiSFET) [112] by using transitions between superfluid mode and non-superfluid mode, which is researched by the author of [66] and his collaborators.

Moreover, there are some educational applications, showing how quan-

tum effects can become macroscopic in scale under certain extreme conditions as illustrated by Bose-Einstein condensates. Many bosons can be condensed at the same time at the lowest level of quantum states by a bosonization, which means it is quantum effect and can be seen in macroscopic level as do LASERs and superconductors. Superfluids have some impressive and unique properties that distinguish them from other forms of matter. As they have no internal viscosity, a quantum vortex formed within one persists indefinitely and its angular velocity is quantized. A superfluid has zero thermodynamic entropy and infinite thermal conductivity. Superfluids can also climb up and out of a container in a one-atom-thick layer if the container is not sealed; this is called a capillary action and a creep phenomenon. [7]. This superfluid quantum liquid prevails gravity of the Earth on the surface and is able to climb out of any container in a thin film moving up to 35 cm per second. A conventional molecule embedded within a superfluid can move with full rotational freedom, behaving like a gas. Other interesting properties may be discovered and designed to be applied for electronics, among others, in the future.

Despite the usefulness of this model, the theoretical analysis of the weak interacting model is limited in fully understanding the system because the Coulomb interaction at the distance (3nm) that causes room temperature superfluid must be very strong. Therefore, the perturbation theory should be re-summed in ad hoc way to take screening into account. We find non-perturbative model of very strongly coupled multi-monolayer systems[8]. This model is a defect quantum field theory which is the holographic AdS/CFT dual of a D3-probe-D5/anti-D5-branes system and D3-probe-D7/anti-D7-branes system.

We model defect quantum field theory in 2+1 dimensional space-time with double monolayer defects. It is shown in Fig. 1.8. $\mathcal{N} = 4$ SYM theory lives in a 3+1 dimensional bulk and there can be U(1) charged fermionic fields on defect. The interaction between them is mediated by $\mathcal{N} = 4$ SYM gauge fields in bulk. In order to consider a holographic gravity dual of the semimetals, e.g. graphene, we use evidence that D7 brane model resembles graphene in that it has relativistic fermions on defect. D7 branes share the coordinates t, x, y with D3 branes, and intersect probe branes along z.

[7] Readers can watch the remarkable properties of liquid helium when cooled below the lambda point (the superfluid state) through the hyperlink provided in [24]. It is video-recorded in 1963 by Alfred Leitner

[8] Graphenes interact by exchanging photons. The double monolayers in the model interact by exchanging gluons of $\mathcal{N} = 4$ supersymmetric Yang-Mills theory and truncate to planar limit. We do not construct the lattice structure.

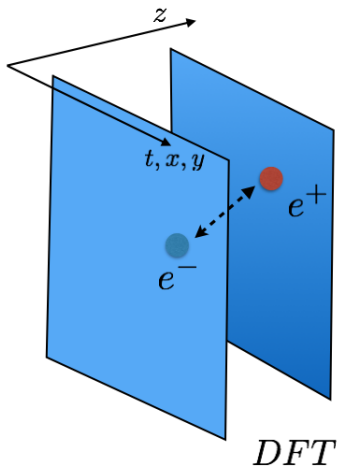

Figure 1.8: The infinite parallel planar (2+1)-dimensional defects bi-secting (3+1)-dimensional spacetime.

This D7 brane model breaks supersymmetry so that it becomes a fermonic theory. On the other hand, D5 brane has supermultiplet of fermions and scalars on defect. Supersymmetry is not broken until an external magnetic field is introduced. Low energy physics is governed by fermions. This is known from research on intra-layer condensates which are seen in graphene. As we mentioned earlier, graphenes interact by exchanging photons of U(1) theory, whereas our model interactions exchange $\mathcal{N} = 4$ super Yang-Mills (SYM) gluons, and truncate to planar limit; $N \to \infty$, $\lambda = g_{YM}^2 N \to \infty$ and $g_{YM} \ll 1$. As we have discussed briefly, large number of D3-branes at low energy limit cause the AdS background geometry, and we consider probe D7 and D5 branes embedded on the background geometry. We also take the no backreaction limit, $N \equiv N_3 \gg N_5,\ N_7$. [9] The motivation of the double layer Dirac Semimetals is well discussed in the later section, 5.1. We recommend reading this introductory section before proceeding.

[9] If the mass of the sun is not heavy enough, it will be much more difficult to calculate the motion of the earth because of the gravitational backreaction. We should consider the movement of the sun at every moment. Similarly, we can fix the geometrical background with the no-backreaction limit, $N_3 \gg N_5, N_7$.

1.5 Overview

The rest of the thesis is summarized as follows. We study a monolayer system before studying a double monolayer system. We probe D5 branes on D3 branes AdS geometry background, $AdS_5 \times S^5$. Fig. 1.9 is the figure to show this brane model. D5 branes span in AdS_4 on AdS_5. D3 and D5 branes are in force equilibrium without an external magnetic field or charges, D5 branes just stretch out toward a Poincaré killing horizon of D3 branes (Left figure of Fig. 1.9). With an external magnetic field perpendicular to D5 branes, the supersymmetry and conformal symmetry are both broken. Then, D5 branes receive repulsive force from D3 branes, and the force becomes stronger as closer as to the Poincaré horizon[10], so the branes pinch off and truncate at a finite AdS_5-radius, before they reach the Poincaré horizon. This is called *Minkowski embedding* (Right figure of Fig. 1.9). It can be considered as dynamical symmetry breaking corresponding to intra-layer condensates in single layer of graphene. This configuration has a charge gap. Charged degrees of freedom are open strings which stretch from the D5 brane to the Poincaré horizon. When, the D5 brane does not reach the Poincaré horizon,the open string has a minimum length and therefore a mass gap. It occurs at any value of an external magnetic field. This phenomenon is elaborated to understand a quantum Hall ferromagnetism in [85] and [77]. The quantum Hall system consists of a bunch of electrons moving in a plane in the presence of an external magnetic field B perpendicular to the plane. The magnetic field is assumed to be sufficiently strong so that the electrons all have spin up, so they can be treated as spinless fermions. The spinless electrons in a magnetic field have Landau quantized energy level. The Coulomb interaction has generated a small energy gap. This gap breaks some symmetry of the system. The phenomenon of interaction induced gaps and broken symmetries at integer filling factors is known as quantum Hall ferromagnetism. The four-fold degeneracy of graphene's Landau levels follows from approximate spin-degeneracy and from Bloch state degeneracy between two inequivalent points in the honeycomb lattice Brillouin zone [86]. For D3/D5 branes model, the gap breaks $SO(3)$ chiral symmetry and makes the neutral state gapped.

When $U(1)$ charge density is introduced, it becomes more interesting. In this case, the tension of D3-D5 strings competes with D5 branes tension. The tension of the strings is so greater than that of D5 branes that the

[10]In Fig. 1.9, $r = 0$ is the Poincaré horizon, and $r = \infty$ is an asymptotic boundary of AdS_5.

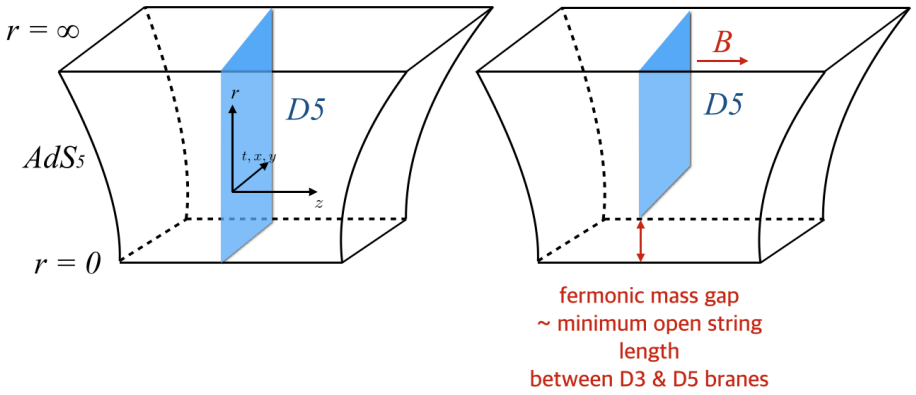

Figure 1.9: Probe D5 branes on D3 branes background geometry without and with an external magnetic field.

strings have zero length and the mass gap vanishes. If the ratio of charge density to the magnetic field, filling fraction, $\frac{q}{b}$[11] is bigger than some critical value, the system restores the symmetry. In other words, D5 branes stretch down to the horizon directly, and the chiral condensate term vanishes with a vanished mass gap. On the other hand, if the filling fraction is smaller than the critical value, the chiral symmetry is still broken without a mass gap. This is called a Berezinski-Kosterlitz-Thouless-like (BKT) phase transition. We have showed that an internal flux on the sphere of D5 branes also behaves like the charge density. The newly defined parameter for the phase transition is $\sqrt{f^2 + (\frac{q}{b})^2}$, where f is a constant factor proportional to the internal flux. We present more detail in the chapter 2. Fig. 1.10 and Fig. 1.11 are the main numerical results obtained in [92] and introduced in chapter 2 of this thesis. We have found the solutions of systems in Fig. 1.10, which interpolate for the Minkowski embedding with an external magnetic field and internal fluxes. Fig. 1.11 is obtained from the data of multiple interpolate solutions as seen in Fig. 1.10. m is a parameter of a fermonic mass, and c is a parameter of an intra-layer chiral condensation in (1.9). We interpret it as a solution with dynamical symmetry breaking, *i.e.*, a chiral condensate with no bare mass term.

In chapter 3, at last do we consider double layer probe branes. For probe D5 brane on D3 brane background geometry, we have a symmetric

[11] q is rescaled charge density. b is rescaled magnetic field. f to be appeared below is a rescaled internal flux on two sphere of five sphere.

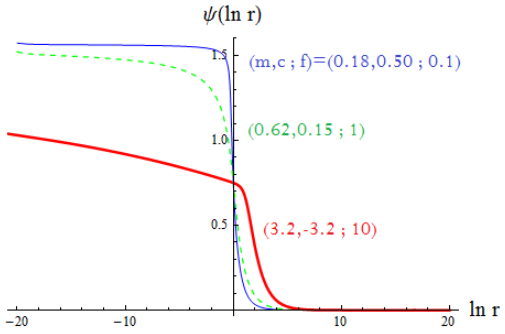

Figure 1.10: Fig. 2.1 in the chapter 2. The solutions of probe D5 branes model with different internal fluxes with the parameter f and the external magnetic field.

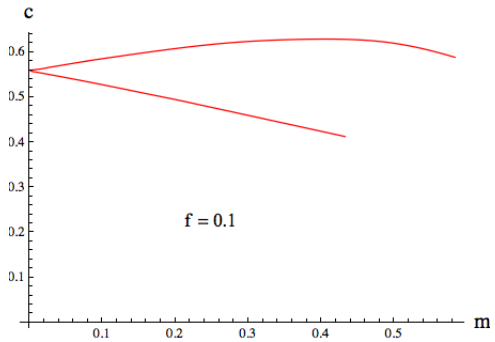

Figure 1.11: Fig. 2.2 in the chapter 2. The graph of c versus v.

trivial phase before breaking supersymmetries. Turning on the B-field, both branes and anti-branes pinch off from the horizon and intra-layer exciton transitions occur for each layer.

The each probe and anti probe brane have symmetries $U(N_f)$ and $U(\bar{N}_f)$ respectively. When the brane pair meets, symmetries of the pair are broken to the symmetry of one set of branes geometrically down there. The Dirac fermions lives on each probe brane and anti-probe brane. Thus, the symmetry breaking corresponds condensate of the fermions and anti-fermion. Note that we do not consider the charge density yet. We have chronologically studied this joined U-shaped model before studying how to introduce a charge density in the model. The readers might wonder why we do not consider the factor of temperature. It is easy to introduce temperature in the model by putting a black hole in AdS. AdS itself is a covariant box in which we can put the black hole and do experiments on it. A black hole pulls probe branes toward the horizon, so symmetry favors to be restored. It is known as symmetry restoration by temperature. Since we know what would happen when we introduce temperature in the model, without a loss of generality, we would consider zero temperature in the model in the later chapters than chapter 3. We also investigate the thermodynamics of brane configurations and obtain a phase diagram of the configurations (symmetric phase/broken symmetric phase), and have found phase diagrams. We load multiple phase transition lines in Fig. 1.12 with respect to different fluxes, $\alpha \equiv \frac{\zeta f}{\sqrt{f^2+4}}$[12]. The dominant solution above any specific curve is given by the two disconnected brane worldvolumes, *i.e.* the symmetric phase. The joined solutions, the broken symmetry phase, dominates below the curve. As a result, we newly see *inverse magnetic catalysis* in some range of internal fluxes of probe branes. For example, see the curve with $\alpha = -0.5$, upper green solid line. The symmetric phase is favored as B increases.

In chapter 4, we study a holographic model of dynamical symmetry breaking in 2+1-dimenisons, where a parallel D7-anti-D7 brane pair fuses into a single object, corresponding to the $U(1) \times U(1) \to U(1)$ symmetry breaking pattern. It is slightly different from the model we have studied in the chapter 2. Simply saying, this model is more symmetrical. Therefore, we show that the current-current correlation functions can be computed analytically and exhibit the low momentum structure that is expected when global symmetries are spontaneously broken. Of interest is that we can choose the $U(1)$ as global or gauged by choice of boundary condition. We

[12] f is a constant proportional to internal flux on S^2. ζ is a coefficient of an orientation. See the detail in chapter 3.

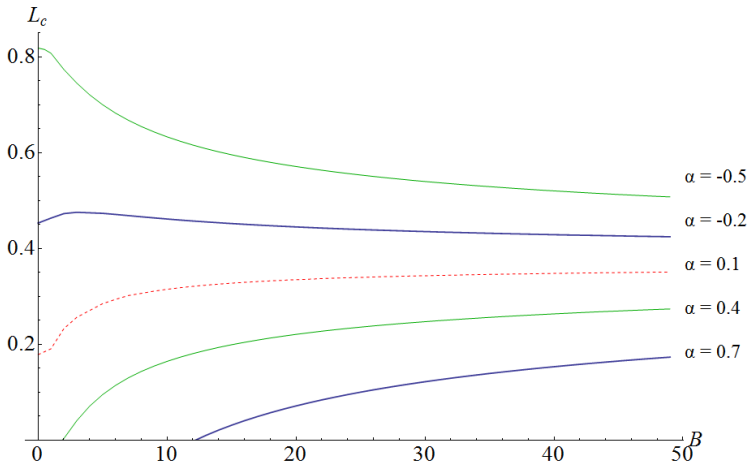

Figure 1.12: Fig. 3.10 in the chapter 3. Phase diagrams for the defect system obtained from D3/probe D7 branes model with an external magnetic field and internal fluxes. $\alpha \equiv \frac{\zeta f}{\sqrt{f^2+4}}$. ζ is a parameter of an orientation, which are *sign* factors $+1/-1$ of Wess-Zumino term. See chapter 3 for the detail.

are able to see 3 different current-current two point functions from Dirchlet-Dirichlet, Neumann-Neumann, and Dirchlet-Neumann boundary condition pair. The most interesting case is that one is global $U(1)$ and the other is gauged (DN boundary condition pair). Then, the global $U(1)$ symmetry is spontaneously broken and its current has a pole in its correlation function. The unbroken gauged $U(1)$ has a massless pole corresponding to the photon. It is seen in bilayer graphenes. We also find that these correlation (2-point) functions have poles attributable to infinite towers of vector mesons with equally spaced masses.

In chapter 5 and 6, we finalize the project we have discussed in the section 1.4. Respectively, we study probe D5 branes in chapter 5, and study probe D7 branes in chapter 6. A D5 brane and an anti-D5 brane are are suspended with a distance L apart at the AdS_5 asymptotic boundary, as shown in Fig. 1.13. When the D5 brane and an anti-D5 brane are exposed to a magnetic field, and if the field is strong enough, they can pinch off and end before they join, Fig. 1.13. So far, it is not different from the model of a single layer. However, the brane and anti-brane tend to join like a particle-hole pair without an external magnetic field. The tendency to join competes with the tendency to pinch off, and the competitions provide the phase diagrams Fig. 1.15 and Fig. 1.16 in [100, 101] , which present the

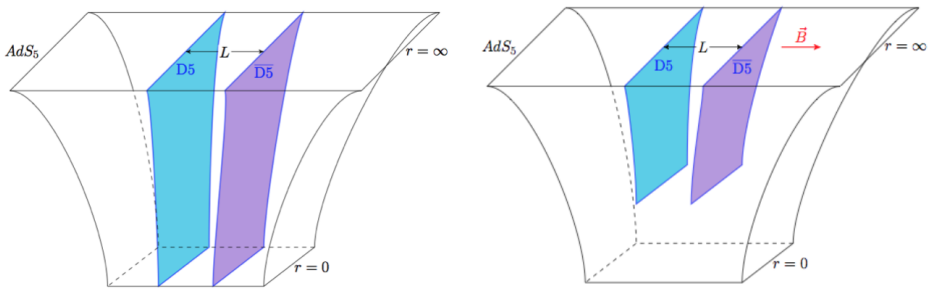

Figure 1.13: A D5 brane and an anti-D5 brane suspended in AdS_5 without an external magnetic field, both branes stretch to Poincaré horizon. When turning on an external magnetic field, they can pinch off before join.

results of a thermodynamical preference between 3 possible phases in the phase diagrams [100, 101].

Let us first see the phase diagram of probe D5 branes at Fig. 1.15. Electric field in the field theory model would effectively change the electric charge density. It is known that a doped bilayer graphene also has a band gap. That is why non-zero charge q is needed for inter-layer phases in the blue/green regions. For the degenerate gapless double monolayer graphene, the Dirac point chemical potential is a non-zero. It is also in agreement with D3/D5 phase diagram we obtained. For a fixed separation L, the red region is gapless and no inter-layer condensation with non-zero charge density, and it corresponds to Minkowski embedding. There are two dotted lines in the phase diagram. One is for the first order phase transition between $L = 1.357$ and 1.7, and the other line is asymptote to the spot BKT transition of single layer model between intra-layer phase and symmetric phase occurs when L is infinite. For infinite separation, L, we can treat the system disconnected, and then recover the behavior of a single layer. For small L, the branes are connected at any value of a chemical potential. It is also notable that there is no symmetric phase corresponds to the left figure in Fig. 1.13. It makes sense because we turned on an external magnetic field for the system.

For the phase diagram of probe D7 branes, the vertical axis is layer separation L in units of the inverse ultraviolet cutoff, R. The horizontal axis is the charge density q in units of R^2, where $R^4 = \lambda\alpha'^2$. The extremal

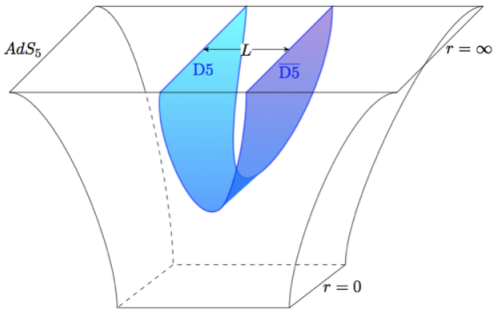

Figure 1.14: When the D5 brane and an anti-D5 brane are suspended as shown, their natural tendency is to join together.

black D3 brane geometry is given as follows :

$$\frac{ds^2}{R^2} = \frac{r^2\left(-dt^2+dx^2+dy^2+dz^2\right)}{\sqrt{1+R^4r^4}} + \sqrt{1+R^4r^4}\left(\frac{dr^2}{r^2}+d\psi^2+\sin^2\psi\sum_{i=1}^{5}(d\theta^i)^2\right) \tag{1.15}$$

where $\Sigma_{i=1}^{5}\ (\theta^i)^2 = 1$. Because $R \sim \alpha^{1/2}$, $1/R$ can be regarded as a UV cutoff. The main merit of using this geometry compared to $AdS_5 \times S^5$ we used for probe D5 branes is that we need an external magnetic field no more in order to break the supersymmetry. The asymptotic large r limit is Minkowski spacetime. In the near horizon limit, $rR \ll 1$, the geometry is $AdS_5 \times S^5$.

We can find a couple of differences below Fig. 1.15 with Fig. 1.16, made by the cutoff factor. The most outstanding one is by cutoff. When L is smaller than about R, inter-layer condensates never occur any more. The brane pair is disconnected shown the red and white area in Fig. 1.16. Moreover, there exists symmetric phase (white). The phase curve between blue and green regions is also a bit different.

We have introduced chemical energy nesting in the weak interacting model. The reader might ask what would happen at strong coupling, and maybe, could expect no need of the perfect nesting. However, inter-layer condensate occurs only if charge densities are balanced. It is sharper than in

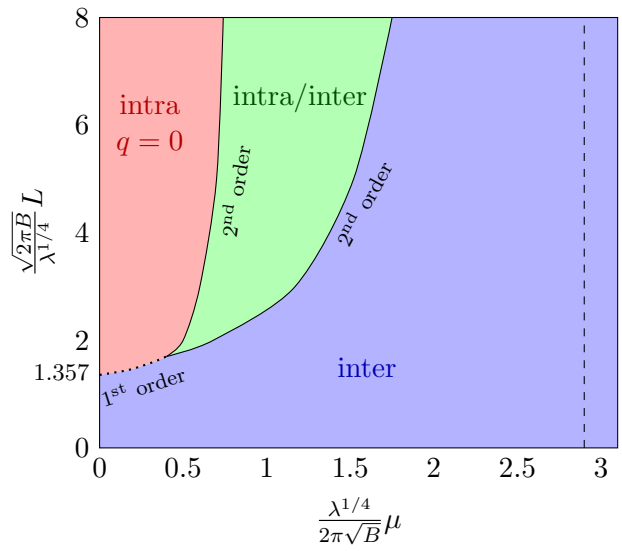

Figure 1.15: (color online)Phase diagram of the D3-probe-D5 brane system

the field theory. Moving away from nesting destroys the mass gap. We newly found that when there is more than one species of fermions, nesting can occur spontaneously. The tendency of interlayer condensate with perfect nesting is the most, so even with unbalanced charges on each layer, they make a perfect nesting at first, and the remaining charged probe branes have an intra-layer condensate and the left non-charged probe branes remain symmetric. This kind of perfect nesting is hard to achieve in the lab. Graphenes or semimetals we concern have crystal structure, whereas our model assume the density of the matter is uniform. Then it would be a bit difficult to match the atomic structures of two layers in the lab. We need more work in this part.

It is interesting to think why the green and blue region extend to an infinite separation, $L \to \infty$. It also agrees with weakly coupled systems. At weak coupling, the Coulomb force is a long-range interaction. For example, superfluidity can exist inside neutron stars. By analogy with electrons inside superconductors forming Cooper pairs due to electron-lattice interaction, it is expected that nucleons in a neutron star at sufficiently high density and low temperature can also form Cooper pairs due to the long-range attractive nuclear force and lead to superfluidity and superconductivity. From this point of view we expect that the strong correlations to play an important role in delimiting the magnitude of the pairing gap [68]. As we mentioned

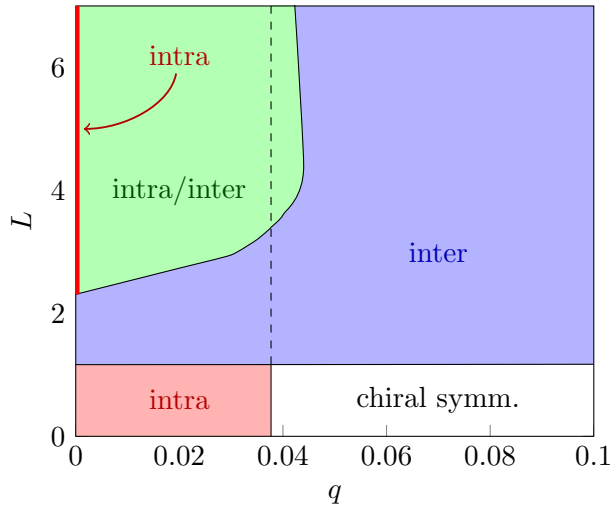

Figure 1.16: (color online)Phase diagram of the D3-probe-D7 brane system. We have used charge density, q, instead of chemical potential, μ as an x-axis. If we use chemical potential (x-axis), the diagram with $L \gtrsim 1$ looks almost the same to Fig. 1.15. The q and L are rescaled with $\frac{\sqrt{2\pi B}}{\lambda^{1}/4} = 1$.

in the previous section, the balanced Fermi surface seems more crucial to form condensates than the distance between layers. This also agrees with weakly interacting theory.

Chapter 2

D3-probe-D5 Holography with Internal Flux

Three quarks for Muster Mark!
Sure he hasn't got much of a bark
And sure any he has it's all beside the mark.

- Finngans wake by James Joyce

The AdS/CFT duality of an appropriately oriented probe D5-brane embedded in $AdS_5 \times S^5$ space-time and a supersymmetric defect conformal field theory is a well-studied example of holography [87]-[99]. In the limit of large N and large radius of curvature, the D5-brane geometry is found as an extremum of the Dirac-Born-Infeld action with appropriate Wess-Zumino terms added. Its world-volume is the product space $AdS_4(\subset AdS_5) \times S^2(\subset S^5)$ which preserves an $OSp(4|4)$ subgroup of the $SU(2,2|4)$ superconformal symmetry of the $AdS_5 \times S^5$ background. The superconformal field theory which is dual to this D3-D5 system, and which is described by it in the strong coupling limit, has a flat co-dimension one membrane that is embedded in 3+1-dimensional flat space. The bulk of the 3+1-dimensional space is occupied by $\mathcal{N} = 4$ supersymmetric Yang-Mills theory with $SU(N)$ gauge group. A bi-fundamental chiral hypermultiplet lives on the membrane defect and its field theory is dual to the low energy modes of open strings connecting the D5-branes and the D3-branes. These fields transform in the fundamental representation of the $SU(N)$ bulk gauge group and in the fundamental representation of the global $U(N_5)$, where N_5 is the number of D5-branes (in the probe limit, $N_5 << N$ and we will take $N_5 = 1$). The defect field theory preserves half of the supersymmetries of the bulk $\mathcal{N} = 4$ theory, resulting in the residual $OSp(4|4)$ super-conformal symmetry. It is massless with a hypermultiplet mass operator which breaks an SU(2) R-symmetry [89].

An external magnetic field has a profound effect on this system. In the quantum field theory, the magnetic field is constant and is perpendicular to

the membrane defect. In the string theory, the magnetic field destabilizes the conformal symmetric state to one which spontaneously breaks the SU(2) R-symmetry and generates a mass gap for the D3-D5 strings [76]. The only solution for the D5-brane embedding has it pinching off before it reaches the Poincaré horizon of AdS_5. As a result, the D3-D5 strings which, when excited, must reach from the D5-brane to the Poincaré horizon, have a minimum length and an energy gap. This occurs for any value of the magnetic field, in fact, since the theory has conformal invariance, the magnetic field is the only dimensional parameter and there is no distinction between large field and small field. A mass and a mass operator condensate for the D3-D5 strings can readily be identified (their conformal dimensions are protected by supersymmetry) and there is simply no solution of the probe D5-brane embedding problem with a magnetic field when both the mass and the condensate are zero. There can be a solution when one of those parameters vanishes and the other does not vanish. Such a solution can be interpreted as presence of a condensate in the absence of a mass operator, that is, as dynamical symmetry breaking. This phenomenon is regarded as a holographic realization of the "magnetic catalysis" of chiral symmetry breaking that has been studied in 2+1-dimensional quantum field theories [71]-[78] . The field theory studies rely on weak coupling expansions and re-summation of Feynman diagrams. Whether the phenomenon can persist at strong coupling is an interesting question which appears to have an affirmative answer in the context of this construction. It and many other aspects of the phase diagram of the D5-brane have been well studied in what is by now an extensive literature [36, 76, 99, 102].

This interesting behavior becomes more complex when a U(1) charge density is introduced. The state then has a non-zero density of D3-D5 strings as well as a magnetic field. There is also a tuneable dimensionless parameter, the ratio of charge density to the field, the "filling fraction" $\nu = \frac{2\pi\rho}{B}$. In this case, there is no charge gap. The D5-brane must necessarily reach the Poincaré horizon. This is due to the fact that, to have a nonzero charge density, there must be a density of fundamental strings suspended between the D5-brane and the Poincaré horizon. However, the fundamental string tension is always greater than the D5-brane tension [36] and such strings would therefore pull the D5-brane to the horizon. The result is a gapless state: the D3-D5 strings could have zero length, and therefore have no energy gap. At weak coupling, the analogous process is the formation of a fermi surface and a gapless metallic state when the charge density is nonzero.

What is more, if the filling fraction is large enough, the state with no

mass term and mass operator condensate equal to zero exists and is stable. In this state, the SU(2) R-symmetry is not broken. As the filling fraction is lowered from large values where the system takes up this symmetric phase, as pointed out in the beautiful paper [102], the system undergoes a Berezinski-Kosterlitz-Thouless-like (BKT) phase transition. This phase transition has BKT scaling and is one of the rare examples on non-mean field phase transitions in holographic systems. When the filling fraction is less than the critical value, again, even though the D5-brane world-volume now reaches the Poincaré horizon, there is no solution of the theory unless either the mass operator or mass operator condensate or both are turned on.

In this chapter, we shall observe that, as well as density, there is a second parameter which can drive the BKT transition. The parameter is the value of a magnetic flux which forms a U(1) monopole bundle on the D5-brane world-volume 2-sphere. The possibility of adding this flux was suggested by Myers and Wapler [36]. They found that the idea could be used to construct stable D3-D7 systems, in particular, and a modification of their idea was subsequently used to study holography in D3-D7 systems [37, 39, 54] In the limit where the string theory is classical, the problem of embedding a D5-brane in the $AdS_5 \times S^5$ geometry reduces to that of finding an extremum of the Dirac-Born-Infeld and Wess-Zumino actions,

$$S = \frac{T_5}{g_s} \int d^6\sigma \left[-\sqrt{-\det(g + 2\pi\alpha' F)} + C^{(4)} \wedge 2\pi\alpha' F \right] \tag{2.1}$$

where g_s is the closed string coupling constant, which is related to the $\mathcal{N} = 4$ Yang-Mills coupling by $4\pi g_s = g_{YM}^2$, $g_{ab}(\sigma)$ is the induced metric of the D5 brane, $C^{(4)}$ is the 4-form of the $AdS_5 \times S^5$ background, F is the world-volume gauge field and $T_5 = \frac{1}{(2\pi)^5 \alpha'^3}$. We shall use the metric of $AdS_5 \times S^5$

$$\begin{aligned} ds^2 = L^2 \Big[& r^2(-dt^2 + dx^2 + dy^2 + dx^2) + \frac{dr^2}{r^2} + \\ & + d\psi^2 + \cos^2\psi(d\theta^2 + \sin^2\theta d\phi^2) + \sin^2\psi(d\tilde{\theta}^2 + \sin^2\tilde{\theta} d\tilde{\phi}^2) \Big] \end{aligned} \tag{2.2}$$

Here the 5-sphere is represented by two 2-spheres fibered over the interval $\psi \in [0, \frac{\pi}{2}]$. The 4-form is

$$C^{(4)} = L^4 r^4 dt \wedge dx \wedge dy \wedge dz + L^4 \frac{c(\psi)}{2} d\cos\theta \wedge d\phi \wedge d\cos\tilde{\theta} \wedge d\tilde{\phi} \tag{2.3}$$

with $\partial_\psi c(\psi) = 8\sin^2\psi\cos^2\psi$ The radius of curvature of AdS is L and $L^2 = \sqrt{\lambda}\alpha'$ with $\lambda = g_{YM}^2 N$. The embedding of the D5-brane is mostly

determined by symmetry. The dynamical variables are

$$\{x(\sigma), y(\sigma), z(\sigma), t(\sigma), r(\sigma), \psi(\sigma), \theta(\sigma), \phi(\sigma), \tilde{\theta}(\sigma), \tilde{\phi}(\sigma)\}$$

We look for a solution of the form

$$\sigma_1 = x, \sigma_2 = y, \sigma_3 = t, \sigma_4 = r, \sigma_5 = \theta, \sigma_6 = \phi, \tilde{\theta} = 0, \tilde{\phi} = 0 \tag{2.4}$$

and the remaining coordinates depending only on $\sigma_4 = r$, $(z(r), \psi(r))$.[13] With this Ansätz, the D5-brane world-volume metric is

$$ds^2 = L^2 \left[r^2(-dt^2 + dx^2 + dy^2) + \frac{dr^2}{r^2}(1 + r^2\psi'^2 + r^4 z'^2) + \cos^2\psi(d\theta^2 + \sin^2\theta d\phi^2) \right] \tag{2.7}$$

where prime denotes derivative by r and the world-volume gauge fields are

$$F = \frac{L^2}{2\pi\alpha'}\ a'(r)\ dr \wedge dt + \frac{L^2}{2\pi\alpha'}\ b\ dx \wedge dy + \frac{L^2}{2\pi\alpha'}\ \frac{f}{2}\ d\cos\theta \wedge d\phi \tag{2.8}$$

Here, f is the strength of the monopole bundle.[14] b is a constant magnetic field which is proportional to a constant magnetic field in the field theory dual. $a(r)$ is the temporal world-volume gauge field which must be non-zero in order to have a uniform charge density in the field theory dual. The bosonic part of the R-symmetry is $SU(2) \times SU(2)$. One SU(2) is the isometry

[13] This ansatz is symmetric under spacetime parity which can be defined for the Wess-Zumino terms

$$\int d^6\sigma \epsilon^{\mu_1\mu_2\cdots\mu_6} \partial_{\mu_1} x(\sigma) \partial_{\mu_2} y(\sigma) \partial_{\mu_3} z(\sigma) \partial_{\mu_4} t(\sigma) r^4(\sigma)\ \partial_{\mu_5} A_{\mu_6}(\sigma) \tag{2.5}$$

$$\int d^6\sigma \epsilon^{\mu_1\mu_2\cdots\mu_6} \partial_{\mu_1} \cos\theta(\sigma) \partial_{\mu_2}\phi(\sigma)\ \partial_{\mu_3} \cos\tilde{\theta}(\sigma) \partial_{\mu_4}\tilde{\phi}(\sigma) c(\psi) \partial_{\mu_5}\ A_{\mu_6}(\sigma) \tag{2.6}$$

in the following way. The world-volume coordinates transform as $\{\sigma'_1, \sigma'_2, \ldots, \sigma'_6\} = \{-\sigma_1, \sigma_2, \ldots, \sigma_6\}$ and the embedding functions as $x'(\sigma') = -x(\sigma)$, $\tilde{\theta}'(\sigma') = \pi - \tilde{\theta}(\sigma)$, $A'_1(\sigma') = -A_1(\sigma)$ with all other variables obeying $\chi(\sigma') = \chi(\sigma)$. This is a symmetry of the Wess-Zumino terms and the solution (2.4) is invariant. Charge conjugation flips the sign of all gauge fields, $A \to -A$ and we augment it by $\{\sigma'_1, \ldots, \sigma'_5, \sigma'_6\} \to \{\sigma_1, \ldots, -\sigma_5, \sigma_6\}$. The Wess-Zumino terms are invariant. The background field $f d\cos\theta \wedge d\phi$ is also invariant once we choose $\sigma_5 = \frac{\pi}{2} - \theta$. The fields $a(r)$ breaks C and preserves P. b breaks C and P and preserves CP.

[14] A monopole bundle has quantized flux. Here the number of quanta is very large in the strong coupling limit $n_D \sim \sqrt{\lambda}$, so that it is to a good approximation a continuously variable parameter. b and q are related to the physical magnetic field and charge density as $b = \frac{2\pi}{\sqrt{\lambda}}B$, $q = \frac{4\pi^3}{\sqrt{\lambda}N}\rho$ so that $\frac{q}{b} = \frac{\pi}{N}\frac{2\pi\rho}{B} \equiv \frac{\pi}{N}\nu$ where the dimensionless parameter ν is the filling fraction. A Landau level would have degeneracy N. so filling fraction of a set of N degenerate levels naturally scales like N to give order one b and q in the large N limit.

of the S^2 which is wrapped by the D5 brane (2.7) and is also a symmetry of the background fields (2.8). The other is the rotation in the transverse $S^2 \subset S^5$ with S^5 coordinates $\tilde{\theta}, \tilde{\phi}$. This is a symmetry of the embedding only when the former S^2 is maximal, that is, when $\psi(r) = 0$ for all r. If $\psi(r)$ deviates from zero, it must choose a direction in the transverse space, and the choice breaks the second SU(2). The hypermultiplet mass shows up in the D5 brane embedding as

$$M \sim m \equiv \lim_{r\to\infty} r \sin\psi(r) \tag{2.9}$$

and deviation of $\psi(r)$ from the constant $\psi = 0$ so that the parameter m is nonzero is a signal of having switched on a hypermultiplet mass operator in the dual field theory.

With (2.7) and (2.8), the action (4.5) is

$$S = \mathcal{N} \int d^3x dr \left[-\sqrt{(f^2 + 4\cos^4\psi)(b^2 + r^4)(1 + r^2\psi'^2 + r^4 z'^2) - a'^2} + f r^4 z' \right] \tag{2.10}$$

where $\mathcal{N} = \frac{2\pi T_5 L^6}{g_s} = \frac{\sqrt{\lambda}N}{4\pi^3}$. The factor of 2π in the numerator comes from half of the volume of the unit 2-sphere (the other factor of 2 is still in the action). The Wess-Zumino term gives a source for $z(r)$.

Now, we must solve the equations of motion for the functions $\psi(r)$, $a(r)$ and $z(r)$ which result from (2.10) and the variational principle. The variables $a(r)$ and $z(r)$ are cyclic and they can be eliminated using their equations of motion,

$$\frac{d}{dr}\frac{\delta S}{\delta z'(r)} = 0 \quad \rightarrow \quad \frac{\sqrt{(f^2 + 4\cos^4\psi)(b^2 + r^4)}\, r^4 z'}{\sqrt{1 + r^2\psi'^2 + r^4 z'^2 - a'^2}} - f r^4 = p_z \tag{2.11}$$

$$\frac{d}{dr}\frac{\delta S}{\delta a'(r)} = 0 \quad \rightarrow \quad \frac{\sqrt{(f^2 + 4\cos^4\psi)(b^2 + r^4)}\, a'}{\sqrt{1 + r^2\psi'^2 + r^4 z'^2 - a'^2}} = -q \tag{2.12}$$

where p_z and q are constants of integration. If these equations are to hold near $r \to 0$, we must set $p_z = 0$. q is proportional to the charge density in the field theory dual. Then, we can solve for z' and a',

$$z' = \frac{f\sqrt{1 + r^2\psi'^2}}{\sqrt{4\cos^4\psi(b^2 + r^4) + f^2 b^2 + q^2}} \tag{2.13}$$

$$a' = \frac{-q\sqrt{1 + r^2\psi'^2}}{\sqrt{4\cos^4\psi(b^2 + r^4) + f^2 b^2 + q^2}} \tag{2.14}$$

We must then use the Legendre transformation

$$\mathcal{R} = S - \int a'(r)\frac{\partial L}{\partial a'(r)} - \int z'(r)\frac{\partial L}{\partial z'(r)}$$

to eliminate z' and a'. We obtain the Routhian

$$\mathcal{R} = \mathcal{N}\int d^3x dr \sqrt{4\cos^4\psi(b^2+r^4)+b^2f^2+q^2}\sqrt{1+r^2\psi'^2} \tag{2.15}$$

which must now be used to find an equation of motion for $\psi(r)$,

$$\frac{\ddot{\psi}}{1+\dot{\psi}^2} + \dot{\psi}\left[1+\frac{8r^4\cos^4\psi}{4(b^2+r^4)\cos^4\psi+f^2b^2+q^2}\right] + \frac{8(b^2+r^4)\cos^3\psi\sin\psi}{4(b^2+r^4)\cos^4\psi+f^2b^2+q^2} = 0 \tag{2.16}$$

where the overdot is the logarithmic derivative $\dot{\psi} = r\frac{d}{dr}\psi$.

First, we note that, if $\psi(r)$ is to be finite at $r\to\infty$, its logarithmic derivatives should vanish. Then, the only boundary condition which is compatible with the equation of motion is $\psi(r\to\infty)=0$.

If we set $b=0$, f does not appear in the Routhian (2.15) or in the equation of motion (2.16). $\psi(r)$ which is then f-independent. In fact, the constant solution, $\psi=0$ is a stable solution of (2.16). $z(r)$ is f and r-dependent. Equation (2.13) has the solution $z(r) = \int dr\frac{f}{\sqrt{4r^4+f^2}}$. The worldvolume metric is still that of $AdS_4\times S^2$,

$$ds^2 = L^2\left[r^2(-dt^2+dx^2+dy^2)+\frac{dr^2}{r^2}\left(1+\frac{f^2}{4}\right)\right] + L^2\left[d\theta^2+\sin^2\theta d\phi^2\right] \tag{2.17}$$

where, now, the radii of the two spaces differ, the S^2 still has radius L whereas AdS_4 has radius $L\sqrt{1+\frac{f^2}{4}}$. The field theory dual of this system was discussed in reference [36]. It has a planar defect dividing three dimensional space into two half-spaces with $\mathcal{N}=4$ Yang-Mills theory with gauge group $SU(N+n_D)$ on one side of the defect and $\mathcal{N}=4$ Yang-Mills theory with gauge group $SU(N)$ on the other side. Here n_D is the number of Dirac monopole quanta in f. The r-dependence of the embedding function $z(r)$ can be viewed as an energy-scale dependent position of the defect in the field theory.

When b is not zero, scaling $r\to\sqrt{b}r$, removes b from most of equation (2.16), the dependence which remains is only inthe parameter $f^2+\left(\frac{q}{b}\right)^2$. If this parameter is large enough, the solution $\psi(r)=0$ is still a stable

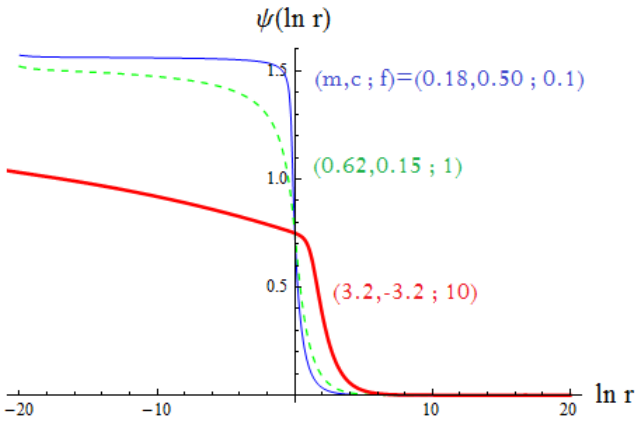

Figure 2.1: We integrate equation (2.16) with $q = 0$, $f^2 = 0.01$ and $f^2 = 100$. The solution interpolates between the correct asymptotic values, $\psi(r = \infty) = 0$ and $\psi(r = 0) = \frac{\pi}{2}$. With larger f^2, it clearly has a slower approach to $\psi = \frac{\pi}{2}$. The AdS radius r is measured in units of $1/\sqrt{b}$.

solution of (2.16). The BKT phase transition found in reference [102] was driven by the change in behavior of the equation for $\psi(r)$ in the small r region and, in that paper, it was found by adjusting $\frac{q}{b}$ (they had $f = 0$) with the critical value being $\left(\frac{q}{b}\right)^2\Big|_{\text{crit.}} = 28$. At that point, the symmetric solution $\psi = 0$ becomes unstable. This is easily seen by looking at solutions of the linearized equation which, at small r, must be $\psi \sim c_1 r^{\nu_+} + c_2 r^{\nu_-}$ with $\nu_\pm = -\frac{1}{2} \pm \frac{1}{2}\sqrt{1 - 32/\left(4 + f^2 + \frac{q}{b}\right)^2}$ and the instability sets in when the exponents become complex, that is, at $\left[f^2 + \left(\frac{q}{b}\right)^2\right]_{\text{crit.}} = 28$. The complex exponents are due to the fact that, in the $r \sim 0$ regime, the fluctuations obey a wave equation for AdS_2 with a mass that violates the Breitenholder-Freedman bound. Since, in the stable regime, $f^2 + \left(\frac{q}{b}\right)^2 > 28$ both of the exponents in the fluctuations are negative, deviation from $\psi(r) = 0$ is not allowed, it is an isolated solution. We can find this solution and the phase transition even when $\frac{q}{b}$ vanishes by varying f, stability where $f^2 > 28$ and the phase transition at $f^2_{\text{crit}} = 28$. In particular, this allows us to study the theory in the charge neutral state where $q = 0$. From the point of view of the space-time symmetry, the flux f is charge conjugation symmetric, whereas the finite charge density state is not. In fact f itself does not violate any 2+1-dimensional spacetime symmetries associated with Lorentz, C, P or T invariance.

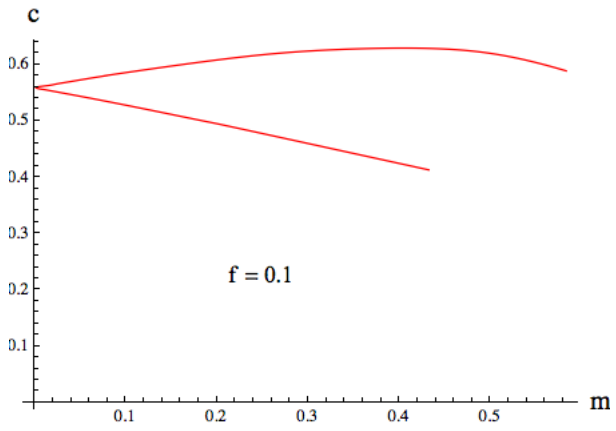

Figure 2.2: The constants c versus m are plotted for a sequence of embeddings of the D5-brane in the region where the constant ψ solutions are unstable. Here $f^2 = .01$. Note that there is a special value of the condensate c where $m = 0$. We interpret this as a solution with dynamical symmetry breaking, i.e. as a chiral condensate with no bare mass term.

When the symmetric solution $\psi = 0$ is unstable, we must find another solution of equation (2.16) for $\psi(r)$, where we now assume that it depends on r. $\psi = 0$ was an isolated solution, there are no other solutions closeby. As soon as it depends on r, if $\psi(r)$ is to remain finite in the small r region, it must go to the other solution of (2.16) at small r, $\psi(r \to 0) = \frac{\pi}{2}$.

When either or both of q and f are nonzero, the D5-brane must reach the Poincaré horizon. Otherwise, the charge density q and magnetic monopole flux f would have to have sources on the D5-brane worldvolume. q would be sourced by a uniform density of fundamental strings and the magnetic monopole flux f by n_D D3-branes which are suspended between the world-volume and the Poincaré horizon. However, as in the case of fundamental strings, it is possible to show that the D3-brane tension is always greater than the D5-brane tension. Like the fundamental string, a suspended D3-brane would drag the D5-brane to the horizon. The D5-brane world-volume could still reflect this behavior with a spike or funnel-like configuration. When there are both suspended fundamental strings and D3-branes, it is interesting that the embedding problem depends on the combination $\sqrt{f^2 + \left(\frac{q}{b}\right)^2}$, reminiscent of bound states of F-strings and D-branes. We then expect to find solutions of (2.16) which interpolate between $\psi = 0$ at $r \to \infty$ to $\psi = \frac{\pi}{2}$ at $r \to 0$. Indeed, for generic asymptotic behavior, such solutions are easy to find by a shooting technique. Examples are given in figure 2.1.

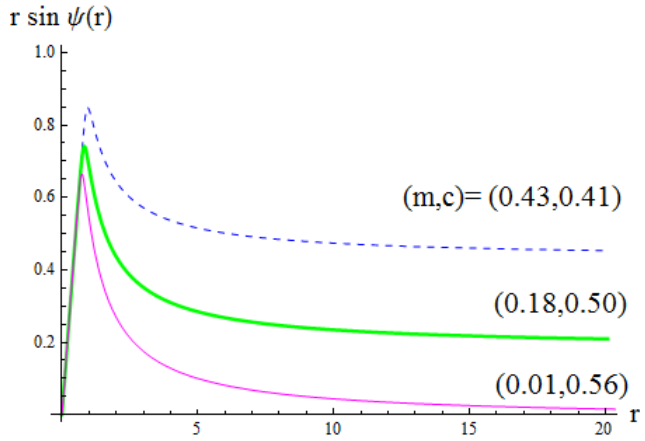

Figure 2.3: The function $r\sin(\psi(r))$ is plotted versus r for some embeddingsparameterized by the asymptotic m and c, including the one which is close the solution with $m = 0$ which is associated with dynamical symmetry breaking.

It is also possible to find solutions that can be interpreted as chiral symmetry breaking, although the D5-brane still reaches the Poincaré horizon and we expect that the D3-D5 strings are still gapless. In the region of large r, the linearized equation for $\psi(r)$ is solved by

$$\psi(r) = \frac{m}{r} + \frac{c}{r^2} + \dots$$

The two asymptotic behaviors have power laws associated with the ultraviolet conformal dimension of the mass and the chiral condensate in the dual field theory. These are the same as their classical dimensions since they are protected by supersymmetry. A symmetry breaking solution would have one of these equal to zero (and the other one interpreted as a condensate). Indeed, it is easy to find a family of solutions of (2.16) which, as we tune m, still exists and has nonzero c in the limit where m goes to zero. The c versus m behavior of this family of solutions is shown in figure 2.2. The behavior if $r\sin(\psi(r))$ which can be interpreted as the separation of the D5 and D3-branes is plotted in figure 2.3 for some values of m and c.

As an extension of our results here, it would be interesting to analyze the electromagnetic properties of the solution with finite f and $q = 0$. This is a charge neutral state and it has a mass operator condensate. It is possible to study Maxwell equations for fluctuations of the worldvolume gauge field and though it is difficult to obtain an analytic solution, it is relatively straightforward to show that they have no solution when the field strength

is a constant. This implies that the charged matter is still gapless and provides the singularities in response functions which make the theory singular at low energy and momentum.

Chapter 3

Dynamical Symmetry Breaking with Charged Probe Pair

> But you've ceased to believe in your theory already,
> what will you run away with?
>
> *- Crime and Punishment by Fydor Dostoevsky*

3.1 Introduction

The AdS/CFT correspondence [12], and holographic duality in general, is a powerful, conjectured technique for the analysis of strongly coupled field theories. While originally pursued to address questions about low-energy QCD, it has expanded to include studies of a variety of strongly coupled field theories in diverse dimensions.[15]

Of much interest in recent years has been the study of defect theories and the interaction of defects. Such defects can be constructed holographically by the intersection of different stacks of D-branes, one of the earliest known examples being the supersymmetric $(2+1)$-dimensional intersection of the $D3/D5$ system [89], a defect in the ambient $(3+1)$-dimensional $\mathcal{N}=4$ super Yang-Mills native to the $D3$ worldvolume. A common technique for studying these systems is to consider the quenched approximation of the field theory, where one stack, say of Dp-branes, has parametrically more branes than the other, say of Dq-branes. The gravity description of this scenario can then be reliably computed at strong coupling by using a probe Dq-brane action in the near-horizon region of a classical p-brane supergravity solution [26].

[15] For older review articles see [8, 14], while [19, 21] are more recent with an emphasis on applications for condensed matter.

The full dual field theory lives at the asymptotic boundary of this spacetime and the defect theory lives where the probe brane intersects the boundary.

Multiple defects may be studied by allowing several stacks of Dq-branes to intersect the boundary. As discussed first in [27, 28], a coherent state of spatially separated defects can be achieved by a continuous probe brane configuration with a multiply connected intersection with the boundary. Since the boundary components must have opposite orientation in this scenario, it can be understood as brane/anti-brane recombination. In the scenario of [27, 28], the defect degrees of freedom were $d = 3 + 1$ chiral fermions, with those on the brane component of opposite chirality from those on the anti-brane. The coherent state where the worldvolumes join in the bulk thus describes chiral symmetry breaking. In [30, 31], this scenario was generalized to allow for intersections of other dimension and brane species as well as for the joining process to occur dynamically.[16] Further generalizations have included adding external magnetic and electric fields as well as chemical potential [29, 32–34].

In this chapter, we consider scenarios of bulk brane/anti-brane recombination in $AdS_5 \times S^5$,

$$ds^2 \sim r^2 \left(-dt^2 + dx^2 + dy^2 + dz^2\right) + \frac{dr^2}{r^2} + d\Omega_5^2 \ . \tag{3.1}$$

As an additional ingredient to previous studies, we consider probes which are electrically charged under the background F_5 Ramond-Ramond field. The probe branes form two stacks, each spanning some cycle in S^5, the non-compact directions (t, x, y) and some curve $z(r)$. The stacks have opposite orientation and are separated in the z direction along the boundary.

An uncharged probe brane – such as in the studies cited above – experiences no force in the non-compact directions from the F_5. For such a case there are then two qualitative classes of solutions, depicted in Fig. 3.1. The first solution is the so-called "black hole embedding" which reaches all the way down to the spacetime horizon. These embeddings are "straight" in the sense that $\frac{dz}{dr} = 0$. The second solution is a joined embedding which has two disconnected boundaries of opposite orientation although the entire worldvolume is a simply connected and oriented manifold. Only these solutions have $\frac{dz}{dr} \neq 0$. Note that since there is no Ramond-Ramond force, the brane orientation does not play a role.

On the other hand, if the probe branes are charged under the spacetime Ramond-Ramond field, the situation is somewhat different. This can occur

[16] In [27, 28], topological considerations force the branes to join while in [30, 31] and later works there are multiple consistent solutions and only the minimum energy one dominates.

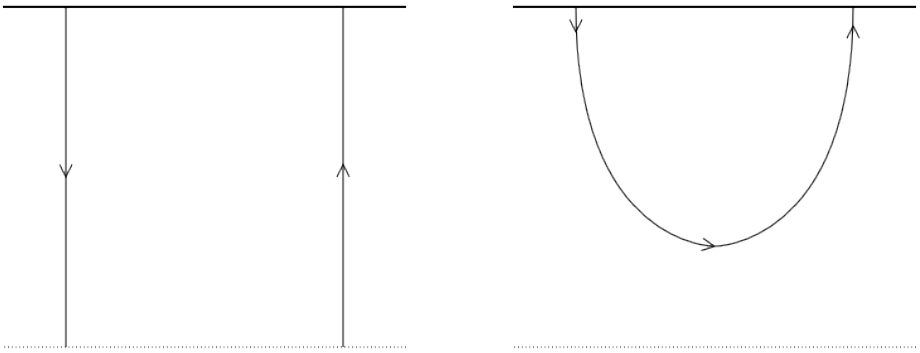

Figure 3.1: Straight embeddings and a joined embedding where there is no force from the background Ramond-Ramond flux. The arrows represent worldvolume orientation. There would be no change in the embedding if the arrows were reversed.

either because the probe itself is a $D3$-brane, or the charge could be induced by worldvolume fluxes on the probe. The $D3/D5$ system where the $D5$ brane carries q unit of $D3$-brane charge was first introduced in [87]. In [36], black-hole embeddings of $D5$ and $D7$ probe branes with induced $D3$-brane charge were studied in $AdS_5 \times S^5$. Additional $D7$ brane embeddings carrying $D3$ charge were introduced in [37] and studied further in [38, 39]. These probes are affected by the background F_5 and even the black hole embeddings have $\frac{dz}{dr} \neq 0$. In Fig. 3.2, we see such a black-hole embedding. The brane orientation plays a major role in this situation; an oppositely oriented probe would bend in the opposite z-direction.

These electrically charged probe branes have a richer space of joined solutions than their uncharged cousins. Due to the force in the z-direction, the qualitative features of the solution depend strongly on the orientation, specifically the left-right ordering of the boundary components. The choice of orientation gives rise to the classes of solutions seen in Fig. 3.3. The top left figure pictures a brane/anti-brane pair which tend toward each other despite not actually connecting, while the top right figure pictures a joined pair. These two solutions have the same boundary conditions and so it is a dynamical question which has the lower energy and is therefore stable. The figures in the bottom row also depict solutions with the same boundary conditions, but with the worldvolume orientations all opposite of the figures above. Note the surprising feature in the bottom right figure, where the joined embedding becomes wider in the bulk than at the boundary. We

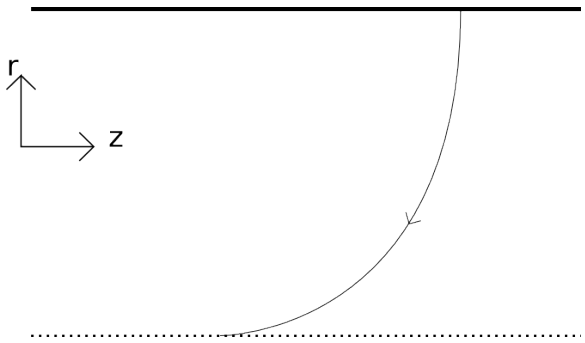

Figure 3.2: A $D3$-charged probe brane in (finite-temperature) $AdS_5 \times S^5$. The probe bends in the z-direction as it descends from the boundary (the solid line at the top) to enter the horizon represented by the dotted line at the bottom. The arrow represents the orientation of the $D3$ charge. An oppositely oriented brane would bend in the opposite z-direction.

will call these joined solutions "chubby" and conversely the more typical solutions in the top right (which are widest at the boundary) we will call "skinny."

There are multiple perspectives on what these brane systems are holographically dual to. Firstly, the $(2+1)$-dimensional intersection of a probe brane with the boundary is conventionally associated with a defect in $\mathcal{N}=4$ super-Yang-Mills gauge theory. The field content of the defect is given by the lowest level open string modes which are localized at the D-brane intersection. For a $D5$-brane probe, the defect theory is supersymmetric since the intersection is $\#ND = 4$; this is the spectrum studied in [89]. For the $D7$-brane probe, the intersection is $\#ND = 6$ and the spectrum is simply massless fermions [40], in fact T-dual to the $D4/D8$ intersections of the Sakai-Sugimoto model [27, 28]. As a caveat, it should be mentioned that it is not clear if this picture of the spectrum still holds when internal fluxes exist on the probe, but is often nonetheless used to guide intuition.

A defect dual to a stack of N branes or anti-branes is associated with a $U(N)$ global flavor symmetry inherited from the gauge field living on the brane worldvolume. Thus the recombination of an equal number of branes and anti-branes describes a breaking of symmetry $U(N) \times U(N) \to U(N)$. Since the defects are separated in space, the duals of these scenarios can be considered interacting $(2+1)$-dimensional defect bi-layer systems or as discussed in [31], $(2+1)$-dimensional effective field theories with non-local interactions.

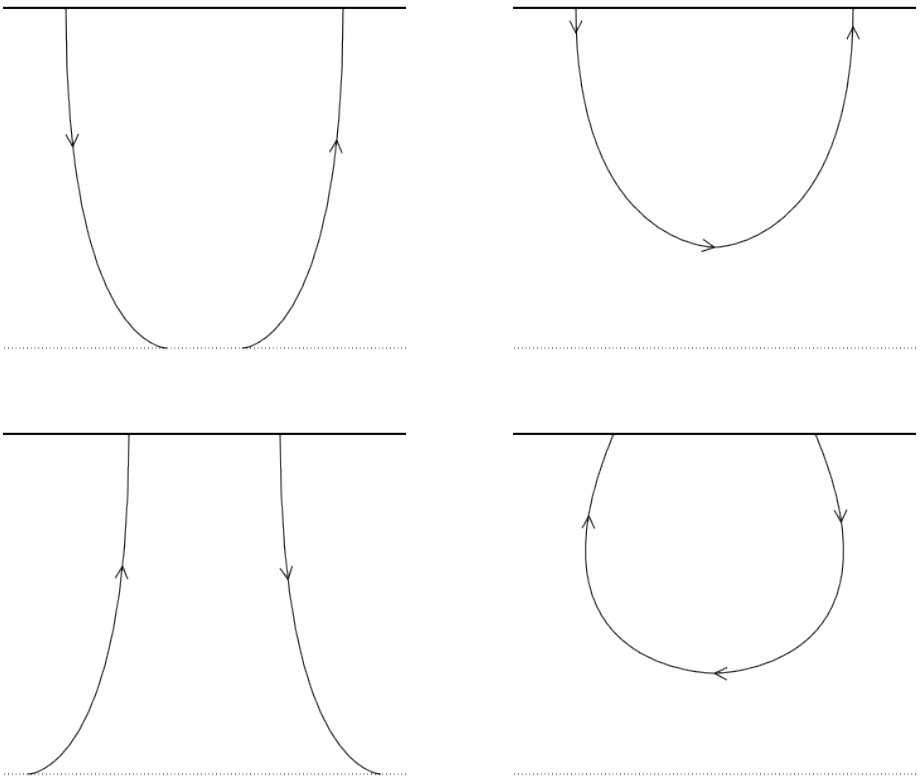

Figure 3.3: The top row pictures possible solutions of a brane/anti-brane pair in the presence of a Ramond-Ramond force. Note that the branes bend toward each other as they extend into the bulk even if they don't join. If the orientations are reversed, we have instead the bottom set of solutions. These always bend away from each other when initially leaving the boundary even if they eventually join in the bulk.

The dual interpretation above holds for probes with or without $D3$-charge. However, for $D3$-charged probes there are some other interesting properties of these solutions. A $D3$-charged probe brane – even a higher dimensional brane with an induced $D3$ charge – contributes to the overall Ramond-Ramond flux of the system. This flux is in turn related by the AdS/CFT dictionary to the rank of the dual gauge group. Therefore a defect of $D3$-charge k forms a domain wall in the dual gauge theory with $SU(N)$ gauge symmetry on one side and $SU(N+k)$ on the other [36]. A cartoon representation of this situation is depicted in Fig. 3.4. Once the probe enters the horizon, it is effectively parallel to the original stack of $D3$-branes sourcing the geometry, adding to the overall $D3$-brane charge as measured by a Gaussian surface outside the horizon. This is interpreted as a larger gauge symmetry existing in the region to the left. It follows that if there are multiple $D3$-charged defects, that we have a spatially non-trivial pattern of symmetry breaking in the dual theory, with a gauge group between the defects which is different from that outside. Thus the joined solutions should be considered dual to finite-width domain walls.

In this chapter, we will study the thermodynamics of these domain walls, mostly from the bulk perspective. In Section 2, we introduce a class of $D3$-charged probe branes and derive a one-dimensional effective particle mechanics action that describes the entire class. The solutions of the equation of motion of this effective action are studied in Section 3 and a renormalized free energy computed in Section 4. Finally, in Section 5, we examine the phase diagram of this system in the space of external magnetic field and asymptotic separation with some comments on the phenomenon of magnetic catalysis.

3.2 $D3$-charged probes in $AdS_5 \times S^5$

Consider the background IIB supergravity solution thermal $AdS_5 \times S^5$, the near-horizon geometry of N_3 $D3$-branes at finite temperature. The line-element is given by

$$L^{-2}ds^2 = r^2\left(-h(r)dt^2 + dx^2 + dy^2 + dz^2\right) + \frac{dr^2}{h(r)r^2} + d\Omega_5^2 \ . \tag{3.2}$$

The S^5 line element is represented as a bundle over $S^2 \times S^2$,

$$d\Omega_5^2 = d\psi^2 + \sin^2\psi d\Omega_2^2 + \cos^2\psi d\tilde{\Omega}_2^2 \ , \tag{3.3}$$

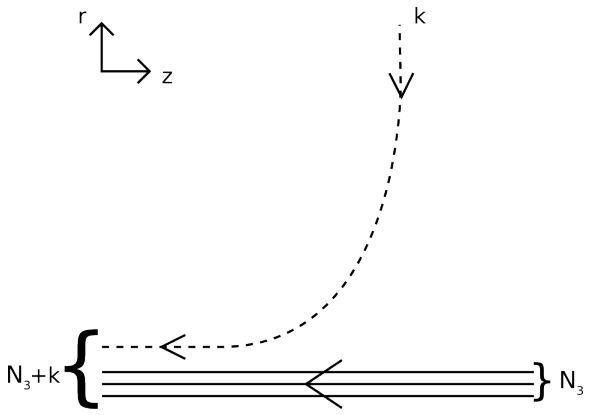

Figure 3.4: A cartoon representation of a probe brane (dashed line) carrying $D3$-charge k bending to become parallel with the stack of N_3 $D3$-branes sourcing the AdS geometry, represented by the solid lines at the bottom. The arrows represent brane worldvolume orientation. The dual gauge group is $SU(N_3)$ towards the right while it is enhanced to $SU(N_3 + k)$ to the left.

where $\psi \in \left(0, \frac{\pi}{2}\right)$ and

$$d\Omega_2^2 = d\theta^2 + \sin^2\theta d\phi^2 \ , \tag{3.4}$$

is the line-element for a unit S^2. The blackening function is

$$h(r) = 1 - \frac{r_h^4}{r^4} \ . \tag{3.5}$$

At zero-temperature, $r_h = 0$. However, any non-zero value of r_h can be rescaled by a coordinate transformation. Therefore, for finite temperature, we can choose without loss of generality $r_h = 1$. The scale of the geometry is related to the microscopic string theory parameters via

$$L^4 = 4\pi g_s N_3 (\alpha')^2 \ . \tag{3.6}$$

There is also a self-dual five-form Ramond-Ramond flux

$$F_5 = \frac{4L^4}{g_s}\left(r^3 dt \wedge dx \wedge dy \wedge dz \wedge dr + \omega_5\right) \ . \tag{3.7}$$

Here ω_5 is the volume form on the unit five-sphere

$$\omega_5 = \sin^2\psi \cos^2\psi d\psi \wedge \omega_2 \wedge \tilde{\omega}_2 \ , \tag{3.8}$$

where $\omega_2 = \sin\theta d\theta \wedge d\phi$ is the S^2 volume form. We encode this flux with the four-form potential

$$\frac{g_s}{L^4} C_4 = r^4 h(r) dt \wedge dx \wedge dy \wedge dz + \frac{1}{2} c\left(\psi\right) \omega_2 \wedge \tilde{\omega}_2 \ . \tag{3.9}$$

The function $c\left(\psi\right)$ is

$$c(\psi) = \psi - \frac{1}{4}\sin\left(4\psi\right) + c_0 \tag{3.10}$$

where c_0 is an arbitrary constant, a residual ambiguity due to the gauge symmetry of the Ramond-Ramond field. A similar constant could be added to the coefficient of $dt \wedge dx \wedge dy \wedge dz$, but we have chosen to partially fix the gauge by requiring that the first term in C_4 vanish at the horizon. This ensures that the term is well-defined on the Euclidean section of (3.2) which simplifies the treatment of the Wess-Zumino terms.

We will now consider the following set of branes

	t	x	y	z	r	ψ	Ω_2	$\tilde{\Omega}_2$
$D3'$	–	–	–	–	·	·	·	·
$D3$	–	–	–	$\sim$	$\sim$	·	·	·
$D5$	–	–	–	$\sim$	$\sim$	·	–	·
$D7$	–	–	–	$\sim$	$\sim$	·	–	–

(3.11)

The $D3'$ row refers to the large stack of $D3$ branes which source the AdS geometry while the other rows record the configurations of the probes. A dash indicates the brane is extended in that direction, with support over the entire range of the coordinate. A dot indicates the respective brane is completely localized in that coordinate. Finally the $\sim$ symbols indicate that the brane traces a curve in those directions. For example, the $D5$-brane extends along the non-compact (t, x, y) directions, wraps one of the two S^2 factors in the S^5, is localized in ψ and on the other S^2, and finally, lies along a curve in the (z, r) space.

These probes all intersect the boundary on some $2+1$ dimensional subspace at a fixed value of z (although for the $D3$ probes, this will turn out to be $z = \pm\infty$). In order to induce $D3$-brane charge,[17] the probe $D5$ and $D7$-branes will carry internal flux topologically supported on one or both S^2 factors, respectively. We will also allow for magnetic field in the three dimensional defect on the boundary, *i.e.* a non-zero F_{xy} component. In [37],

[17] Such flux is actually required to stabilize the $D7$ probe at a non-trivial value of ψ at the AdS boundary [37].

$D7$ branes with a more general *ansatz* were studied. However, our focus will be a class of solutions with different boundary conditions.

The $D5$ and $D7$ probes outlined above have $3+1$ non-compact directions and wrap some compact cycles. If one imagines integrating over these cycles, one would obtain an effective $3+1$ dimensional object which carries $D3$ charge in AdS_5. In other words, the higher-dimensional $D3$-charged branes act as effective $D3$-branes. These effective branes are much like excited states of a proper $D3$, they carry $D3$ charge but the effective tension is greater than the charge. This will become clearer in the next few sections. First, we will calculate an effective action for a $D3$ probe with the *ansatz* (3.11). We will then see that $D5$ and $D7$ probes will yield an effective action of the same form.

3.2.1 $D3$-brane probe

First, let us introduce a $D3$-brane probe as a model system. The action comprises the familiar DBI and Wess-Zumino terms

$$S_3 = -T_3 \int d^{3+1}\xi e^{-\phi}\sqrt{-\det\left(g + 2\pi\alpha' F\right)} - T_3 \int C_4 \ . \tag{3.12}$$

The three-brane tension is

$$T_3 = \frac{1}{(2\pi)^3}\frac{1}{\alpha'^2} \ . \tag{3.13}$$

We choose a static gauge where $\xi^a = \{t, x, y, r\}$ are brane coordinates and the embedding is given by the function $z(r)$. The induced metric is thus

$$\frac{ds_3^2}{L^2} = r^2\left(-hdt^2 + dx^2 + dy^2\right) + \left(1 + r^4 h\dot{z}^2\right)\frac{dr^2}{r^2 h} \ , \tag{3.14}$$

where a dot indicates differentiation by r. We also allow a magnetic field normalized as

$$\frac{2\pi\alpha'}{L^2}F = B dx \wedge dy \ . \tag{3.15}$$

This information is sufficient to compute the Born-Infeld term

$$S_{DBI} = \mathcal{N}_3 \int dr\sqrt{\left(r^4 + B^2\right)\left(1 + r^4 h\dot{z}^2\right)} \ , \tag{3.16}$$

where the overall constant is

$$\mathcal{N}_3 = \frac{T_3 L^4 V_{2+1}}{g_s} \ , \tag{3.17}$$

with V_{2+1} the infinite volume factor of the (t, x, y) directions.

To compute the Wess-Zumino term we also need to specify an orientation, which we encode via an orientation parameter $\zeta = \pm 1$. Evaluating,

$$\int C_4 = V_{2+1}\zeta \int r^4 h\dot{z} dr \ . \tag{3.18}$$

Note that while orientation is an invariant geometric feature intrinsic to the entire D-brane worldvolume, the parameter ζ is partly an artifact of the coordinates we use. Therefore ζ may take different values on separate branches of the same continuous brane. For example, in a brane/anti-brane recombination, the left branch has $\zeta = 1$ and the right branch $\zeta = -1$, yet the worldvolume is continuous.

Putting together the terms above – and dropping an overall constant factor – yields an effective particle mechanics Lagrangian

$$L_3 = \sqrt{(r^4 + B^2)\left(1 + r^4 h\dot{z}^2\right)} + \zeta r^4 h\dot{z} \ . \tag{3.19}$$

We will find similar effective Lagrangians for the $D5$ and $D7$ probes, differing only in the coefficient of the second term. Here that coefficient is of unit magnitude since physically it is the $D3$-brane charge per tension.

3.2.2 $D5$ probes

The probe action for $D5$-branes is

$$S_5 = -T_5 \int d^{5+1}\xi e^{-\phi} \sqrt{-\det\left(g + 2\pi\alpha' F\right)} - 2\pi\alpha' T_5 \int C_4 \wedge F \ , \tag{3.20}$$

where the tension is

$$T_5 = \frac{1}{(2\pi)^5} \frac{1}{\alpha'^3} \ . \tag{3.21}$$

We choose a static gauge with coordinates $\xi^a = \{t, x, y, r, \theta, \phi\}$ and embedding function $z(r)$. The induced metric is

$$\frac{ds_5^2}{L^2} = r^2\left(-h dt^2 + dx^2 + dy^2\right) + \left(1 + r^4 h\dot{z}^2\right)\frac{dr^2}{r^2 h} + \sin^2\psi d\Omega_2^2 \ . \tag{3.22}$$

The *ansatz* for worldvolume flux is

$$\frac{2\pi\alpha'}{L^2} F = B dx \wedge dy + \frac{f}{2}\omega_2 \ . \tag{3.23}$$

The magnetic field is a continuous quantity but the flux on the compact sphere is, of course, quantized

$$f = \frac{2\pi\alpha'}{L^2} n \ , \qquad n \in \mathbb{Z} \ . \tag{3.24}$$

Substituting all this into the action yields

$$S_5 = -\mathcal{N}_5 \int dr \left[\sqrt{(r^4 + B^2)\left(f^2 + 4\sin^4\psi\right)(1 + r^4 h \dot{z}^2)} + \zeta f r^4 h \dot{z} \right] , \tag{3.25}$$

with the normalization

$$\mathcal{N}_5 = \frac{2\pi T_5 L^6 V_{2+1}}{g_s} \ , \tag{3.26}$$

and once again we have introduced an orientation parameter $\zeta = \pm 1$. Our *ansatz* is for constant ψ but we see that ψ has a potential. The ψ equation of motion is

$$\frac{d}{d\psi}\sqrt{f^2 + 4\sin^4\psi} = 0 \ , \tag{3.27}$$

yielding[18]

$$\psi = \frac{\pi}{2} \ . \tag{3.28}$$

We insert this back into the $D5$ action. Up to an overall constant we again obtain an effective particle Lagrangian for $z(r)$,

$$L_5 = \sqrt{(r^4 + B^2)(1 + r^4 h \dot{z}^2)} + \frac{\zeta f}{\sqrt{f^2 + 4}} r^4 h \dot{z} \ . \tag{3.29}$$

The only difference from the $D3$ is in the coefficient of the second term, the effective $D3$-brane charge per unit tension. The magnitude of this ratio is less than unity here, in keeping with the picture that this $D5$ probe is a $D3$-brane in an excited state.

3.2.3 $D7$ probes

The $D7$-brane action is

$$S_7 = -T_7 \int d^{7+1}\xi e^{-\phi} \sqrt{-\det\left(g + 2\pi\alpha' F\right)} - \frac{(2\pi\alpha')^2}{2} T_7 \int C_4 \wedge F \wedge F \ , \tag{3.30}$$

[18] Another solution is $\psi = 0$ but it is physically trivial since the brane volume is then exactly zero.

with tension

$$T_7 = \frac{1}{(2\pi)^7}\frac{1}{\alpha'^4} \ . \tag{3.31}$$

In a static gauge with coordinates $\xi^a = \left\{t, x, y, r, \theta, \phi, \tilde{\theta}, \tilde{\phi}\right\}$, we describe the embedding with the function $z(r)$. The induced metric is

$$\frac{ds_7^2}{L^2} = r^2\left(-hdt^2 + dx^2 + dy^2\right) + \left(1 + r^4 h\dot{z}^2\right)\frac{dr^2}{r^2 h} + \sin^2\psi d\Omega_2^2 + \cos^2\psi d\tilde{\Omega}_2^2 \ . \tag{3.32}$$

For the worldvolume flux we use the *ansatz*

$$\frac{2\pi\alpha'}{L^2}F = Bdx \wedge dy + \frac{f_1}{2}\omega_2 + \frac{f_2}{2}\tilde{\omega}_2 \ . \tag{3.33}$$

The fluxes on the S^2 factors are quantized

$$f_i = \frac{2\pi\alpha'}{L^2}n_i \ , \qquad\qquad n_i \in \mathbb{Z} \ . \tag{3.34}$$

The DBI portion of the action is

$$S_{DBI} = -\mathcal{N}_7 \int dr \sqrt{\left(r^4 + B^2\right)\left(f_1^2 + 4\sin^4\psi\right)\left(f_2^2 + 4\cos^4\psi\right)\left(1 + r^4 h\dot{z}^2\right)} \tag{3.35}$$

with

$$\mathcal{N}_7 = \frac{4\pi^2 T_7 L^8 V_{2,1}}{g_s} \ . \tag{3.36}$$

The Wess-Zumino term is given by

$$S = -\mathcal{N}_7 \zeta f_1 f_2 \int dr r^4 h\dot{z} \ , \tag{3.37}$$

with ζ the orientation parameter. We minimize the ψ potential

$$\frac{d}{d\psi}\sqrt{\left(f_1^2 + 4\sin^4\psi\right)\left(f_2^2 + 4\cos^4\psi\right)} = 0 \ , \tag{3.38}$$

yielding the implicit equation[19]

$$f_2^2\sin^2\psi - f_1^2\cos^2\psi + 4\cos^2\psi\sin^2\psi\left(\cos^2\psi - \sin^2\psi\right) = 0 \ . \tag{3.39}$$

[19] While this can be solved for general f_i, it can be seen that fluctuations $\delta\psi$ around the solution can violate the BF bound [42, 43]. In particular, for absolutely no internal fluxes $f_i = 0$, the $D7$ will be unstable [44]. See [37] for more discussion of stabilizing this $D7$ brane embedding.

Substituting this back into the action yields, up to an overall constant, an effective particle Lagrangian for the $D7$-brane

$$L_7 = \sqrt{(r^4 + B^2)\,(1 + r^4 h\dot{z}^2)} + \frac{\zeta f_1 f_2}{\sqrt{\left(f_1^2 + 4\sin^4\psi_0\right)\left(f_2^2 + 4\cos^4\psi_0\right)}} r^4 h\dot{z}\ , \quad (3.40)$$

where ψ_0 is a constant that solves (3.39). This again takes the form of the effective $D3$ Lagrangian with a charge per tension smaller than unity.

3.3 Solutions to effective Lagrangian

We found that all three of the $D3$-charged probes under consideration are described by an effective particle Lagrangian of the form

$$S_{eff} = \int dr\sqrt{r^4 + B^2}\sqrt{1 + r^4 h\dot{z}^2} + \alpha \int dr r^4 h\dot{z}\ . \quad (3.41)$$

The parameter α is the effective $D3$-brane charge per tension and is given by

$$\alpha = \begin{cases} \zeta & D3-\text{brane} \\ \frac{\zeta f}{\sqrt{f^2+4}} & D5-\text{brane} \\ \frac{\zeta f_1 f_2}{\sqrt{\left(f_1^2+4\sin^4\psi_0\right)\left(f_2^2+4\cos^4\psi_0\right)}} & D7-\text{brane} \end{cases} \quad (3.42)$$

with ψ_0 solving (3.39) in the case of the $D7$. Note that $|\alpha| < 1$ for both the $D5$ and $D7$ probes.

The equation of motion derived from (3.41) can be immediately integrated since the variable $z(r)$ is cyclic

$$P \equiv \sqrt{\frac{r^4 + B^2}{1 + r^4 h\dot{z}^2}} r^4 h\dot{z} + \alpha r^4 h = constant\ . \quad (3.43)$$

Define the intermediate function

$$g(r) = \frac{P}{r^4 h} - \alpha\ , \quad (3.44)$$

then solve for $\dot{z}$ to obtain

$$\dot{z} = \frac{g(r)}{\sqrt{r^4 + B^2 - r^4 h g(r)^2}}\ . \quad (3.45)$$

The full profile $z(r)$ is obtained by integration. This cannot be done analytically in general, but for any choice of B, P and α the integration of (3.45) is easily evaluated numerically.

These solutions are completely specified by the integration constant P. For any brane profile that enters the black hole horizon, substituting $r = 1$ into (3.43) shows that P must vanish since $h\,(r = r_h = 1) = 0$,

$$\boxed{P = 0 \text{ for solutions with support at } r = 1} \tag{3.46}$$

In keeping with the literature we call these solutions *black hole embeddings*. Since $P = 0$, we have $g(r) = -\alpha$. Thus, we see from (3.45) that for the black hole embeddings $z(r)$ is single-valued and monotonic.

The other possibility is that the profile has a minimum value of r. Without loss of generality, we can choose this minimum to be located at $z = 0$. The signal of a minimum would be $\dot{z}$ diverging at some $r = r_0$. This yields the expression for the integration constant

$$P = r_0^4\sqrt{h_0}\left(\sqrt{1+\frac{B^2}{r_0^4}}\text{sign}\,(\dot{z}_0) + \alpha\sqrt{h_0}\right)\ , \tag{3.47}$$

where $h_0 = h(r_0)$ and $\dot{z}_0 = \dot{z}(r \to r_0)$. The presence of an absolute minimum requires that the brane bends back up to the boundary. This other leg of the brane will have opposite orientation parameter ζ so this solution is a joined brane/anti-brane pair. We thus call the $P \neq 0$ solutions *joined embeddings*.

The magnitude of the first term in the parentheses of (3.47) is greater than unity while that of the second term is less than unity. Therefore

$$\text{sign}\,(\dot{z}\,(r \to r_0)) = \text{sign}\,(P)\ . \tag{3.48}$$

However, $\dot{z} \to -\infty$ when approaching from the left of the minimum while $\dot{z} \to +\infty$ when approaching from the right. Furthermore, the orientation parameter ζ changes sign from one branch to the other. Therefore, P changes sign as well,[20] with $P < 0$ for $z < 0$ and $P > 0$ for $z > 0$ (see Fig. 3.5). The joined configuration is clearly symmetric under parity $z \to -z$, so we can without loss of generality focus our attention to a single branch. We will therefore restrict our attention to $P \geq 0$, which includes the black hole embedding and the "right branch" with $\dot{z}_0 > 0$ of the joined solutions.

At the boundary

$$\text{sign}\,(\dot{z}\,(r \to \infty)) = -\text{sign}\,(\alpha)\ , \tag{3.49}$$

[20]The reader may find this disconcerting, since P is playing the role of a conserved quantity. The resolution lies in the multi-valuedness of the function $z(r)$. P need only be constant on a given single-valued branch. The minimum is precisely where the single-valued parameterization $z(r)$ breaks down and so consequently does the definition of P. That the magnitude of P is constant follows from the continuity of the embedding.

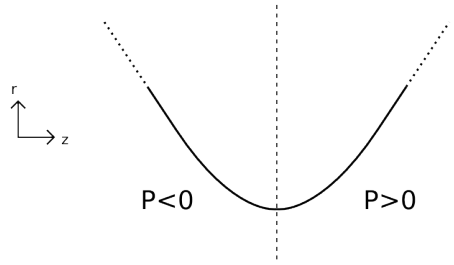

Figure 3.5: The sign of the integration constant P is the same as that of $\dot{z}$ as r_0 is approached and flips accordingly as the minimum at $z = 0$ is crossed.

indicating that the direction in which the brane bends initially on its descent from infinity is given entirely by the sign of the $D3$-brane charge. Comparing (3.48) and (3.49) we see there are thus two qualitative classes of joined solutions, given by the relative sign of P and α. For $\text{sign}(P) = -\text{sign}(\alpha)$, the sign of $\dot{z}$ remains the same throughout the branch, *i.e.* each branch of the brane is separately monotonic. On the other hand, for $\text{sign}(P) = \text{sign}(\alpha)$ even a given branch is not monotonic. We call these two possibilities "skinny" and "chubby," respectively. See Fig. 3.6.

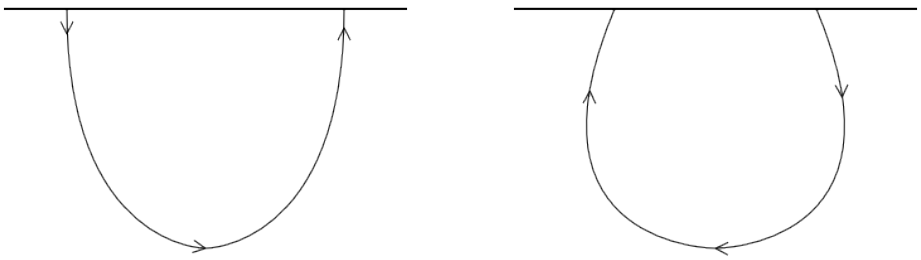

Figure 3.6: "Skinny" and "chubby" joined embeddings.

Physically, we know that the brane and anti-brane have an attraction due to exchange of gravitons and Ramond-Ramond quanta. Further, the background F_5 also deflects branes and anti-branes in opposite directions. In the skinny solutions, the background F_5 pushes the two stacks together while in the chubby solutions the Ramond-Ramond field forces them apart.

3.3.1 Asymptotics

The asymptotic separation in z of a joined brane/anti-brane pair is not independent of r_0. Define L as

$$L(r_0) = 2\int_{r_0}^{\infty} \dot{z}(r) \ , \tag{3.50}$$

where the factor of two arises since the integral is only over one branch of the brane system. For a joined solution, *i.e.* any solution with $r_0 > 1$, L is the asymptotic separation in the z direction of the two ends of the solution. For $r_0 = 1$ however, the brane and anti-brane are disconnected black hole embeddings. In this case the asymptotic separation is truly a free parameter and $L(r_0 = 1)$ simply records (twice) the range in z that each branch of the embedding spans.

The probe branes for generic α have the large r behavior

$$\dot{z}\,(r \gg 1) = -\frac{\alpha}{\sqrt{1-\alpha^2}}\frac{1}{r^2} + O\left(\frac{1}{r^6}\right) \ , \qquad (|\alpha| < 1) \ . \tag{3.51}$$

The case $|\alpha| = 1$ is non-generic. Indeed, expanding (3.45) in yields

$$\dot{z}\,(r \gg 1) = -\frac{\alpha}{\sqrt{1+B^2+2\alpha P}} + O\left(\frac{1}{r^4}\right) \ , \qquad (|\alpha| = 1) \ . \tag{3.52}$$

It follows that L converges for $|\alpha| < 1$ and diverges for $|\alpha| = 1$, which means that $|\alpha| = 1$ branes (*i.e.* $D3$-brane probes) do not intersect the AdS boundary at finite z while those with generic α do. The impossibility of the $D3$ probe to intersect the AdS boundary at finite z may be a symptom of the open string tachyon present at weak coupling at the $(2+1)$-dimensional intersection of $D3$-branes.[21] Whatever the explanation, we will now restrict our attention to $D5$-branes and $D7$-branes so that we can study probes which intersect the boundary at a finite location.

The right-hand side of (3.50) is a complicated function of r_0 since $\dot{z}$ depends on it through the integration constant P. We do not have an analytic expression but can plot it numerically. As an example, see Fig. 3.7, which plots $L(r_0)$ for a $D7$-brane probe with $B = 0$ and $f_1 = f_2 = \frac{1}{\sqrt{2}}$. Note that $L(r_0)$ is not monotonic and has a maximum. Therefore, when the brane/anti-brane pair are sufficiently separated at the boundary (with an $L \gtrsim 1.3$) there are no joined solutions, only black hole-embeddings. Further,

[21] Since such a system has $\#ND = 2$. See [40].

due to the maximum there is a range of L where there are two r_0, that is two solutions with the same boundary condition.

Another feature worth noting is the abrupt end of the curve at $r_0 = 1$. The $r_0 = 1$ solution is a black-hole embedding and $L(1)$ is (twice) the Δz spanned by a single branch of that embedding. The curve $L(r_0)$ does not continue past this point.

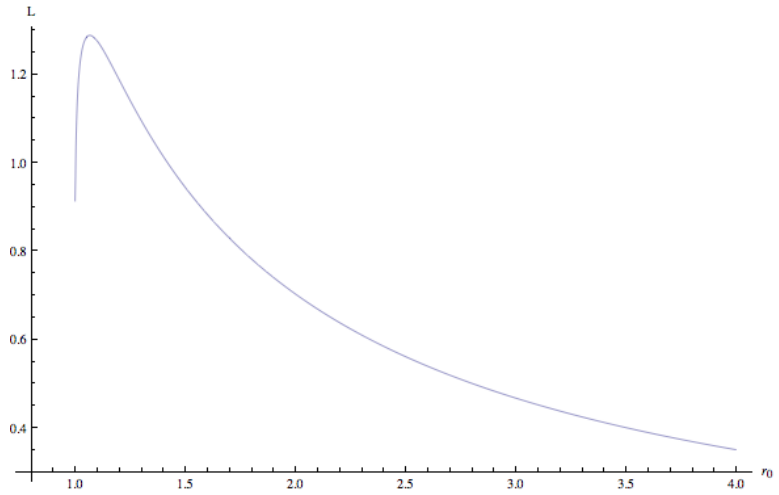

Figure 3.7: Asymptotic brane separation L of a joined solution ($\alpha = -\frac{1}{3}$ and no magnetic field) as a function of minimum radius r_0.

There is a class of unphysical solutions lurking within the family that we have been discussing. Some of the non-monotonic branches, *i.e.* those with $\text{sign}(P) = \text{sign}(\alpha)$, will turn out to have negative L. Qualitatively these solutions appear as in Fig. 3.8. Note that they have the same boundary conditions as a "skinny" solution. These solutions are clearly unstable to brane reconnection at the intersection point and will not be considered further.

3.4 Free energy

Now that we have classified the solutions, we investigate the phases of a pair of brane/anti-brane probes. The dynamical problem is to find the solution in a given ensemble, with given boundary conditions, which has the lowest free energy. This solution will dominate and be thermodynamically stable. In the present case, the boundary conditions are given by the asymptotic brane positions and orientations and the values of the fluxes, including magnetic

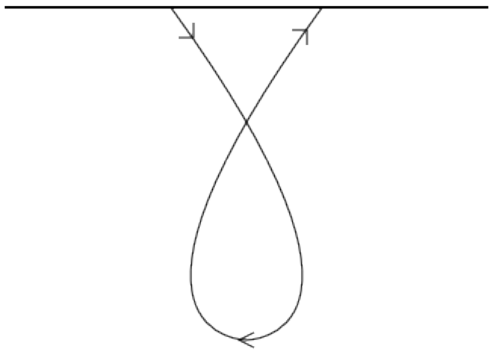

Figure 3.8: An unphysical solution with negative L.

field. Without loss of generality, we can assume[22] that the center of the pair is at $z = 0$, *i.e.* if they join, they join at $z = 0$. Then the boundary conditions are given by L, B, and α.

The free energy is conventionally given as the negative of the on-shell action. This is, up to a positive constant, simply the effective action (3.41)

$$F(r_0) = \int_{r_0}^{\infty} dr \left\{ \sqrt{(r^4 + B^2)\left(1 + r^4 h \dot{z}^2\right)} + \alpha r^4 h \dot{z} \right\} , \tag{3.53}$$

This is the free energy of a single leg of the brane/anti-brane system. In the case of $r_0 = 1$, (3.53) is the energy of one entire worldvolume, from horizon to boundary. For $r_0 > 1$, it computes the free energy of one half of the joined brane/anti-brane system. In all cases since the other branch is obtained by symmetry, the true free energy is just twice (3.53). Substituting in the general solution (3.45) we get

$$\begin{aligned} F(r_0) &= \int_{r_0}^{\infty} dr \sqrt{\frac{r^4 + B^2}{1 - \frac{r^4}{r^4+B^2} h g^2}} \left(1 + \frac{r^4}{r^4 + B^2} \alpha h g\right) , \\ &= \int_0^{\frac{1}{r_0}} \frac{du}{u^4} \frac{1 + B^2 u^4 + \alpha h \left(\frac{1}{u}\right) g \left(\frac{1}{u}\right)}{\sqrt{1 + B^2 u^4 - h \left(\frac{1}{u}\right) g \left(\frac{1}{u}\right)^2}} , \end{aligned} \tag{3.54}$$

where we changed integration variables to $u = r^{-1}$ in the second line.

[22] Due to translation invariance in the z direction.

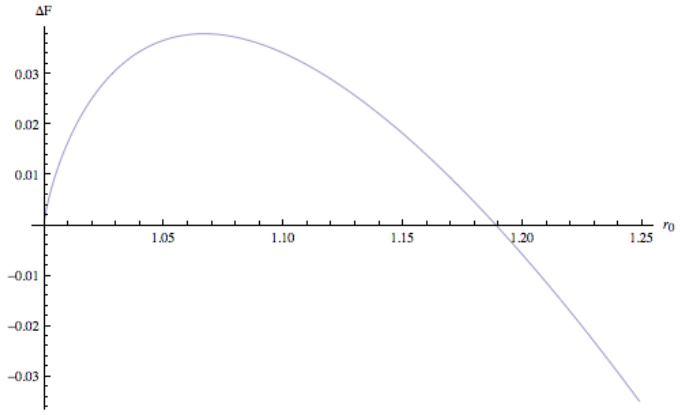

Figure 3.9: The renormalized free energy as a function of r_0 for $B = 0$ and $\alpha = -\frac{1}{3}$.

Note that (3.54) is generically infinite. Indeed, placing a cut-off at the lower end of the u integral yields

$$F(r_0) = \int_\epsilon \frac{du}{u^4} \frac{1 + B^2u^4 + \alpha h\left(\frac{1}{u}\right) g\left(\frac{1}{u}\right)}{\sqrt{1 + B^2u^4 - h\left(\frac{1}{u}\right) g\left(\frac{1}{u}\right)^2}} \sim \frac{\sqrt{1-\alpha^2}}{3\epsilon^3} + \text{finite} \ . \tag{3.55}$$

Since this divergence is independent of r_0, the difference in free energy between any two embeddings will be finite and numerically computable. We will thus compute a renormalized free energy

$$\Delta F(r_0) \equiv F(r_0) - F_0 \ , \tag{3.56}$$

with F_0 the divergent free energy of the black hole embedding with $r_0 = 1$,

$$F_0 = \int_0^1 \frac{du}{u^4} \sqrt{1 + B^2u^4 - \alpha^2 h\left(\frac{1}{u}\right)} \ . \tag{3.57}$$

When $\Delta F < 0$, the joined solution has less energy than the black hole embeddings and so it dominates, indicating flavor symmetry breaking in the bi-layer description.

In Fig. 3.9 we plot the renormalized free energy as a function of r_0 for the case $B = 0$ and $\alpha = -\frac{1}{3}$. This is the same set of solutions whose asymptotic separation versus r_0 is plotted in Fig. 3.7. The only joined solutions with negative free energy are those with $r_0 \gtrsim 1.19$ which corresponds to $L \lesssim 1.2$. For any larger L, the black hole embedding is less energetic or the joined embedding does not exist.

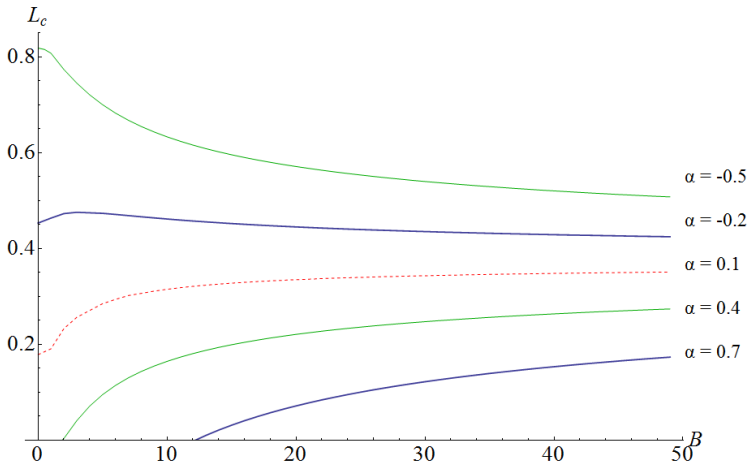

Figure 3.10: Phase diagrams for the defect system. Above any fixed α curve, the dominant solution is given by the two disconnected brane worldvolumes, *i.e.* the symmetric phase. The joined solutions, the broken symmetry phase, dominates below the curve.

3.5 Phase diagram and discussion

In Fig. 3.10, we plot the phase diagram of the brane/anti-brane system in the L-B plane. Each curve is at fixed α, above the curve being the flavor symmetric phase where the stacks do not join while below the curve the symmetry is broken to the diagonal subgroup by brane recombination. We can see that for α negative, the stacks always join at small enough L. This is quite intuitive since the background F_5 assists the native attraction of the brane and anti-brane so there is no effect to prevent their joining. On the other hand, we see that for large enough positive α, the stacks do not join at small L unless there is also a strong enough external magnetic field. Intuitively, the force from the background F_5 is strong enough to overcome the brane/anti-brane attraction even at arbitrarily small separation.

In these types of studies, there is a general expectation of *magnetic catalysis*, that an external magnetic field favors the breaking of flavor symmetry. This effect has been seen both in perturbative and large-N calculations in quantum field theory [48]. It is also known to be a common feature in holographic scenarios of various dimensional brane intersections [29, 53, 76]. However, in [51] the Sakai-Sugimoto model was studied at finite chemical potential and magnetic field and an inverse magnetic catalysis was found in a certain region of the phase diagram, *i.e.* at zero temperature and fixed finite

chemical potential, an increase in magnetic field can prompt a transition to a symmetric state.

We see in Fig. 3.10 both catalysis and inverse catalysis, depending on the value of α and the region of the curve in question. One can see that all positive α embeddings exhibit catalysis, *i.e.* all of the chubby solutions. In these cases, it appears that external magnetic field always enhances the attraction of the brane/anti-brane pair. However, for $0 \gtrsim \alpha \gtrsim -.2$ the curves are similar to positive α so the sign of the induced $D3$ charge is not sufficient to determine the behavior with respect to magnetic field. For $\alpha \approx -.2$, we see a maximum, indicating a region of inverse catalysis for small B. This region expands as α is decreased until there is inverse catalysis for all B.

It is not clear from the point of view of the field theory what dictates whether the system exhibits catalysis or inverse catalysis. We will refrain from speculating on the exact mechanism here and leave this question to future work.

Chapter 4

D7-anti-D7 Double Monolayer : Holographic Dynamical Symmetry Breaking

Now they have beaten me, he thought.
I am too old to club sharks to death.
But I will try it as long as I have the oars
and the short club and the tiller

- The Old Man and the Sea by Ernest Hemingway

Note that the title of the original paper was *Bilayer* instead of *Double Monolayers*. Double monolyer should be distinguished from bilayer by whether allows hop or not between each monolayers.

In weakly coupled quantum field theory, spontaneous symmetry breaking is a familiar paradigm. It is based on formation of a condensate, usually an order parameter obtaining a nonzero expectation value and the resulting features of the spectrum such as goldstone bosons and a Higgs field. String theory holography has given an alternative picture of dynamical symmetry breaking in terms of geometry. Particularly with probe branes, the symmetry breaking corresponds to the branes favoring a less symmetric worldvolume geometry over a more symmetric one. This is seen in the Sakai-Sugimoto model of holographic quantum chromodynamics [27]. There, chiral symmetry breaking corresponds to the fact that a $D8$-$\overline{D8}$ brane pair prefer to fuse into a cigar-like geometry, rather than remaining in a more symmetric independent configuration. In this chapter, we shall study a model which is close in spirit to the Sakai-Sugimoto model, the $D7$-$\overline{D7}$ system which has a 2+1-dimensional overlap with a stack of $D3$-branes. It can be considered a toy model of chiral symmetry breaking in strongly coupled

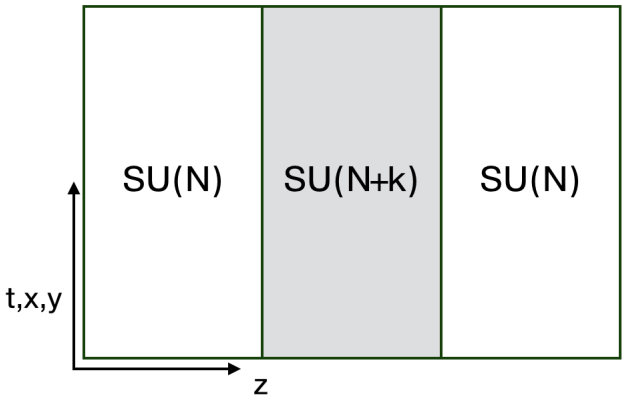

Figure 4.1: Two parallel 2-dimensional spaces, depicted by the vertical dark lines, are inhabited by fundamental representation fermions which interact via fields of $\mathcal{N} = 4$ supersymmetric Yang-Mills theory in the bulk. The Yang-Mills theory in the region between the layers has a different rank gauge group than that in the regions external to the double monolayer.

2+1-dimensional quantum field theories containing fermions and it is explicitly solvable. The symmetry breaking pattern is $U(N) \times U(N) \to U(N)$ and, at least in principle, it is possible to gauge various subgroups of the global symmetry group and to study the Higgs mechanism at strong coupling. In the following we shall concentrate on the case $U(1) \times U(1) \to U(1)$ which displays the essential features of the mechanism.

Before analyzing the $D7$-$\overline{D7}$ system, let us discuss its quantum field theory dual, the double monolayer system depicted in figure 4.1. Massless relativistic 2+1-dimensional fermions are confined to each of two parallel but spatially separated layers. They are two-component spinor representations of the SO(2,1) Lorentz group with a U(1) global symmetry for the fermions inhabiting each layer. The overall global symmetry is thus $U(1) \times U(1)$. The 3+1-dimensional bulk contains $\mathcal{N} = 4$ supersymmetric Yang-Mills theory. The fermions transform in the fundamental representation of the gauge groups of the Yang-Mills theories. As shown in figure 1, the rank of the Yang-Mills gauge groups differ in the interior and exterior of the double monolayer by an integer k which arises from the worldvolume flux in the $D7$-$\overline{D7}$ system. The D-brane system which we shall discuss studies this theory in the strong coupling planar limit where, first, the Yang-Mills coupling $g_{\rm YM}$ is taken to zero and N to infinity while holding $\lambda \equiv g^2_{YM} N$ fixed and,

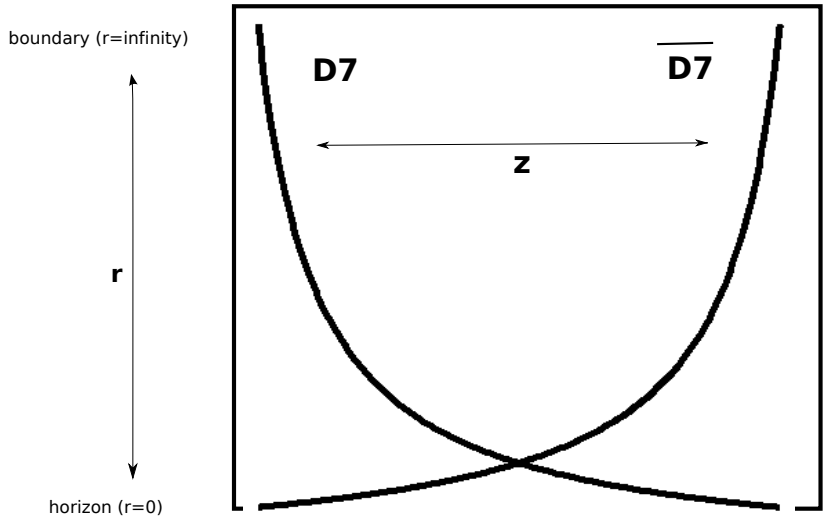

Figure 4.2: The z-position of the D7-branes depends on AdS-radius and with the appropriate orientation the branes would always intersect.

subsequently, a strong coupling limit of large λ is taken. The field theory mechanism for the symmetry breaking which we shall analyze is an exciton condensate which binds a fermion on one layer to an anti-fermion on the other layer and breaks the $U(1) \times U(1)$ symmetry to a diagonal $U(1)$.

There has been significant recent interest in graphene double monolayer systems where formation of an exciton driven dynamical symmetry breaking of the kind that we are discussing has been conjectured [12]. The geometry is similar, with the layers in figure 4.1 replaced by graphene sheets and the space in between with a dielectric insulator. In spite of some differences: graphene is a relativistic electron gas with a strong non-relativistic Coulomb interaction, whereas what we describe is an entirely relativistic non-Abelian gauge theory, there are also similarities and perhaps lessons to be learned. For example, we find that the exciton condensate forms in the strong coupling limit even in the absence of fermion density whereas the weak coupling computations that analyze graphene need nonzero electron and hole densities in the sheets to create an instability. We also find "coulomb drag", where the existence of an electric current in one layer induces a current in the other[47]. In the holographic model, the drag would vanish in the absence of a condensate, whereas it is large when a condensate is present. The correlator between the electric current in the two sheets (from (4.10) below)

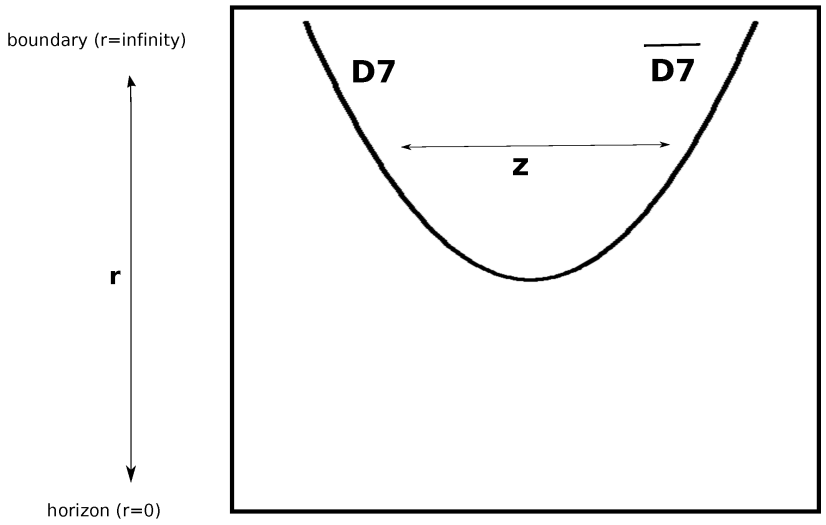

Figure 4.3: Joined configuration.

is

$$< j_a(k)\tilde{j}_b(\ell) >= \frac{4\lambda(1+f^2)|k|}{(2\pi)^2 \sinh 2|k|\rho_m}\left(\delta_{ab} - \frac{k_a k_b}{k^2}\right)\delta(k+\ell) \tag{4.1}$$

where $|k| = \sqrt{\vec{k}^2 - \omega^2/v_F^2}$, there is a factor of 4 from the degeneracy of graphene, v_F is the electron fermi velocity and λ and f^2 are parameters and ρ_m, given in (A.5), is proportional to the interlayer spacing. Aside from the superfluid pole at $k^2 = 0$, this correlator has an infinite series of poles at $k^2 = (n\pi/\rho_m)^2$, $n = 1, 2, ...$ due to vector mesons. Parameters partially cancel in the ratio of the current-current correlator in (4.1) to the single layer correlator, $< j\tilde{j} > / < jj >= \text{csch}2|k|\rho_m$.

Symmetry breaking in the $D7$-$\overline{D7}$ system has already been studied in reference [54]. The mechanism is a joining of the $D7$ and $\overline{D7}$ worldvolumes as depicted in figure 4.3. The $D7$ and $\overline{D7}$ are probe branes [87] in the $AdS_5 \times S^5$ geometry which is the holographic dual of 3+1-dimensional $\mathcal{N} = 4$ supersymmetric Yang-Mills theory. A single probe D7-brane is stable when it has magnetic flux added to its worldvolume [37]. Its most symmetric configuration is dual to a defect conformal field theory [37][39] where the flux (f in the following) is an important parameter which determines, for example, the conformal dimension of the fermion mass operator. The $D7$-$\overline{D7}$ pair would tend to annihilate and are prevented from doing so by

boundary conditions that contain a pressure (the parameter P in the following) which holds them apart. The problem to be solved is that of finding the configuration of the $D7$ and $\bar{D}7$ in the $AdS_5 \times S^5$ background, subject to the appropriate boundary conditions. We shall impose the parity and time-reversal invariant boundary conditions that were discussed in reference [39]. We differ from reference [54] in that we use the zero temperature limit, a simplification that allows us to obtain our main result, explicit current-current correlation functions for the theory described by the joined solution (4.11)-(4.13). The $AdS_5 \times S^5$ metric is

$$\begin{aligned} ds^2 = R^2[r^2(-dt^2 + dx^2 + dy^2 + dz^2) + \frac{dr^2}{r^2} \\ +d\psi^2 + \sin^2\psi d\Omega_2^2 + \cos^2\psi d\tilde{\Omega}_2^2] \end{aligned} \tag{4.2}$$

where $d\Omega_2^2$ and $d\tilde{\Omega}_2^2$ are metrics of unit 2-spheres and $\psi \in [0, \frac{\pi}{2}]$. The radius of curvature is $R^2 = \sqrt{4\pi g_s N}\alpha'$, where g_s is the closed string coupling constant and N the number of units of Ramond-Ramond 4-form flux of the IIB string background. The holographic dictionary sets $g_{\rm YM}^2 = 4\pi g_s$, and N becomes the rank of the Yang-Mills gauge group. The embedding of the $D7$ in this space is mostly determined by symmetry. We take the $D7$ and $\overline{D7}$ embeddings to wrap (t, x, y), S^2 and $\tilde{S}^2$ and to sit at the parity symmetric point $\psi = \frac{\pi}{4}$. To solve embedding equations, the transverse coordinate z must depend on the radius r. At the boundary of AdS_5 ($r \to \infty$), we impose the boundary condition that the $\overline{D7}$ is located at $z = -L/2$ and $D7$ at $z = L/2$. The worldvolume metric of one of the branes is then

$$\begin{aligned} d\sigma^2 = R^2[r^2(-dt^2 + dx^2 + dy^2) + \frac{dr^2}{r^2}(1 + r^4\dot{z}(r)^2) \\ +\frac{1}{2}d\Omega_2^2 + \frac{1}{2}\tilde{d\Omega}_2^2] \end{aligned} \tag{4.3}$$

where $\dot{z} = dz/dr$. The field strength of the world-volume gauge fields are

$$F = \frac{R^2}{2\pi\alpha'}\frac{f}{2}\Omega_2 + \frac{R^2}{2\pi\alpha'}\frac{f}{2}\tilde{\Omega}_2 \tag{4.4}$$

where Ω_2 and $\tilde{\Omega}_2$ are the volume forms of the unit 2-spheres. The flux forms two Dirac monopole bundles with monopole number $n_D = \sqrt{\lambda}f^2$. Stability and other properties of the theory [37][39] require that $23/50 < f^2 < 1$, otherwise it is a tunable parameter. The embedding is determined

by extremizing the Dirac-Born-Infeld plus Wess-Zumino actions,

$$S = -\frac{T_7 N}{g_s}\int d^8\sigma \left[\sqrt{-\det(g(\sigma)+2\pi\alpha' F)} \mp \frac{(2\pi\alpha')^2}{2} F\wedge F\wedge C_4\right] \tag{4.5}$$

$T_7 = 1/(2\pi)^7\alpha'^4$ is the brane tension, C_4 is the Ramond-Ramond 4-form of the IIB string background and the $\mp$ refer to the $D7$ and $\overline{D7}$, respectively. With our Ansatz, this reduces to a variational problem with Lagrangian

$$\mathcal{L} = (1+f^2)r^2\sqrt{1+r^4\dot{z}(r)^2} \mp f^2 r^4 \dot{z}(r) \tag{4.6}$$

$z(r)$ is a cyclic variable whose equation of motion is solved by $z_\pm(r) = \pm\frac{L}{2} \mp \int_r^\infty dr \dot{z}_+(r)$ is the position of the brane to the right (upper sign) or left (lower sign) of $z=0$ and $\dot{z}_\pm(r) = \pm\frac{f^2r^4+P}{r^2\sqrt{(r^4-P)((1+2f^2)r^4+P)}}$. P is an integration constant proportional to the pressure needed to hold the branes with their asymptotic separation L. When they are not joined, they do not interact, at least in this classical limit, and P must be zero. Then $z_\pm(r) = \pm\frac{L}{2} \mp \frac{f^2}{\sqrt{1+2f^2}\ r}$ as depicted in figure 4.2. When they are joined, as depicted in figure 4.3, P must be nonzero and they are joined at a minimum radius $r_0 = P^{\frac{1}{4}}$ and L and P are related by $LP^{\frac{1}{4}} = 2\int_1^\infty dr \frac{f^2r^4+1}{r^2\sqrt{(r^4-1)((1+2f^2)r^4+1)}}$.

The joined solution will always be the lower energy solution when the branes are oriented as in figures 4.2 and 4.3. They are also stable for any value of L when the brane and antibrane are interchanged, the "chubby solutions" discussed in reference [54], only when $23/50 \le f^2 \lesssim .56$. When $f^2 > .56$ the chubby solutions are unstable for any L. (As noted in reference [54], there can be a much richer phase structure when temperature, density or external magnetic fields are introduced.) For the chubby solution, the gauge group ranks N and $N+k$ in figure 4.1 trade positions.

A simple diagnostic of the properties of the fermion system in the strongly coupled quantum field theory which is dual to the joined branes is the current-current correlation function. It is obtained by solving the classical dynamics of the gauge field on the world-volume of the branes with the Dirichlet boundary condition. The quadratic form in boundary data in the on-shell action yields the current-current correlator. Here, the brane geometry is simple enough that, to quadratic order, AdS components of the vector field decouple from the fluctuations of the worldvolume geometry, as well as from those components on $S^2, \tilde{S}^2$. To find them, we simply need to solve

Maxwell's equations on the worldvolume,

$$\partial_A \left[\sqrt{g} g^{BC} g^{DE} (\partial_C A_E - \partial_E A_C)\right] = 0$$

where the worldvolume metric is given in equation (4.3) above and the gauge fields have indices $A, B... = (t, x, y, r)$. In the $A_r = 0$ gauge,

$$\partial_r(\partial_a A_a) = 0 \quad , \quad \partial_\rho^2 A_a + \partial_b(\partial_b A_a - \partial_a A_b) = 0 \tag{4.7}$$

where indices $a, b, ... = (t, x, y)$ and we have redefined the radial coordinate as $\rho = \int_r^\infty \frac{dr}{r^2}\sqrt{1 + r^4 \dot{z}^2}$. In the simpler case of a single D7-brane, say the brane which originates on the right in figure 4.2, whose geometry is AdS_4, these equations are solved by [39]

$$A_a(\rho, k) = A_a(k) \cosh |k|\rho + \frac{1}{|k|} A'_a(k) \sinh |k|\rho$$

where $A_a(k, \rho) = \int d^3x e^{ikx} A_a(x, \rho)$, $k_a A_a(k) = 0 = k_a A'(k)$ and $|k| = \sqrt{\vec{k}^2 - k_0^2}$. Regularity at the Poincare horizon ($\rho \to \infty$) requires $A'_a(k) = -|k| A_a(k)$. Moreover, with the on-shell action,

$$S = -\frac{N(f^2+1)}{4\pi^2} \int d^3k |k| A_a(-k) \left(\delta_{ab} - k_a k_b / k^2\right) A_b(k) + \dots$$

e^{-S} is a generating function for current-current correlators in the dual conformal field theory where the U(1) symmetry is global, ($j_a(k) = g_{\rm YM} \delta / \delta A_a(-k)$)

$$< j_a(k) j_b(\ell) >= \frac{\lambda(f^2+1)}{2\pi^2} |k| \left(\delta_{ab} - k_a k_b / k^2\right) \delta(k + \ell) \tag{4.8}$$

Alternatively, if instead of the Dirichlet boundary conditions used above, we impose the Neuman boundary condition that $\partial_\rho A_a(k, \rho)$ approaches $A'_a(k)$ as $\rho \to 0$, we can write the on-shell action as a functional of $A'(k)$ and it generates correlators of the gauge field in a different conformal field theory where the U(1) symmetry is gauged and the gauge field is dynamical. It yields the Landau gauge 2-point function of the photon field in that theory [56] ($a_a(k) = \delta / \delta A'(-k)$),

$$< a_a(k) a_b(\ell) >= \frac{N(f^2+1)}{2\pi^2} \frac{1}{|k|} \left(\delta_{ab} - k_a k_b / k^2\right) \delta(k + \ell)$$

The momentum dependence of these correlation functions is consistent with conformal symmetry.

To analyze the joined configuration, we note that in that case ρ reaches a maximum

$$\rho_m = \frac{L}{2}\frac{\int_0^1 \frac{dx(1+f^2)}{\sqrt{(1-x^4)((1+2f^2)-x^4)}}}{\int_0^1 \frac{dx(f^2+x^4)}{\sqrt{(1-x^4)((1+2f^2)-x^4)}}} \tag{4.9}$$

We use a variable $s = \rho$ for the left branch and $s = 2\rho_m - \rho$ for the right branch of figure 4.3. With the Dirichlet boundary conditions $A_a(s = 0, k) = A_a(k)$ and $A_a(s = 2\rho_m, k) = \tilde{A}_a(k)$ the on-shell action is

$$\begin{aligned}\tilde{S} = -\frac{N(f^2+1)}{4\pi^2}\int d^3k \Big[&(|A_a(k)|^2 + |\tilde{A}_a(k)|^2)\coth 2|k|\rho_m \\ &-2A_a(-k)A_a(k)\mathrm{csch}2|k|\rho_m] + \dots\end{aligned} \tag{4.10}$$

The current-current correlation functions can are diagonalized by $j_+ \equiv j+\tilde{j}$, $j_- \equiv j - \tilde{j}$, so that

$$< j_{a+}j_{b-} > = 0 \tag{4.11}$$

$$< j_{a+}j_{b+} > = \frac{\lambda(f^2+1)}{2\pi^2}k\tanh k\rho_m\left(\delta_{ab} - \frac{k_a k_b}{k^2}\right) \tag{4.12}$$

$$< j_{a-}j_{b-} > = \frac{\lambda(f^2+1)}{2\pi^2}k\coth k\rho_m\left(\delta_{ab} - \frac{k_a k_b}{k^2}\right) \tag{4.13}$$

At large Euclidean momenta, (4.12) and (4.13) revert to the conformal field theory correlators in (4.8). At time-like momenta the correlator $< j_{a-}j_{b-} >$ has a pole at $k^2 = 0$ which is the signature of dynamical breaking of a diagonal $U(1)$ subgroup of the $U(1) \times U(1)$ symmetry and gives rise to superfluid linear response. On the other hand, the correlator $< j_{a+}j_{b+} > \sim k^2$ for small k, which indicates that the system is an insulator in the channel which couples to the other diagonal U(1) subgroup with current j_{a+}. In addition, both correlators have an interesting analytic structure. They have no cut singularities. $< j_{a+}j_{b+} >$ has poles at the (Minkowski signature) energies

$$k_0^2 = k_1^2 + k_2^2 + \left(\frac{\pi(2n+1)}{2\rho_m}\right)^2 \quad , \qquad n = 0, 1, \dots \tag{4.14}$$

and $< j_{a-}j_{b-} >$ has poles at

$$k_0^2 = k_1^2 + k_2^2 + \left(\frac{\pi n}{\rho_m}\right)^2 \quad , \qquad n = 0, 1, \dots \tag{4.15}$$

indicating two infinite towers of massive spin-one particles. These would be narrow bound state resonances with decay widths that vanish as $N \to \infty$, as one expects in the large-N limit that we are studying here [57]. The current operators create these single-particle states from the vacuum. Their creation of multi-particle states, which would normally result in cut singularities, is suppressed in the large N planar limit. The resonances are simply the tower of vector mesons whose masses (4.14) and (4.15) occur at eigenvalues of $-\partial_s^2$ with Dirichlet boundary conditions on the interval $s \in [0, 2\rho_m]$. The fact that currents create either even or odd harmonics is due to $L \to -L$ reflection symmetry.

In the above, we used Dirichlet boundary conditions for the worldvolume gauge field. It is possible, alternatively, to select Neumann boundary conditions by choosing $\partial_s A_a$ rather than A_a on the asymptotic boundary. The result is dual to a field theory where the U(1) symmetries are gauged and the on-shell action generates photon correlation functions [56]. Most relevant are mixed Neuman and Dirichlet boundary conditions. For example, in graphene, a diagonal electromagnetic U(1) is gauged whereas the orthogonal U(1) is a global symmetry. This is obtained by applying the Dirichlet condition to $A(s = 0, k) - A(s = 2\rho_m, k)$ and the Neuman condition to $\partial_s A(s = 0, k) - \partial_s A(s = 2\rho_m, k)$. In this case, the correlation functions are

$$< j_a a_b > = 0 \tag{4.16}$$

$$< j_a j_b > = \frac{\lambda(f^2+1)}{4\pi^2} k \coth k\rho_m \left(\delta_{ab} - \frac{k_a k_b}{k^2}\right) \tag{4.17}$$

$$< a_a a_b > = \frac{N(f^2+1)}{4\pi^2} \frac{1}{k} \coth k\rho_m \left(\delta_{ab} - \frac{k_a k_b}{k^2}\right) \tag{4.18}$$

The global U(1) symmetry is spontaneously broken and its current j_a has a pole in its correlation function. The unbroken gauged U(1) has a massless pole corresponding to the photon. In addition, the two towers of intermediate states have the same masses with values (4.15). There is a family of more general mixed boundary conditions which are interesting and which will be examined in detail elsewhere.

Chapter 5

Holographic D3-probe-D5 Model of a Double Layer Dirac Semimetals

I have ugly lips.
It was all my fault.
I sobbed standing next to the coat left behind.
None of the laughs could raise my heavy heart.
I want to forget the tavern.
There is none like you in this world.
I lost my love in that narrow place.

- In Front of the House by Ki, Hyung-do

5.1 Introduction and Summary

The possibility of Coulomb drag-mediated exciton condensation in double monolayer graphene or other multi-layer heterostructures has recently received considerable attention [63]-[106]. The term "double monolayer graphene" refers to two monolayers of graphene[23], each of which would be a Dirac semi-metal in isolation, and which are brought into close proximity but are still separated by an insulator so that direct transfer of electric charge carriers between the layers is negligible. The system then has two conserved charges, the electric charge in each layer. The Coulomb interaction between an electron in one layer and a hole in the other layer is attractive. A bound state of an electron and a hole that forms due to this attraction is called an exciton. Excitons are bosons and, at low temperatures they can condense to a form a charge-neutral superfluid. We will call this an inter-layer exciton

[23] It should be distinguished from bilayer graphene where electrons are allowed to hop between the layers.

condensate. Electrons and holes in the same monolayer can also form an exciton bound state, which we will call this an intra-layer exciton and its Bose condensate an intra-layer condensate.

Inter-layer excitons have been observed in some cold atom analogs of double monolayers [107]-[109] and as a transient phenomenon in Gallium Arsenide/ Aluminium-Gallium-Arsenide double quantum wells, albeit only at low temperatures and in the presence of magnetic fields[109]-[111]. Their study is clearly of interest for understanding fundamental issues with quantum coherence over mesoscopic distance scales and dynamical symmetry breaking. Recent interest in this possibility in graphene double layers has been inspired by some theoretical modelling which seemed to indicate that the exciton condensate could occur at room temperature [66]. A room temperature superfluid would have interesting applications in electronic devices where proposals include ultra-fast switches and dispersionless field-effect transistors [112]-[117]. This has motivated some recent experimental studies of double monolayers of graphene separated by ultra-thin insulators, down to the nanometer scale [118][119]. These experiments have revealed interesting features of the phenomenon of Coulomb drag. However, to this date, coherence between monolayers has yet to be observed in a stationary state of a double monolayer.

One impediment to a truly quantitative analysis of inter-layer coherence is the fact that the Coulomb interaction at sub-nanoscale distances is strong and perturbation theory must be re-summed in an ad hoc way to take screening into account [105][120]. In fact, inter-layer coherence will likely always require strong interactions. The purpose of this chapter is to point out the existence of an inherently nonperturbative model of very strongly coupled multi-monolayer systems. This model is a defect quantum field theory which is the holographic AdS/CFT dual of a D3-probe-D5 brane system. It is simple to analyze and exactly solvable in the limit where the quantum field theory interactions are strong. External magnetic field and charge density can be incorporated into the solution and it exhibits a rich phase diagram where it has phases with inter-layer exciton condensates.

It might be expected that, with a sufficiently strong attractive electron-hole interaction, an inter-layer condensate would always form. One of the lessons of our work will be that this is not necessarily so. In fact, it was already suggested in reference [94] that, when both monolayers are charge neutral, and in a constant external magnetic field, there can be an inter-layer or an intra-layer condensate but there were no phases where the two kinds of condensate both occur at the same time. What is more, the inter-layer condensate only appears for small separations of the monolayers, up to a

critical separation. As the spacing between the monolayers is increased to the critical distance, there is a phase transition where an intra-layer condensate takes over. Intra-layer condensates in a strong magnetic field are already well known to occur in monolayer graphene in the integer quantum Hall regime [124]-[128]. They are thought to be a manifestation of "quantum Hall ferromagnetism" [129]-[134] or the "magnetic catalysis of chiral symmetry breaking" [71]-[83] which involve symmetry breaking with an intra-layer exciton condensate. It has been argued that the latter phenomenon, intra-layer exciton condensation, in a single monolayer is also reflected in symmetry breaking behaviour of the D3-probe-D5 brane system [84]-[85].

Another striking conclusion that we will come to is that, even in the strong coupling limit, there is no inter-layer exciton condensate unless the charge densities of the monolayers are fine-tuned in such a way that, at weak coupling, the electron Fermi surface on one monolayer and the hole Fermi surface in the other monolayer are perfectly nested, that is, they have identical Fermi energies. In this particle-hole symmetric theory, this means that the charge densities on the monolayers are of equal magnitude and opposite sign. It is surprising that this need for charge balance is even sharper in the strong coupling limit than what is seen at weak coupling, where the infrared singularity from nesting does provide the instability needed for exciton condensation, but where, also, there is a narrow window near perfect nesting where condensation is still possible [65]. In our model, at strong coupling, there is inter-layer condensate only in the perfectly nested (or charge balanced) case. This need for such fine tuning of charge densities could help to explain why such a condensate is hard to find in experiments where charged impurities would disturb the charge balance.

When the charge densities of the monolayers are non-zero, and when they are balanced, there can be an inter-layer condensate at any separation of the monolayers. The phase diagram which we shall find for the D3-probe-D5 brane system in a magnetic field and with nonzero, balanced charge densities is depicted in figure 5.1. The blue region has an inter-layer condensate and no intra-layer condensate. The green region has both inter-layer and intra-layer condensates. The red region has only an intra-layer condensate. From the vertical axis in figure 5.1 we see that, in the charge neutral case. the inter-layer condensate exists only for separation less than a critical one.

It has recently been suggested [101] that there is another possible behaviour which can lead to inter-layer condensates when the charges of the monolayers are not balanced. This can occur when the material of the monolayers contain more than one species of fermions. For example, graphene has four species and emergent SU(4) symmetry [98]. In that case, the most sym-

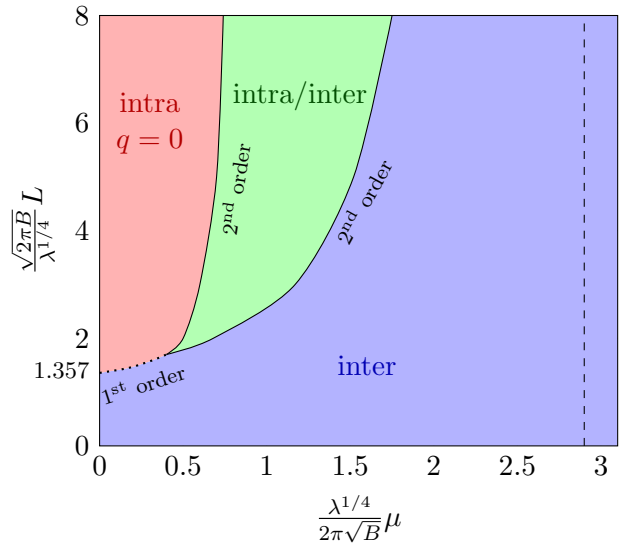

Figure 5.1: Phase diagram of the D3-probe-D5 brane system with balanced charge densities. Layer separation is plotted on the vertical axis and the chemical potential μ for electrons in one monolayer and holes in the other monolayer is plotted on the horizontal axis. The units employed set the length scale $\sqrt{\frac{\sqrt{\lambda}}{2\pi B}}$ equal to one. The blue region is a phase with an inter-layer condensate and with no intra-layer condensate. The green region is a phase with both an inter-layer and an intra-layer condensate. The red region has only an intra-layer condensate. In that region, the chemical potential is too small to induce a density of the massive electrons (μ is in the charge gap) and the charge densities on both of the monolayers vanishes. The electrons and holes are massive in that phase due to the intra-layer exciton condensate. The dotted line, separating a pure inter-layer from a pure intra-layer condensate, is a line of first order phase transitions. The solid lines, on the other hand, indicate second order transitions.

metric state of a monolayer has the charge of that monolayer shared equally by each of the four species of electrons. Other less symmetric states are possible.

Consider, for example, the double monolayer with one monolayer having electron charge density Q and the other monolayer having hole density $\bar{Q}$ (or electron charge density $-\bar{Q}$), with $Q > \bar{Q} > 0$. On the hole-charged monolayer, some subset, which must be one, two or three of the fermion species could take up all of the hole charge density, $\bar{Q}$. Then, in the electron monolayer, the same number, one, two or three species of electrons would

take up electron charge density $\bar{Q}$ and the remainder of the species will take electron charge density $Q-\bar{Q}$. The (one, two or three) species with matched charge densities will then spawn an inter-layer exciton condensate. The remaining species on the hole monolayer is charge neutral. A charge-neutral monolayer will have an intra-layer condensate. The remaining species in the electron monolayer, with charge density $Q-\bar{Q}$, would also have an intra-layer condensate and it would not have a charge gap (all of the fermions are massive, but this species has a finite density and it does not have a charge gap). A simple signature of this state would be that one of the monolayers is charge gapped, whereas the other one is not. The implication is that perfect fine-tuning of Fermi surfaces is not absolutely necessary for inter-layer condensation. We will show that, in a few examples, this type of spontaneous nesting can occur. However, some important questions, such as how unbalanced the charge densities can be so that there is still a condensate are left for future work.

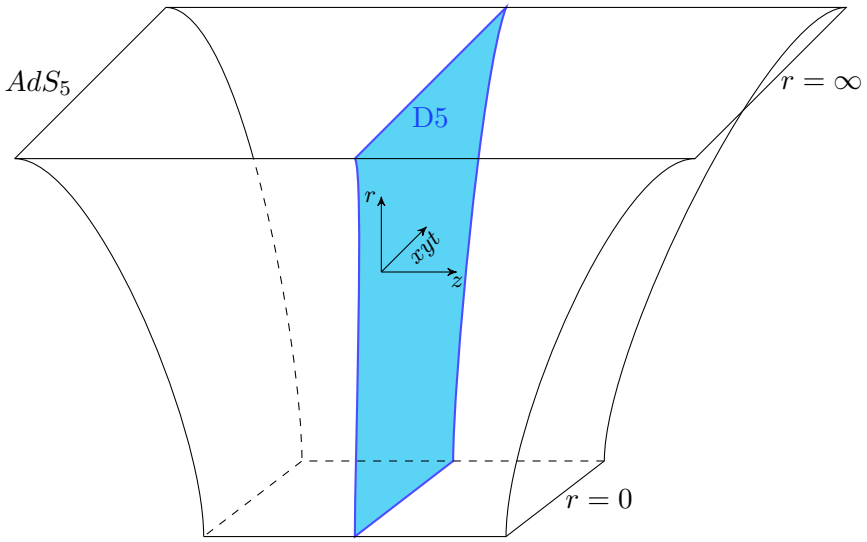

Figure 5.2: A D5 brane is embedded in $AdS_5 \times S^5$ where the metric of AdS_5 is $ds^2 = \sqrt{\lambda}\alpha'[\frac{dr^2}{r^2} + r^2(dx^2+dy^2+dz^2-dt^2)]$ and the D5 brane world-volume is an AdS_4 subspace which fills r, x, y, t and sits at a point in z. The AdS_5 boundary is located at $r=\infty$ and the Poincarè horizon at $r=0$. The D5 brane also wraps a maximal, contractible S^2 subspace of S^5 of the $AdS_5 \times S^5$ background. The internal bosonic symmetries of the configuration are $SO(3)$ of the wrapped S^2 and a further $SO(3)$ symmetry of the position of the maximal S^2 in S^5.

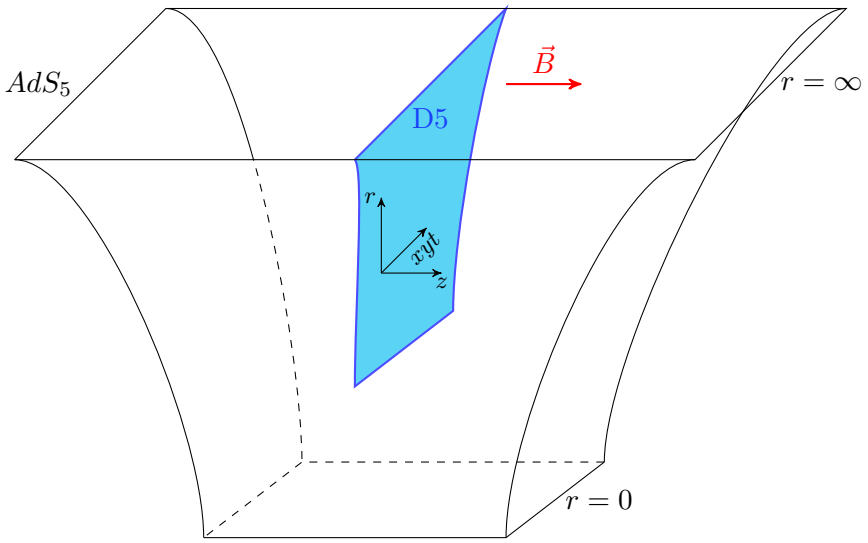

Figure 5.3: When the D5 brane is exposed to a magnetic field, it pinches off before it reaches the Poincarè horizon. It does so for any value of the magnetic field, with the radius at which it pinches off proportional to $\sqrt{\frac{2\pi B}{\sqrt{\lambda}}}$. In this configuration, the embedding of the $S^2 \subset S^5$ depends on the AdS_5 radius. It is still the maximal one which can be embedded in S^5 at the boundary, but it shrinks and collapses to a point at the radius where the D5 brane pinches off.

We will model a double monolayer system with a relativistic defect quantum field theory consisting of two parallel, infinite, planar 2+1-dimensional defects embedded in 3+1-dimensional Minkowski space. The defects are separated by a length, L. Some U(1) charged degrees of freedom inhabit the defects and play the role of the two dimensional relativistic electron gases. We can consider states with charge densities on the monolayers. As well, we can expose them to a constant external magnetic field. We could also turn on a temperature and study them in a thermal state, however, we will not do so in this chapter.

The theory that we use has an AdS/CFT dual, the D3-probe-D5 brane system where the D5 and anti-D5 branes are probes embedded in the $AdS_5 \times S^5$ background of the type IIB superstring theory. The $AdS_5 \times S^5$ is sourced by N D3 branes and it is tractable in the large N limit where we simultaneously scale the string theory coupling constant g_s to zero so that $\lambda \equiv g_s N/4\pi = g_{YM}^2 N$ is held constant. Here, $g_{\rm YM}$ is the coupling constant of the gauge fields in the defect quantum field theory. The D5 and anti-

D5 branes are semi-classical when the quantum field theory on the double monolayer is strongly coupled, that is, where λ is large. It is solved by embedding a D5 brane and an anti-D5 brane in the $AdS_5 \times S^5$ background. The boundary conditions of the embedding are such that, as they approach the boundary of AdS_5, the world volumes approach the two parallel 2+1-dimensional monolayers. The dynamical equations which we shall use are identical for the brane and the anti-brane. The reason why we use a brane-anti-brane pair is that they can partially annihilate. This annihilation will be the string theory dual of the formation of an inter-layer exciton condensate.

The phase diagram of a single D5 brane or a stack of coincident D5 branes is well known [99], with an important modification in the integer quantum Hall regime [84],[85]. In the absence of a magnetic field or charge density, a single charge neutral D5 brane takes up a supersymmetric and conformally invariant configuration. The D5 brane world-volume is itself AdS_4 and it stretches from the boundary of AdS_5 to the Poincarè horizon, as depicted in figure 5.2. It also wraps an $S^2 \subset S^5$. This is a maximally symmetric solution of the theory. It has a well-established quantum field theory dual whose Lagrangian is known explicitly [87]-[90]. The latter is a conformally symmetric phase of a defect super-conformal quantum field theory [24].

Now, let us introduce a magnetic field on the D5 brane world volume. This is dual to the 2+1-dimensional field theory in a background constant magnetic field. As soon as an external magnetic field is introduced, the single D5 brane changes its geometry drastically [76]. The brane pinches off and truncates at a finite AdS_5-radius, before it reaches the Poincarè horizon. This is called a "Minkowski embedding" and is depicted in figure 5.3. This

[24]Of course a supersymmetric conformal field theory is not a realistic model of a semimetal. Here, we will use this model with a strong magnetic field. It was observed in references [84], [85] that the supersymmetry and conformal symmetry are both broken by an external magnetic field, and that the low energy states of the weakly coupled system were states with partial fillings of the fermion zero modes which occur in the magnetic field (the charge neutral point Landau level). The dynamical problem to be solved is that of deciding which partial fillings of zero modes have the lowest energy. It is a direct analog of the same problem in graphene or other Dirac semimetals. It is in this regime that D3-D5 system exhibits quantum Hall ferromagnetism and other interesting phenomena which can argued to be a strong coupling extrapolation of universal features of a semimetal in a similar environment. It is for this reason that we will concentrate on the system with a magnetic field, with the assumption that the very low energy states of the theory are the most important for the physics of exciton formation, and that this situation persists to strong coupling. There have been a number of works which have used D branes to model double monolayers [54]-[96].

configuration has a charge gap. Charged degrees of freedom are open strings which stretch from the D5 brane to the Poincarè horizon. When, the D5 brane does not reach the Poincarè horizon, these strings have a minimum length and therefore a mass gap. This is the gravity dual of the mass generation that accompanies exciton condensation in a single monolayer.

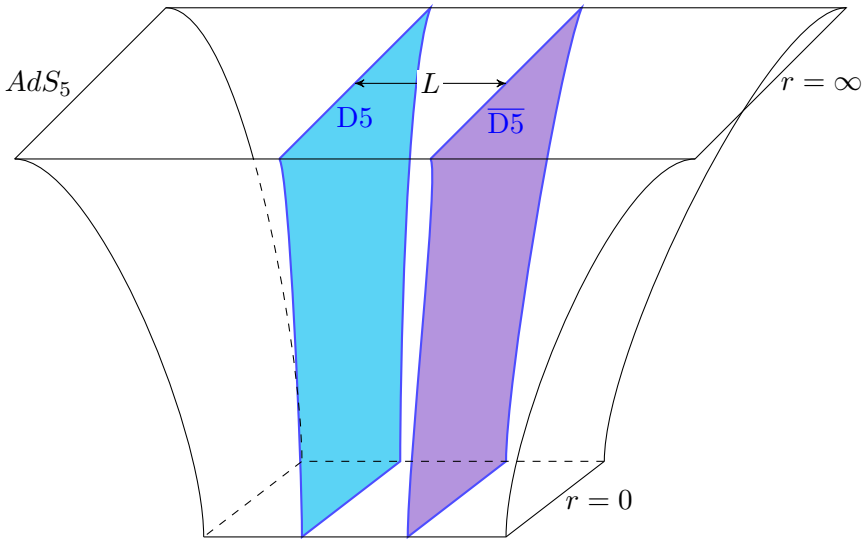

Figure 5.4: A D5 brane and an anti-D5 brane are are suspended in AdS_5 as shown. They are held a distance L apart at the AdS_5 boundary.

Let us now consider the double monolayer system. We will begin with the case where both of the monolayers are charge neutral and there is no magnetic field. We will model the strong coupled system by a pair which consists of a probe D5 brane and a probe anti-D5 brane suspended in the AdS_5 background as depicted in figure 5.4. Like a particle-hole pair, the D5 brane and the anti-D5 brane have a tendency to annihilate. However, we can impose boundary conditions which prevent their annihilation. We require that, as the D5 brane approaches the boundary of the AdS_5 space, it is parallel to the anti-D5 brane and it is separated from the anti-D5 brane by a distance L. Then, as each brane hangs down into the bulk of AdS_5, they can still lower their energy by partially annihilating as depicted in the joined configuration in figure 5.4. This joining of the brane and anti-brane is the AdS/CFT dual of inter-layer exciton condensation. The in this case, when they are both charge neutral, the branes will join for any value of the separation L. In this strongly coupled defect quantum field

theory, with vanishing magnetic field and vanishing charge density on both monolayers, the inter-layer exciton condensate exists for any value of the inter-layer distance.

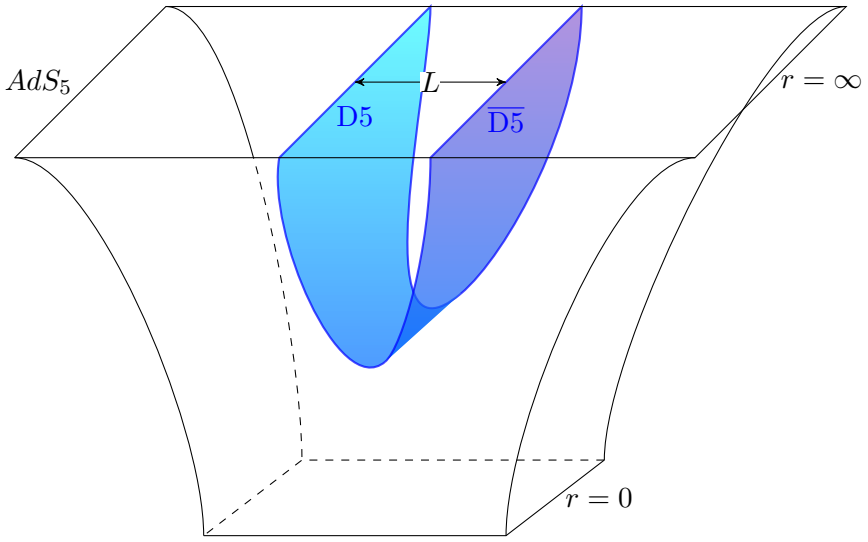

Figure 5.5: When the D5 brane and an anti-D5 brane are suspended as shown, their natural tendency is to join together. This is the configuration with the lowest energy when L is fixed. It is also the configuration which describes the quantum field theory with an inter-layer exciton condensate.

If we now turn on a magnetic field B so that the dimensionless parameter BL^2 is small, the branes join as they did in the absence of the field. However, in a stronger field, as BL^2 is increased, there is a competition between the branes joining and, alternatively, each of the branes pinching off and truncating, as they would do if there were isolated. The pinched off branes are depicted in figure 5.6. This configuration has intra-layer exciton condensates on each monolayer but no inter-layer condensate. We thus see that, in a magnetic field, the charge neutral double monolayer always has a charge gap due to exciton condensation. However, it has an inter-layer condensate only when the branes are close enough.

Now, we can also introduce a charge density on both the D5 brane and the anti-D5 brane. We shall find a profound difference between the cases where the overall density, the sum of the density on the two branes is zero and where it is nonzero. In the first case, when it is zero, joined configurations of branes exist for all separations. Within those configurations, there

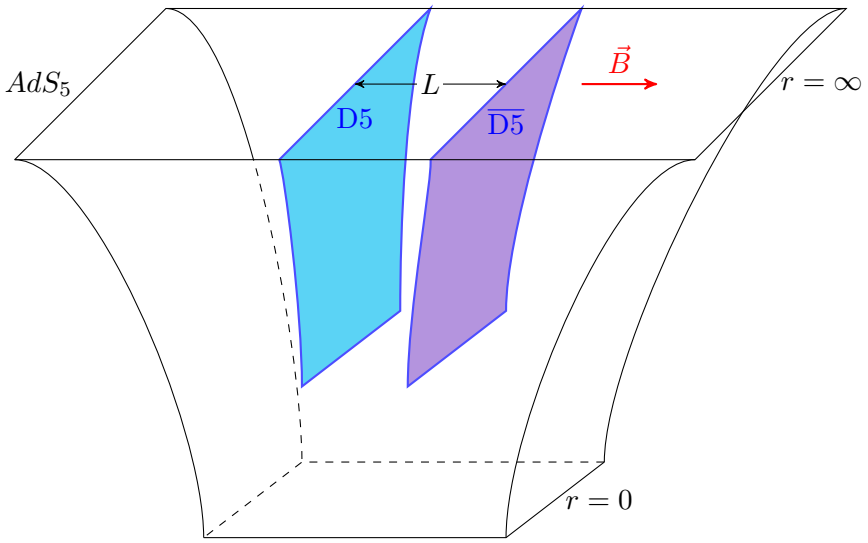

Figure 5.6: When the D5 brane and an anti-D5 brane are exposed to a magnetic field, and if the field is strong enough, they can pinch off and end before they join. This tendency to pinch off competes with their tendency to join and in a strong enough field they will take up the phase that is shown where they pinch off before they can join.

are regions where the exciton condensate is inter-layer only and a region where it is a mixture of intra-layer and inter-layer. These are seen in the phase diagram in figure 5.1. The blue region has only an inter-layer exciton condensate. The green region has a mixed inter-layer and intra-layer condensate. In the red region, the chemical potential is of too small a magnitude to induce a charge density (it is in the charge gap) and the phase is identical to the neutral one, with an intra-layer condensate and no inter-layer condensate.

In the case where the D5 and anti-D5 brane are not overall neutral, they cannot join. There is never an inter-layer condensate. They can have intra-layer condensates if their separation is small enough. However, there is another possibility, which occurs if we have stacks of multiple D5 branes. In that case, there is the possibility that the D5 branes in a stack do not share the electric charge equally. Instead some of them take on electric charges that matches the charge of the anti-D5 branes, so that some of them can join, and the others absorb the remainder of the unbalanced charge and do not join. At weak coupling this would correspond to a spontaneous nesting of the

Fermi surfaces of some species of fermions in the monolayers, with the other species taking up the difference of the charges. At weak coupling, as well as in our strong coupling limit, the question is whether the spontaneously nested system is energetically favored over one with a uniform distribution of charge. We shall find that, for the few values of the charge where we have been able to compare the energies, this is indeed the case.

In the remainder of the chapter, we will describe the quantitative analysis which leads to the above description of the behaviour of the D3-probe-D5 brane system. In section 2 we will discuss the mathematical problem of finding the geometry of probe D5 branes embedded in $AdS_5 \times S^5$ in the configurations which give us the gravity dual of the double monolayer. In section 3 we will discuss the behaviour of the double monolayer where each layer is charge neutral and they are in a magnetic field. In section 4 we will discuss the double monolayer in a magnetic field and with balanced charge densities. In section 5 we will explore the behaviour of double monolayers with un-matched charge densities. Section 6 contains some discussion of the conclusions.

5.2 Geometry of branes with magnetic field and density

We will consider a pair of probe branes, a D5 brane and an anti-D5 brane suspended in $AdS_5 \times S^5$. They are both constrained to reach the boundary of AdS_5 with their world volume geometries approaching $AdS_4 \times S^2$ where the AdS_4 is a subspace of AdS_5 with one coordinate direction suppressed and S^2 is a maximal two-sphere embedded in S^5. What is more, when they reach the boundary, we impose the boundary condition that they are separated from each other by a distance L.

We shall use coordinates where the metric of the $AdS_5 \times S^5$ background is

$$ds^2 = \frac{dr^2}{r^2} + r^2\left(-dt^2 + dx^2 + dy^2 + dz^2\right) + d\psi^2 + \sin^2\psi d^2\Omega_2 + \cos^2\psi d^2\tilde{\Omega}_2 \tag{5.1}$$

where $d^2\Omega_2 = d\theta^2 + \sin^2\theta d\phi^2$ and $d^2\tilde{\Omega}_2 = d\tilde{\theta}^2 + \sin^2\tilde{\theta} d\tilde{\phi}^2$ are the metrics of two 2-spheres, S^2 and $\tilde{S}^2$. The world volume geometry of the D5 brane is for the most part determined by symmetry. We require Lorentz and translation invariance in 2+1-dimensions. This is achieved by both the D5 and the anti-D5 brane wrapping the subspace of AdS_5 with coordinates t, x, y. We will also assume that all solutions have an SO(3) symmetry. This is achieved

when both the D5 and anti-D5 brane world volumes wrap the 2-sphere S^2 with coordinates θ, ϕ. Symmetry requires that none of the remaining variables depend on t, x, y, θ, ϕ. For the remaining internal coordinate of the D5 or anti-D5 brane, it is convenient to use the projection of the AdS_5 radius, r onto the brane world-volume. The D5 and anit- D5 branes will sit at points in the remainder of the $AdS_5 \times S^5$ directions, $z, \psi, \tilde{\theta}, \tilde{\phi}$. The points $z(r)$ and $\psi(r)$ generally depend on r and these functions become the dynamical variables of the embedding (along with world volume gauge fields which we will introduce shortly). The wrapped S^2 has an $SO(3)$ symmetry. What is more, the point $\psi = \frac{\pi}{2}$ where the wrapped sphere is maximal has an additional $SO(3)$ symmetry[25]. The geometry of the D5 brane and the anti-D5 brane are both given by the ansatz

$$ds^2 = \frac{dr^2}{r^2}\left(1 + (r^2 z')^2 + (r\psi')^2\right) + r^2\left(-dt^2 + dx^2 + dy^2\right) + \sin^2\psi d^2\Omega_2 \quad (5.2)$$

The introduction of a charge density and external magnetic field will require D5 world-volume gauge fields. In the $a_r = 0$ gauge, the field strength 2-form F is given by

$$\frac{2\pi}{\sqrt{\lambda}} F = a_0'(r) dr \wedge dt + b dx \wedge dy \quad (5.3)$$

In this expression, b is a constant which will give a constant magnetic field in the holographic dual and $a_0(r)$ will result in the world volume electric field which is needed in order to have a nonzero $U(1)$ charge density in the quantum field theory. The magnetic field B and temporal gauge field A_0 are defined in terms of them as

$$b = \frac{2\pi}{\sqrt{\lambda}} B \ , \qquad a_0 = \frac{2\pi}{\sqrt{\lambda}} A_0 \quad (5.4)$$

In this Section, we will use the field strength (5.3) for both the D5 brane and the anti-D5 brane.

The asymptotic behavior at $r \to \infty$ for the embedding functions in (5.2) and the gauge field (5.3) are such that the sphere S^2 becomes maximal,

$$\psi(r) \to \frac{\pi}{2} + \frac{c_1}{r} + \frac{c_2}{r^2} + \dots \quad (5.5)$$

[25] At that point where S^2 is maximal, $\sin\psi = \sin\frac{\pi}{2} = 1$ and $\cos\psi = 0$, that is, the volume of $\tilde{S}^2$ vanishes. The easiest way to see that this embedding has an $SO(3)$ symmetry is to parameterize the S^5 by $(x_1, ..., x_6)$ with $x_1^2 + \dots x_6^2 = 1$. S^2 is the space $x_1^2 + x_2^2 + x_3^2 = \sin^2\psi$ and $\tilde{S}^2$ is $x_4^2 + x_5^2 + x_6^2 = \cos^2\psi$. The point $\cos\psi = 0$ with $x_4 = x_5 = x_6 = 0$ requires no choice of position on $\tilde{S}^2$ and it thus has $SO(3)$ symmetry. On the other hand, if $\cos\psi \neq 0$ and therefore some of the coordinates (x_4, x_5, x_6) are nonzero, the symmetry is reduced to an $SO(2)$ rotation about the direction chosen by the vector (x_4, x_5, x_6).

and the D5 brane and anti-D5 brane are separated by a distance L,

$$z(r) \to \frac{L}{2} - \frac{f}{r^5} + \dots \tag{5.6}$$

for the D5 brane and

$$z(r) \to -\frac{L}{2} + \frac{f}{r^5} + \dots \tag{5.7}$$

for the anti-D5 brane. The asymptotic behaviour of the gauge field is

$$a_0(r) = \mu - \frac{q}{r} + \dots \tag{5.8}$$

with μ and q related to the chemical potential and the charge density, respectively. There are two constants which specify the asymptotic behavior in each of the above equations. In all cases, we are free to choose one of the two constants as a boundary condition, for example we could choose c_1, q, f. Then, the other constants, c_2, μ, L, are fixed by requiring that the solution is non-singular.

In this chapter, we will only consider solutions where the boundary condition is $c_1 = 0$. This is the boundary condition that is needed for the Dirac fermions in the double monolayer quantum field theory to be massless at the fundamental level. Of course they will not remain massless when there is an exciton condensate. In the case where they are massless, we say that there is "chiral symmetry", or that $c_1 = 0$ is a chiral symmetric boundary condition. Then, when we solve the equation of motion for $\psi(r)$, there are two possibilities. The first possibility is that $c_2 = 0$ and $\psi = \frac{\pi}{2}$, a constant for all values of r. This is the phase with good chiral symmetry. Secondly, $c_2 \neq 0$ and ψ is a non-constant function of r. This describes the phase with spontaneously broken chiral symmetry. The constant c_2 is proportional to the strength of the intra-layer chiral exciton condensate the D5 brane or the anti-D5 brane. The constant f instead is proportional to the strength of the inter-layer condensate.

To be more general, we could replace the single D5 brane by a stack of N_5 coincident D5 branes and the single anti-D5 brane by another stack of $\bar{N}_5$ coincident anti-D5 branes. Then, the main complication is that the world volume theories of the D5 and anti-D5 branes become non-Abelian in the sense that the embedding coordinates become matrices and the world-volume gauge fields also have non-Abelian gauge symmetry. The Born-Infeld action must also be generalized to be, as well as an integral over coordinates, a trace over the matrix indices. For now, we will assume that

the non-Abelian structure plays no significant role. Then, all of the matrix degrees of freedom are proportional to unit matrices and the trace in the non-Abelian Born-Infeld action simply produces a factor of the number of branes, N_5 or $\bar{N}_5$ (see equation (5.9) below). We will also take $N_5 = \bar{N}_5$ and leave the interesting possibility that $N_5 \neq \bar{N}_5$ for future work. (This generalization could, for example, describe the interesting situation where a double monolayer consists of a layer of graphene and a layer of topological insulator.) We also have not searched for interesting non-Abelian solutions of the world volume theories which would provide other competing phases of the double monolayer system. Some such phases are already known to exist. For example, it was shown in references [84] and [85] that, when the Landau level filling fraction, which is proportional to Q/B, is greater than approximately 0.5, there is a competing non-Abelian solution which resembles a D7 brane and which plays in important role in matching there integer quantum Hall states which are expected to appear at integer filling fractions. In the present work, we will avoid this region by assuming that the filling fraction is sub-critical. Some other aspects of the non-Abelian structure will be important to us in section 5.

The Born-Infeld action for either the stack of D5 branes or the stack of anti-D5 branes is given by

$$S = \mathcal{N}_5 \int dr \sin^2\psi \sqrt{r^4+b^2}\sqrt{1+(r\psi')^2+(r^2z')^2-(a_0')^2} \tag{5.9}$$

where

$$\mathcal{N}_5 = \frac{\sqrt{\lambda}NN_5}{2\pi^3}V_{2+1}$$

with V_{2+1} the volume of the 2+1-dimensional space-time, N the number of D3 branes, N_5 the number of D5 branes. The Wess-Zumino terms that occur in the D brane action will not play a role in the D5 brane problem.

The variational problem of extremizing the Born-Infeld action (5.9) involves two cyclic variables, $a_0(r)$ and $z(r)$. Being cyclic, their canonical momenta must be constants,

$$Q = -\frac{\delta S}{\delta A_0'} \equiv \frac{2\pi\mathcal{N}_5}{\sqrt{\lambda}}q \ , \qquad q = \frac{\sin^2\psi\sqrt{r^4+b^2}a_0'}{\sqrt{1+(r\psi')^2+(r^2z')^2-(a_0')^2}} \tag{5.10}$$

$$\Pi_z = \frac{\delta S}{\delta z'} \equiv \mathcal{N}_5 f \ , \qquad f = \frac{\sin^2\psi\sqrt{r^4+b^2}r^4z'}{\sqrt{1+(r\psi')^2+(r^2z')^2-(a_0')^2}} \ , \tag{5.11}$$

Solving (5.10) and (5.11) for $a_0'(r)$ and $z'(r)$ in terms of q and f we get

$$a_0' = \frac{qr^2\sqrt{1+r^2\psi'^2}}{\sqrt{r^4\left(b^2+r^4\right)\sin^4\psi + q^2r^4 - f^2}} \tag{5.12}$$

$$z' = \frac{f\sqrt{1+r^2\psi'^2}}{r^2\sqrt{r^4\left(b^2+r^4\right)\sin^4\psi + q^2r^4 - f^2}} \tag{5.13}$$

The Euler-Lagrange equation can be derived by varying the action (5.9). We eliminate $a_0'(r)$ and $z'(r)$ from that equation using equations (5.12) and (5.13). Then the equation of motion for ψ reads

$$\frac{r\psi''+\psi'}{1+r^2\psi'^2} - \frac{\psi'\left(f^2+q^2r^4+r^4\left(b^2+3r^4\right)\sin^4\psi\right) - 2r^3\left(b^2+r^4\right)\sin^3\psi\cos\psi}{f^2-q^2r^4-r^4\left(b^2+r^4\right)\sin^4\psi} = 0 \tag{5.14}$$

This equation must be solved with the boundary conditions in equation (5.5)-(5.8) (remembering that we can choose only one of the integration constants, the other being fixed by regularity of the solution) in order to find the function $\psi(r)$. Once we know that function, we can integrate equations (5.12) and (5.13) to find $a_0(r)$ and $z(r)$.

Clearly, $\psi = \frac{\pi}{2}$, a constant, for all values of r, is always a solution of equation (5.14), even when the magnetic field and charge density are nonzero. However, for some range of the parameters, it will not be the most stable solution.

5.2.1 Length, Chemical Potential and Routhians

The solutions of the equations of motion are implicitly functions of the integration constants. We can consider a variation of the integration constants in such a way that the functions $\psi(r), a_0(r), z(r)$ remain solutions as the constants vary. Then, the on-shell action varies in a specific way. Consider the action (5.9) evaluated on solutions of the equations of motion. We call the on-shell action the free energy $\mathcal{F}_1 = S[\psi, z, a_0]/\mathcal{N}_5$. If we take a variation of the parameters in the solution, here, specifically μ and L, while keeping $c_1 = 0$, and assuming that the equations of motion are obeyed, we obtain

$$\begin{aligned}\delta\mathcal{F}_1 &= \int_0^\infty dr\left(\delta\psi\frac{\partial\mathcal{L}}{\partial\psi'} + \delta a_0\frac{\partial\mathcal{L}}{\partial a_0'} + \delta z\frac{\partial\mathcal{L}}{\partial z'}\right)' \\ &= -q\delta\mu + f\delta L\end{aligned} \tag{5.15}$$

The first term, with $\delta\psi$ vanishes because $\delta\psi \sim \delta c_2/r^2$. We see that $\mathcal{F}_1$ is a function of the chemical potential μ and the distance L and the conjugate

variables, the charge density and the force needed to hold the D5 brane and anti-D5 brane apart are gotten by taking partial derivatives,

$$q = -\frac{\partial \mathcal{F}_1}{\partial \mu}\bigg|_L \quad , \quad f = \frac{\partial \mathcal{F}_1}{\partial L}\bigg|_\mu \tag{5.16}$$

When the dynamical system relaxes to its ground state, with the parameters μ and L held constant, it relaxes to a minimum of $\mathcal{F}_1$.

There are other possibilities for free energies. For example, the quantity which is minimum when the charge density, rather than the chemical potential, is fixed, is obtained from $\mathcal{F}_1[L,\mu]$ by a Legendre transform,

$$\mathcal{F}_2[L,q] = \mathcal{F}_1[L,\mu] + q\mu \tag{5.17}$$

If we formally consider $\mathcal{F}_2$ off-shell as an action from which, for fixed q and f, we can derive equations of motion for $\psi(r)$ and $z(r)$,

$$\mathcal{F}_2 = \frac{S}{\mathcal{N}_5} + \int q a_0' dr = \int dr \sqrt{\sin^4\psi (r^4+b^2)+q^2}\sqrt{1+(r\psi')^2+(r^2 z')^2} \tag{5.18}$$

where we have used

$$a_0' = \frac{q\sqrt{1+r^4 z'^2 + r^2\psi'^2}}{\sqrt{(b^2+r^4)\sin^4\psi + q^2}}$$

obtained by solving equation (5.10) for a_0'. The equation of motion for $\psi(r)$, equation (5.14), can be derived from (5.18) by varying $\psi(r)$. Moreover, we still have

$$f = \frac{\sin^2\psi\sqrt{r^4+b^2}r^4 z'}{\sqrt{1+(r\psi')^2+(r^2z')^2-(a_0')^2}} = \frac{\sqrt{(b^2+r^4)\sin^4\psi+q^2}\, r^4 z'}{\sqrt{1+r^4 z'^2+r^2\psi'^2}} \tag{5.19}$$

which was originally derived from (5.9) by varying z and then finding a first integral of the resulting equation of motion. It can also be derived from (5.18).

Once the function $\psi(r)$ is known, we can solve equation (5.19) for $z'(r)$ and then integrate to compute the separation of the D5 and anti-D5 branes,

$$L = 2\int_{r_0}^{\infty} dr\, z'(r) = 2f\int_{r_0}^{\infty} dr\, \frac{\sqrt{1+r^2\psi'^2}}{r^2\sqrt{r^4\,(b^2+r^4)\sin^4\psi + q^2 r^4 - f^2}} \tag{5.20}$$

where $\psi(r)$ is a solution of (5.14) and r_0 is the turning point, that is the place where the denominator in the integrand vanishes. This turning point depends on the value of $\psi(r_0)$. When ψ is the constant solution $\psi = \pi/2$,

$$r_0 = \frac{\sqrt[4]{\sqrt{\left(b^2+q^2\right)^2+4f^2}-b^2-q^2}}{\sqrt[4]{2}} \tag{5.21}$$

and the integral in (5.20) can be done analytically. It reads

$$L = 2f\int_{r_0}^{\infty} dr\,\frac{1}{r^2\sqrt{r^4\left(b^2+r^4\right)+q^2r^4-f^2}} = \frac{f\,\sqrt{\pi}\Gamma\left(\frac{5}{4}\right)\,{}_2F_1\left(\frac{1}{2},\frac{5}{4};\frac{7}{4};-\frac{f^2}{{r_0}^8}\right)}{2{r_0}^5\Gamma\left(\frac{7}{4}\right)\sqrt{b^2+q^2}} \tag{5.22}$$

For $b = q = 0$, $f = r_0^4$, we get

$$L = \frac{2\sqrt{\pi}\Gamma\left(\frac{5}{8}\right)}{r_0\Gamma\left(\frac{1}{8}\right)}$$

in agreement with the result quoted in reference [94] .

Analogously, the chemical potential is related to the integral of the gauge field strength on the brane in the $(r, 0)$ directions, (5.12),

$$\mu = \int_{r_0}^{\infty} a_0'(r)\,dr = q\int_{r_0}^{\infty} dr\,\frac{r^2\sqrt{1+r^2\psi'^2}}{\sqrt{r^4\left(b^2+r^4\right)\sin^4\psi+q^2r^4-f^2}} \tag{5.23}$$

When ψ is the constant solution $\psi = \pi/2$ the integral in (5.23) can again be done analytically and reads

$$\mu = q\int_{r_0}^{\infty} dr\,\frac{r^2}{\sqrt{r^4\left(b^2+r^4\right)+q^2r^4-f^2}} = \frac{q\,\sqrt{\pi}\Gamma\left(\frac{5}{4}\right)\,{}_2F_1\left(\frac{1}{4},\frac{1}{2};\frac{3}{4};-\frac{f^2}{{r_0}^8}\right)}{r_0\Gamma\left(\frac{3}{4}\right)} \tag{5.24}$$

Through equations (5.20) and (5.23), L and μ are viewed as functions of f and q, this equations can in principle be inverted to have f and q as functions of L and μ.

We can now use (5.12) and (5.13) to eliminate a_0' and z' from the action (5.9) to get the expression of the free energy $\mathcal{F}_1$

$$\mathcal{F}_1[L,\mu] = \int_{r_0}^{\infty} dr\,\left(b^2+r^4\right)\sin^4\psi\,\frac{r^2\sqrt{1+r^2\psi'^2}}{\sqrt{r^4\left(b^2+r^4\right)\sin^4\psi+q^2r^4-f^2}} \tag{5.25}$$

this has to be thought of as a function of L and μ, where f and q are considered as functions of L and μ, given implicitly by (5.20) and (5.23). Note that

we do not do a Legendre transform here since we need the variational functional which is a function of L and μ the D5 brane separation and chemical potential that are the physically relevant parameters.

Using (5.13) to eliminate z' in the Routhian (5.18), we now get a function of L and q

$$\mathcal{F}_2[L,q] = \int_{r_0}^{\infty} dr\ \left(\left(b^2+r^4\right)\sin^4\psi + q^2\right)\frac{r^2\sqrt{1+r^2\psi'^2}}{\sqrt{r^4\left(b^2+r^4\right)\sin^4\psi + q^2r^4 - f^2}} \tag{5.26}$$

The Routhian (5.26) is a function of L through the fact that it is a function of f and f is a function of L given implicitly by (5.20). Of course had we performed the Legendre transform of the Routhian also with respect to L, the result would be

$$\mathcal{F}_3[f,q] = \mathcal{F}_2[L,q] - \int f z' dr = \int_{r_0}^{\infty} dr\ \frac{\sqrt{1+r^2\psi'^2}}{r^2}\sqrt{r^4\left(b^2+r^4\right)\sin^4\psi + q^2r^4 - f^2} \tag{5.27}$$

which is the variational functional appropriate for variations which hold both q and f fixed.

Note that, for convenience, from now on we shall scale the magnetic field b to 1 in all the equations and formulas we wrote: This can be easily done implementing the following rescalings

$$r \to \sqrt{b}r\,, \quad f \to b^2 f\,, \quad q \to b\,q\,, \quad L \to \sqrt{b}L\,, \quad \mu \to \frac{\mu}{\sqrt{b}}\,, \quad \mathcal{F}_i \to b^{3/2}\mathcal{F}_i\,. \tag{5.28}$$

5.3 Double monolayers with a magnetic field

In reference [94] the case of a double monolayer where both of the monolayers are charge neutral was considered with an external magnetic field. In this section, we will re-examine their results within our framework and using our notation. The equation of motion for $\psi(r)$ in this case is

$$\frac{r\psi'' + \psi'}{1+r^2\psi'^2} - \frac{\psi'\left(f^2 + r^4\left(1+3r^4\right)\sin^4\psi\right) - 2r^3\left(1+r^4\right)\sin^3\psi\cos\psi}{f^2 - r^4\left(1+r^4\right)\sin^4\psi} = 0 \tag{5.29}$$

There are in principle four type of solutions for which $c_1 = 0$ in (5.5) [94]:

1. An unconnected, constant solution that reaches the Poincaré horizon. An embedding of the D5 brane which reaches the Poincaré horizon is called a "black hole (BH) embedding". Being a constant solution,

this corresponds to a state of the double monolayer where both the intra-layer and inter-layer condensates vanish.

2. A connected constant $\psi = \frac{\pi}{2}$ solution. Since this is a connected solution, $z(r)$ has a non trivial profile in r and its boundary behaviour is given by equation (5.7) with f non-zero. This solution corresponds to a double monolayer with a non-zero inter-layer condensate and a vanishing intra-layer condensate.

3. An unconnected solution with zero force between the branes, with $f = 0$ and z(r) constant functions for both the D5 brane and the anti-D5 brane, but where the branes pinch off before reaching the Poincaré horizon. An embedding of a single D brane which does not reach the Poincaeé horizon is called a "Minkowski embedding". Since $\psi(r)$ must be r-dependent, its asymptotic behaviour is given in (5.5) with a non-vanishing c_2. This embedding corresponds to a double monolayer with a non-zero intra-layer condensate and a vanishing inter-layer condensate.

4. A connected r-dependent solution, where both $z(r)$ and $\psi(r)$ are non-trivial functions of r. This solution corresponds to the double monolayer with both an intra-layer and an inter-layer condensate.

This classification of the solutions is summarized in table 5.1.

	$f = 0$	$f \neq 0$
$c_2 = 0$	**Type 1** unconnected, $\psi = \pi/2$ BH, chiral symm.	**Type 2** connected, $\psi = \pi/2$ inter
$c_2 \neq 0$	**Type 3** unconnected, r-dependent ψ Mink, intra	**Type 4** connected, r-dependent ψ intra/inter

Table 5.1: Types of possible solutions, where Mink stands for Minkowski embeddings and BH for black hole embeddings.

For type 2 and 4 solutions the D5 and the anti-D5 world-volumes have to join smoothly at a finite $r = r_0$. For these solution the charge density on the brane and on the anti-brane, as well as the value of the constant f that

gives the interaction between the brane and the anti-brane, are equal and opposite.

Consider now the solutions of the type 3, types 1 and 2 are just $\psi = \pi/2$.

The equation for ψ (5.29) with $f = 0$ simplifies further to

$$\frac{r\psi'' + \psi'}{1 + r^2\psi'^2} - \frac{\psi' r \left(1 + 3r^4\right) \sin^4\psi - 2\left(1 + r^4\right) \sin^3\psi \cos\psi}{r\left(1 + r^4\right) \sin^4\psi} = 0 \qquad (5.30)$$

In this case it is obvious from (5.13) that $z(r)$ is a constant. Solutions of type 3 are those for which $\psi(r)$ goes to zero at a finite value of r, $r_{\min}$, so that the two-sphere in the world-volume of the D5 brane shrinks to zero at $r_{\min}$.

A solution to (5.30) of this type can be obtained by a shooting technique. The differential equation can be solved from either direction: from $r_{\min}$ or from the boundary at $r = \infty$. In either case, there is a one-parameter family of solutions, from $r_{\min}$ the parameter is $r_{\min}$, from infinity it is the value of the modulus c_2 in (5.5), which can be used to impose the boundary conditions at $r \to \infty$ with $c_1 = 0$. The parameters at the origin $r_{\min}$ and at infinity can be varied to find the unique solution that interpolates between the Poincaré horizon and the boundary at $r = \infty$.

Consider now the solution of equation (5.29) of type 4. In this case we look for a D5 that joins at some given r_0 the corresponding anti-D5. At r_0, $z'(r_0) \to \infty$ and r_0 can be determined by imposing this condition, that, from (5.13) with $q = 0$ and b scaled out, reads

$$f^2 - r_0^4\left(1 + r_0^4\right) \sin^4\psi(r_0) = 0 \qquad (5.31)$$

which yields

$$\psi(r_0) = \sin^{-1}\left(\sqrt[4]{\frac{f^2}{r_0^4\left(1 + r_0^4\right)}}\right) \qquad (5.32)$$

The lowest possible value of r_0 is obtained when $\psi = \dfrac{\pi}{2}$ and is given by

$$r_{0,\min}(f) = \frac{\sqrt[4]{\sqrt{1 + 4f^2} - 1}}{\sqrt[4]{2}}$$

Note that $r_{0,\min}$ grows when f grows.

Using (5.32) we can derive from the equation of motion (5.29) the condition on $\psi'(r_0)$, it reads

$$\psi'(r_0) = \frac{\left(r_0^4 + 1\right)\sqrt{\frac{\sqrt{r_0^4+1}}{f} - \frac{1}{r_0^2}}}{2r_0^4 + 1} \qquad (5.33)$$

To find the solution let us fix some $\bar{r}$ between r_0 and $r = \infty$. Start with shooting from the origin with boundary conditions (5.32) and (5.33). (5.32) leads to $z'(r_0) \to \infty$, but for a generic choice of r_0 the solution for $\psi(r)$ does not encounter the solution coming from infinity that has $c_1 = 0$, we then need to vary the two parameters r_0 and c_2 in such a way that the two solutions, coming from r_0 and from $r = \infty$ meet at some intermediate point.

For ψ and ψ' given by (5.32) and (5.33) at the origin, integrate the solution outwards to $\bar{r}$ and compute ψ and its derivative at $\bar{r}$. For each solution, put a point on a plot of $\psi'(\bar{r})$ vs $\psi(\bar{r})$, then do the same thing starting from the boundary, $r = \infty$, and varying the coefficient c_2 of the expansion around infinity. Where the two curves intersect the r-dependent solutions from the two sides match and give the values of the moduli for which there is a solution.

5.3.1 Separation and free energy

There are then four types of solutions of the equation of motion (5.29) representing double monolayers with a magnetic field, of type 1, 2, 3 and 4. Solutions 1 and 3 are identical to two independent copies of a single monolayer with B field solution, sitting at a separation L. The brane separation for the solutions of type 2 and 4 is given in (5.20) (for $q = 0$ in this case) and it is plotted in fig. 5.7, the blue line gives the analytic curve (5.22), keeping into account that also r_0 is a function of f through equation (5.21). For the r-dependent solution, green line, instead, r_0 is defined as a function of f by equation (5.31), once the solution $\psi(r)$ is known numerically.

We shall now compare the free energies of these solutions as a function of the separation to see at which separation one becomes preferred with respect to the other.

Since we want to compare solutions at fixed values of L the correct quantity that provides the free energy for each configuration is given by the action evaluated on the corresponding solution

$$\mathcal{F}_1[L] = \int_{r_0}^{\infty} dr \, \left(1 + r^4\right) \sin^4\psi \frac{r^2\sqrt{1 + r^2\psi'^2}}{\sqrt{r^4\left(1 + r^4\right)\sin^4\psi - f^2}} \,. \tag{5.34}$$

Note that this formula is obtained from (5.25), by setting $q = 0$ and performing the rescaling (5.28). The dependence of $\mathcal{F}_1$ on L is implicit (recall that we can in principle trade f for L). This free energy is divergent since in the large r limit the argument of the integral goes as $\sim r^2$. However, in order to find the energetically favored configuration, we are only interested in the difference between the free energies of two solutions, which is always

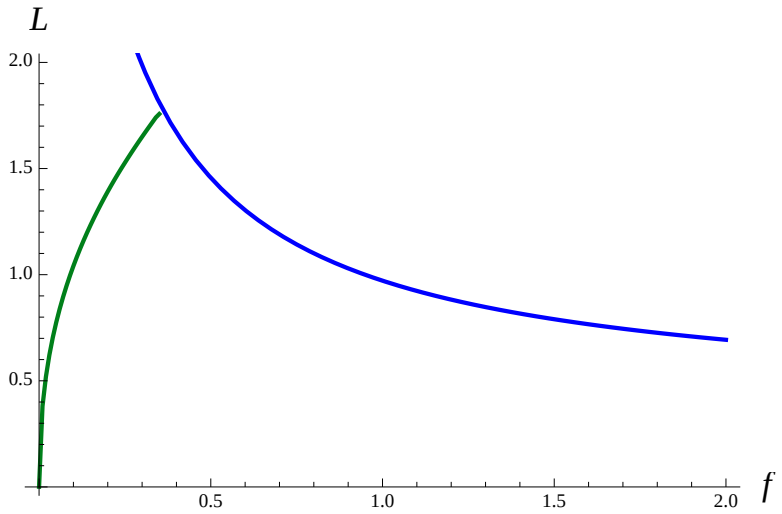

Figure 5.7: The separation of the monolayers, L, is plotted on the vertical axis and the force parameter f is plotted on the horizontal axis. The branch indicated by the blue line is for the constant connected (type 2) solution. (It is a graph of equation (5.22).) The green line is for the r-dependent connected (type 4) solution.

finite. We then choose the free energy of the unconnected ($f = 0$) constant $\psi = \pi/2$ solution, type 1, as the reference free energy (zero level), so that any other (finite) free energy can be defined as

$$\Delta\mathcal{F}_1(\psi; f) = \mathcal{F}_1(\psi; f) - \mathcal{F}_1(\psi = \pi/2; f = 0) = \int_{r_0}^{\infty} dr \left(\left(1 + r^4\right) \sin^4\psi \frac{r^2\sqrt{1 + r^2\psi'^2}}{\sqrt{r^4\left(1 + r^4\right)\sin^4\psi - f^2}} - \sqrt{1 + r^4} \right) - r_0\, {}_2F_1\left(-\frac{1}{2}, \frac{1}{4}; \frac{5}{4}; -{r_0}^4\right) . \tag{5.35}$$

where the last term is a constant that keeps into account that the $\psi = \pi/2$ disconnected solution reaches the Poincaré horizon, whereas the other solutions do not. It turns out that, in this particular case where the D5 brane and the anti-D5 brane are both charge neutral, the solutions of type 1 and 4 always have a higher free energy than solutions 2 and 3. By means of numerical computations we obtain for the free energy $\Delta\mathcal{F}_1$ of the solutions 2, 3 and 4, the behaviours depicted in Figure 5.8. This shows that the dominant configuration is the connected one with an inter-layer condensate for small brane separation L and the disconnected one, with only an intra-layer condensate, for large L. The first order transition between the two

phases takes place at $L \simeq 1.357$ in agreement with the value quoted in reference [94].

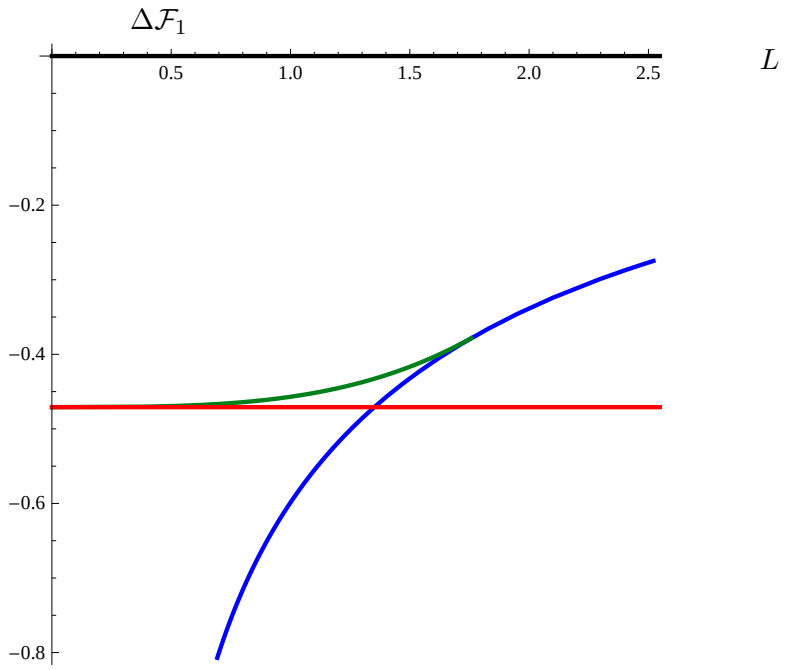

Figure 5.8: Double monolayer in a magnetic field, where each monolayer is charge neutral. The regularized free energy $\Delta\mathcal{F}_1$ is plotted on the vertical axis, and the inter-layer separation L (in units of $1/\sqrt{b}$), which is plotted on the horizontal axis. The blue line corresponds to the connected solution (type 2), the red line to the unconnected solution (type 3) and the green line to the connected r-dependent solutions (type 4). All solutions are regulated by subtracting the free energy of the constant unconnected solution of type 1. The latter is the black line at the top of the diagram. The type 1 and type 4 solutions exist but they never have the lowest energy. For large L, the type 3 solution is preferred and small L the type 2 solution is more stable. This reproduces results quoted in reference [94].

5.4 Double monolayer with a magnetic field and a charge-balanced chemical potential

We shall now study the possible configurations for the D5-anti D5 probe branes in the $AdS_5 \times S^5$ background, with a magnetic field and a chemical potential. The chemical potentials are balanced in such a way that the

chemical potential on one monolayer induces a density of electrons and the chemical potential on the other monolayer induces a density of holes which has identical magnitude to the density of electrons. Moreover, the chemical potentials are exactly balanced so that the density of electrons and the density of holes in the respective monolayers are exactly equal. Due to the particle-hole symmetry of the quantum field theory, it is sufficient that the chemical potentials have identical magnitudes. The parameters that we keep fixed in our analysis are the magnetic field b, the monolayer separation L and the chemical potential μ.

In order to derive the allowed configurations we have to solve equation (5.14) for ψ as well as equation (5.12) for the gauge potential a_0 and equation (5.13) for z. In practice the difficult part is to find all the solutions of the equation of motion for ψ, which is a non-linear ordinary differential equation. Once one has a solution for ψ it is straightforward to build the corresponding solutions for z and a_0, simply by plugging the solution for ψ into the equations (5.12)-(5.13) and integrating them.

It should be noted that any solution of the equation (5.12) for the gauge potential $a_0(r)$ always has an ambiguity in that $a_0(r)$+constant is also a solution. The constant is fixed by remembering that $a_0(r)$ is the time component of a vector field and it should therefore vanish at the Poincaré horizon. When the charge goes to zero, a_0 =constant is the only solution of equation (5.12) and this condition puts the constant to zero. Of course, this is in line with particle-hole symmetry which tells us that the state with chemical potential set equal to zero has equal numbers of particles and holes. The results of the previous section, where μ and q were equal to zero, care a special case of what we will derive below.

5.4.1 Solutions for $q \neq 0$

Now we consider the configurations with a charge density different from zero. The differential equation for ψ in this case is

$$\frac{r\psi'' + \psi'}{1 + r^2\psi'^2} - \frac{\psi'\left(f^2 + q^2r^4 + r^4\left(1 + 3r^4\right)\sin^4\psi\right) - 2r^3\left(1 + r^4\right)\sin^3\psi\cos\psi}{f^2 - q^2r^4 - r^4\left(1 + r^4\right)\sin^4\psi} = 0\,. \tag{5.36}$$

As usual, we shall look for solutions with $c_1 = 0$ in equation (5.5). We can again distinguish four types of solutions according to the classification of table 5.2. The main difference between the solutions summarized in table 5.2 and those in table 1 are that the type 3 solution now has a black hole, rather than a Minkowski embedding. This is a result of the fact that, as explained

in section 1, the world-volume of a D5 brane that carries electric charge density must necessarily reach the Poincaré horizon if it does not join with the anti-D5 brane. The latter, where it reaches the Poincaré horizon, is an un-gapped state and it must be so even when there is an intra-layer exciton condensate. It is, however, incompatible with an inter-layer condensate.

	$f = 0$	$f \neq 0$
$c_2 = 0$	**Type 1** unconnected, $\psi = \pi/2$ BH, chiral symm.	**Type 2** connected, $\psi = \pi/2$ inter
$c_2 \neq 0$	**Type 3** unconnected, r-dependent ψ BH, intra	**Type 4** connected, r-dependent ψ intra/inter

Table 5.2: Types of possible solutions for $q \neq 0$.

Type 1 solutions are trivial both in ψ and z (they are both constants). They correspond to two parallel black hole (BH) embeddings for the D5 and the anti-D5. This configuration is the chiral symmetric one. In type 2 solutions the chiral symmetry is broken by the inter-layer condensate ($f \neq 0$): In this case the branes have non flat profiles in the z direction. Solutions of type 3 and 4 are r-dependent and consequently are the really non-trivial ones to find. Type 3 solutions have non-zero expectation value of the intra-layer condensate and they can be only black hole embeddings, this is the most significant difference with the zero charge case. Type 4 solutions break chiral symmetry in both the inter- and intra-layer channel. For type 2 and 4 solutions the D5 and the anti-D5 world-volumes have to join smoothly at a finite $r = r_0$.

Now we look for the non-trivial solutions of equation (5.36). We start considering the solutions of type 4. We can build such a solution requiring that the D5 profile smoothly joins at some given r_0 the corresponding anti-D5 profile. The condition that has to be satisfied in order to have a smooth solution for the connected D5/anti-D5 world-volumes is $z'(r_0) \to \infty$ which, from (5.13) (with b scaled to 1), corresponds to the condition

$$f^2 - r_0^4 \left[q^2 + \left(1 + r_0^4\right) \sin^4 \psi(r_0)\right] = 0\,. \tag{5.37}$$

From this we can determine the boundary value $\psi(r_0)$

$$\psi(r_0) = \arcsin\left(\sqrt[4]{\frac{f^2 - q^2 r_0^4}{r_0^4\left(1 + r_0^4\right)}}\right) . \tag{5.38}$$

Note that the request that $0 \leq \sin\psi(r_0) \leq 1$ fixes both a lower and an upper bound on r_0

$$r_{0,\min}(f,q) = \frac{\sqrt[4]{\sqrt{(1+q^2)^2 + 4f^2} - 1 - q^2}}{\sqrt[4]{2}} , \qquad r_{0,\max}(f,q) = \sqrt{\frac{f}{q}} .$$

Using (5.32) we can derive from the equation of motion (5.36) the condition on $\psi'(r_0)$, which reads

$$\psi'(r_0) = \frac{\left(r_0^4 + 1\right)\left(f^2 - q^2 r_0^4\right)\sqrt{\sqrt{\frac{r_0^4+1}{f^2 - q^2 r_0^2}} - \frac{1}{r_0^2}}}{f^2\left(2r_0^4 + 1\right) - q^2 r_0^8} \tag{5.39}$$

We can then build such solutions imposing the conditions (5.38) and (5.39) at r_0, where r_0 is the modulus. With the usual shooting technique we then look for solutions that also have the desired behavior at infinity, *i.e.* those that match the boundary conditions (5.5) with $c_1 = 0$. It turns out that in the presence of a charge density there are solutions of type 4 for any value of q, in this case, however, these solutions will play an important role in the phase diagram.

Next we consider the solutions of type 3. These solutions can be in principle either BH or Minkowski embeddings. However when there is a charge density different from zero only BH embeddings are allowed. A charge density on the D5 world-volume is indeed provided by fundamental strings stretched between the D5 and the Poincaré horizon. These strings have a tension that is always greater than the D5 brane tension and thus they pull the D5 down to the Poincaré horizon [104]. For this reason when $q \neq 0$ the only disconnected solutions we will look for are BH embedding. Solutions of this kind with $c_2 \neq 0$ can be built numerically along the lines of ref. [92]. Note that because of the equation of motion they must necessarily have $\psi(0) = 0$[26].

[26] Actually also the condition $\psi(0) = \pi/2$ is allowed by the equation of motion, but this would correspond to the constant solution with $c_2 = 0$, namely the type 1 solution.

5.4.2 Separation and free energy

The brane separation is given in (5.20) and for the solutions of type 2 and 4 is plotted in fig. 5.9 for $q = 0.01$, the blue line gives the curve (5.22), keeping into account that also r_0 is a function of f through equation (5.21). For the r-dependent solution instead r_0 is defined as a function of f by equation (5.37), once the solution $\psi(r)$ is known numerically. The r-dependent connected solution, green line, has two branches one in which L decreases with increasing f and the other one in which L increases as f increases. It is clear from the picture that when $q \to 0$ one of the branches of the green solution disappears and fig. 5.9 will become identical to fig. 5.7.

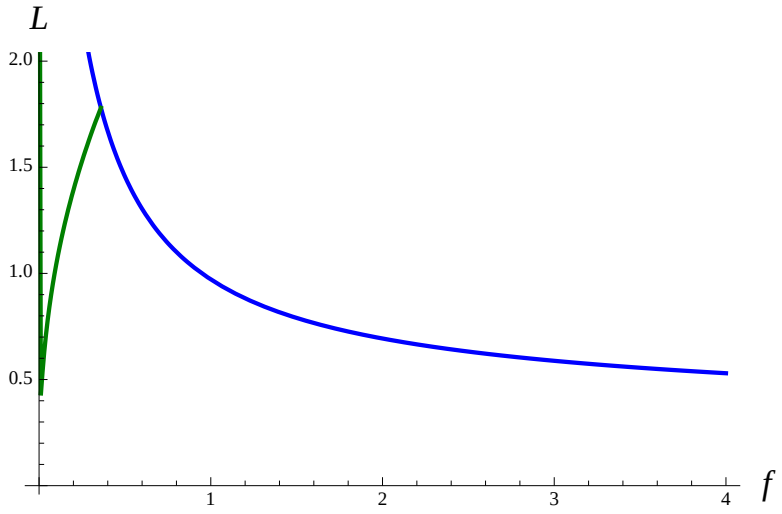

Figure 5.9: The separation of the monolayers, L, is plotted on the vertical axis and the force parameter f is plotted on the horizontal axis, in the case where the monolayers have charge densities and $q = 0.01$. The branch indicated by the blue line is for the constant connected (type 2) solution. The green line is for the r-dependent connected (type 4) solution.

Once we have determined all the possible solutions, it is necessary to study which configuration is energetically favored. We shall compare the free energy of the solutions at fixed values of L and μ, since this is the most natural experimental condition for the double monolayer system. Thus the right quantity to define the free energy is the action (5.25), which after the

rescaling (5.28) is given by

$$\mathcal{F}_1[L,\mu] = \int_{r_0}^{\infty} dr\ \left(1+r^4\right)\sin^4\psi \frac{r^2\sqrt{1+r^2\psi'^2}}{\sqrt{r^4\left(1+r^4\right)\sin^4\psi + q^2r^4 - f^2}} \tag{5.40}$$

As usual we regularize the divergence in the free energy by considering the difference of free energies of pairs of solutions, which is really what we are interested in. So we define a regularized free energy $\Delta\mathcal{F}_1$ by subtracting to each free energy that of the unconnected ($f=0$) constant $\psi=\pi/2$ solution,

$$\Delta\mathcal{F}_1(\psi; f, q) \equiv \mathcal{F}_1(\psi; f, q) - \mathcal{F}_1(\psi=\pi/2; f=0, \hat{q}). \tag{5.41}$$

As we already noticed, the free energy (5.40) and consequently $\Delta\mathcal{F}_1$ are implicit functions of L and μ, via f and q, which are the parameters that we really have under control in the calculations. Thus when computing the regularized free energy $\Delta\mathcal{F}_1$ we have to make sure that the two solutions involved have the same chemical potential.[27] This is the reason why in the definition of $\Delta\mathcal{F}_1$ (5.41) we subtract the free energy of two solutions with different values of q: the $\hat{q}$ in (5.41) is in fact the value of the charge such that the chemical potential of the regulating solution ($\psi=\pi/2; f=0$) equals that of the solution we are considering $(\psi; f, q)$. To be more specific, for a solution with chemical potential μ, which can be computed numerically through (5.23) (or through (5.24) for the $\psi=\pi/2$ case), $\hat{q}$ must satisfy

$$\mu(\psi=\pi/2; f=0, \hat{q}) \equiv \frac{4\Gamma\left(\frac{5}{4}\right)^2\hat{q}}{\sqrt{\pi}(1+\hat{q}^2)^{1/4}} = \mu$$

and therefore it is given by

$$\hat{q} = \sqrt{\frac{\mathcal{J}+\sqrt{\mathcal{J}(\mathcal{J}+4)}}{2}}\,, \qquad \mathcal{J} \equiv \frac{\pi^2\mu^4}{\left(2\Gamma\left(\frac{5}{4}\right)\right)^8}\,.$$

For the type 2 solution the regularized free energy density can be com-

[27] In principle we also have to make sure that the two solutions have the same L. However this is not necessary in practice, since in $\Delta\mathcal{F}_1$ we use as reference free energy that of an unconnected solution, which therefore is completely degenerate in L. Indeed the unconnected configuration is given just by two copies of the single D5 brane solution with zero force between them, which can then be placed at any distance L.

puted analytically. Reintroducing back the magnetic filed, it reads

$$\begin{aligned}\Delta\mathcal{F}_1[L,\mu] = &\int_{r_0}^{\infty} dr\left(b^2+r^4\right)\left(\frac{r^2 r_0^2}{\sqrt{\left(r^4-r_0^4\right)\left(f^2+r^4 r_0^4\right)}}-\frac{1}{\sqrt{b^2+\hat{q}^2+r^4}}\right)\\ &-\int_0^{r_0} dr\frac{b^2+r^4}{\sqrt{b^2+\hat{q}^2+r^4}}\\ &=\frac{\sqrt{\pi}\Gamma\left(-\frac{3}{4}\right)}{16 r_0\sqrt[4]{b^2+\hat{q}^2}\Gamma\left(\frac{3}{4}\right)}\left[\sqrt[4]{b^2+\hat{q}^2}\left(2r_0^4\,{}_2F_1\left(-\frac{3}{4},\frac{1}{2};\frac{3}{4};-\frac{f^2}{r_0^8}\right)\right.\right.\\ &\left.\left.-3\left(b^2+r_0^4\right)\,{}_2F_1\left(\frac{1}{4},\frac{1}{2};\frac{3}{4};-\frac{f^2}{r_0^8}\right)\right)+\sqrt{2}r_0\left(2b^2-\hat{q}^2\right)\right]\end{aligned} \tag{5.42}$$

where r_0 is given in (5.21).

A comparison of the free energies of the various solutions for $L = 1.5$ and $L = 5$ is given in figure 5.10. The chirally symmetric solution would be along the μ-axis since it is the solution we used to regularize all the free energies. It always has a higher free energy, consequently, the chirally symmetric phase is always metastable.

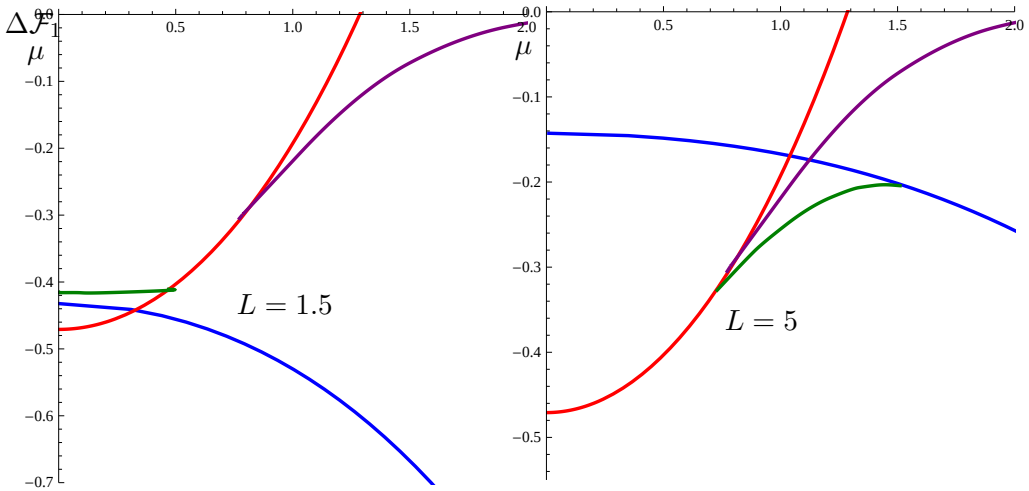

Figure 5.10: Plots of the free energies as a function of the chemical potential: type 2 (blue line), type 3 (red-line) and type 4 (green line) solutions for $L = 1.5$ and $L = 5$.

5.4.3 Phase diagrams

Working on a series of constant L slices we are then able to draw the phase diagram (μ, L) for the system. For the reader convenience we reproduce the phase diagram that we showed in the introduction in fig. 5.11 (here the labels are rescaled however). We see that the dominant phases are three:

- The connected configuration with $c_2 = 0$ (type 2 solution) where the flavor symmetry is broken by the inter-layer condensate (blue area);
- The connected configuration with $c_2 \neq 0$ and $f \neq 0$ (type 4 solution with $q \neq 0$) where the chiral symmetry is broken by the intra-layer condensate and the flavor symmetry is broken by the inter-layer condensates (green area);
- The unconnected Minkowski embedding configuration with $c_2 \neq 0$ (type 3 solution with $q = 0$) where the chiral symmetry is broken by the intra-layer condensate (red area);

Note that in all these three phases chiral symmetry is broken.

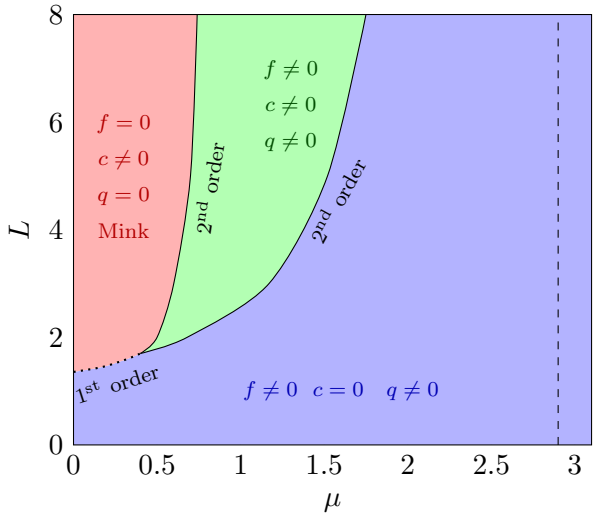

Figure 5.11: Phase diagram of the D3-probe-D5 branes system with balanced charge densities. Layer separation is plotted on the vertical axis and chemical potential μ for electrons in one monolayer and holes in the other monolayer is plotted on the horizontal axis. The units are the same as in figure 5.1.

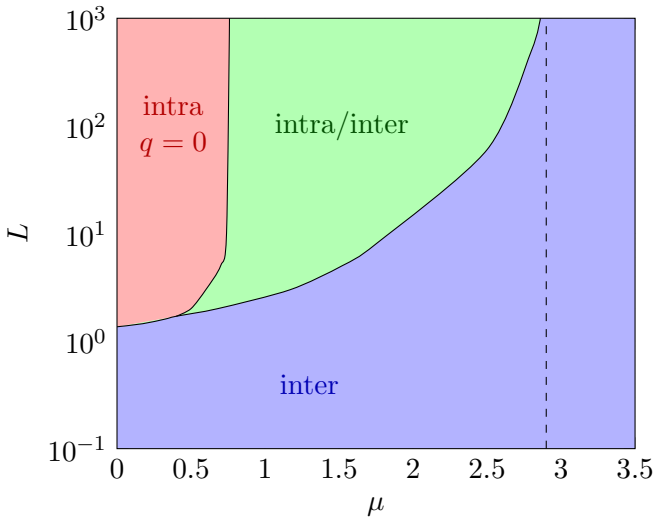

Figure 5.12: Phase diagram for large separation between the layers.

As expected, for small enough L the connected configuration is the dominant one. We note that for $L \lesssim 1.357$, which, as we already pointed out, is the critical value for L in the zero-chemical potential case, the connected configuration is always preferred for any value of μ. When $1.357 \lesssim L \lesssim 1.7$ the system faces a second order phase transition from the unconnected Minkowski embedding phase – favored for small values of μ – to the connected phase – favored at higher values of μ. When $L \gtrsim 1.7$ as the chemical potential varies the system undergoes two phase transitions: The first happens at $\mu \simeq 0.76$ and it is a second order transition from the unconnected Minkowski embedding phase to the connected phase with both condensates. Increasing further the chemical potential the system switches to the connected phase with only an intra-layer condensate again via a second order transition.

Therefore it is important to stress that, with a charge density, a phase with coexisting inter-layer and intra-layer condensates can be the energetically preferred state. Indeed, it is the energetically favored solution in the green area and corresponds to states of the double monolayer with both the inter-layer and intra-layer condensates.

The behavior of the system at large separation between the layers is given in fig. 5.12. For $L \to \infty$ the phase transition line between the green and the blue area approaches a vertical asymptote at $\mu \simeq 2.9$. The connected solu-

tions for $L \to \infty$ become the corresponding, r-dependent or r-independent disconnected solutions. Thus for an infinite distance between the layers we recover exactly the behavior of a single layer [99] where at $\mu \simeq 2.9$ the system undergoes a BKT transition between the intra-layer BH embedding phase to the chiral symmetric one [102].

It is interesting to consider also the phase diagram in terms of the brane separation and charge density fig. 5.14. In this case the relevant free energy function that has to be considered is the Legendre transformation of the action with respect to q, namely the Routhian $\mathcal{F}_2[L, q]$ defined in equation (5.26). For the regularization of the free energy we choose proceed in analogy as before: For each solution of given q and L we subtract the free energy of the constant disconnected (type 1) solution with the same charge q, obtaining the following regularized free energy

$$\Delta\mathcal{F}_2[L, q] \equiv \mathcal{F}_2[L, q] - \mathcal{F}_2(\psi = \pi/2; f = 0)[q]. \tag{5.43}$$

In fig. 5.14 the phase represented by the red region in fig. 5.11, is just given by a line along the $q = 0$ axis. By computing the explicit form of the free energies as function of the brane separation L, it is possible to see in fact that the r-dependent connected solution has two branches. These branches reflect the fact that also the separation L has two branches as a function of f, as illustrated in fig. 5.9. In the limit $q \to 0$ one of these branches tends to overlap to the r-dependent disconnected solution and for $q = 0$ disappears. This is illustrated in fig. 5.13 where one can see that in the $q \to 0$ limit the free energy difference as a function of L goes back to that represented in fig. 5.8.

5.5 Double monolayers with un-matched charge densities

We now consider a more general system of two coincident D5 branes and two coincident anti-D5 branes, with total charges $Q = q_1 + q_2 > 0$ and $-\bar{Q}$ where $\bar{Q} = q_3 + q_4 > 0$. Then, unlike before, this corresponds to a double monolayer with unpaired charge on the two layers. For such a system we are interested in determining the most favored configuration, *i.e.* to find out how the charges Q and $\bar{Q}$ distribute among the branes and which types of solutions give rise to the least free energy for the whole system. Since the parameter that we take under control is the charge, and not the chemical potential, we shall use the free energy $\mathcal{F}_2$, defined in equation (5.17), in order to compare the different solutions.

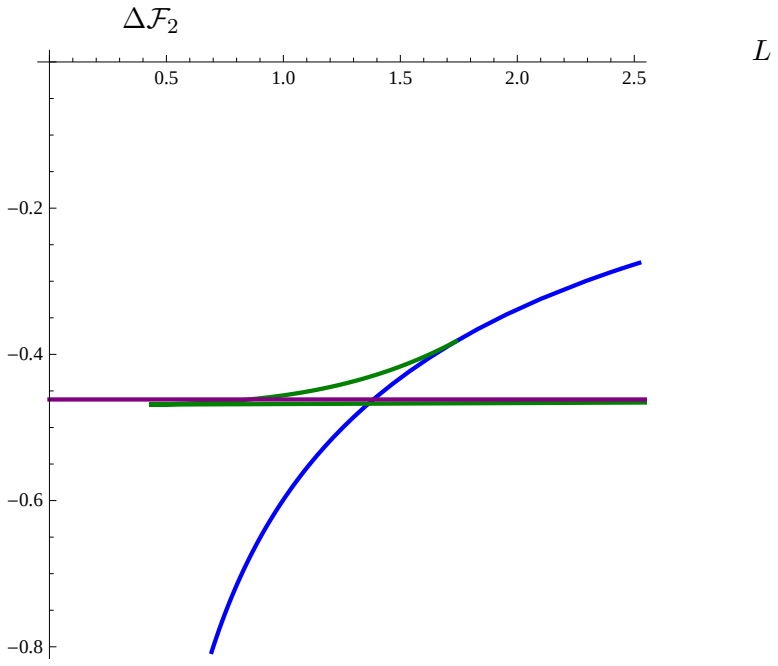

Figure 5.13: Free energy difference $\Delta\mathcal{F}_2$ as a function of L for $q = 0.01$, the two branches of the r-dependent connected solution, green line, tend to become just the one of fig. 5.8.

What we keep fixed in this setup are the overall charges Q and $\bar{Q}$ in the two layers, while we let the charge on each brane vary: Namely the q_i vary with the constraints that $Q = q_1 + q_2$ and $\bar{Q} = q_3 + q_4$ are fixed. Then we want to compare configurations with different values for the charges q_i on the single branes. For this reason we must choose a regularization of the free energy that does not depend on the charge on the single brane, and clearly the one that we used in the previous section is not suitable. The most simple choice of such a regularization consists in subtracting to the integrand of the free energy only its divergent part in the large r limit, which is r^2. We denote this regularized free energy as $\Delta\mathcal{F}_{2,r}$.

Without loss of generality we suppose that $Q > \bar{Q}$. Then for simplicity we fix the values of the charges to $Q = 0.15$ and $\bar{Q} = 0.1$ and the separation between the layers to $L = 1$. There are two possible cases.

(i) A configuration in which the D5 brane with charge q_1 is described by a black hole embedding whereas the D5 brane with charge q_2 is connected with the anti-D5 brane with charge q_3, so that $q_2 = q_3$.

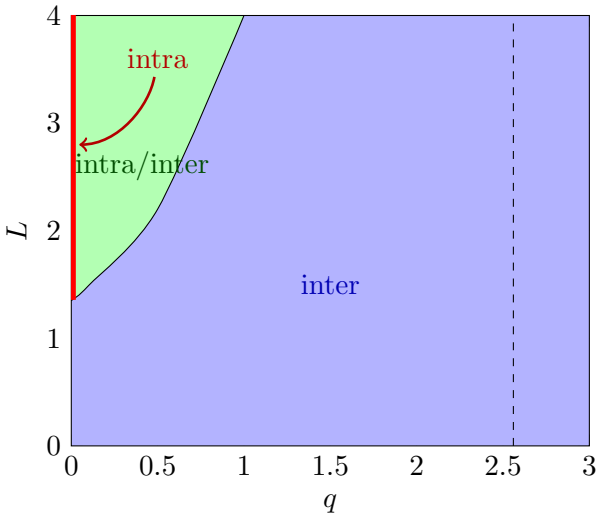

Figure 5.14: Phase diagram in terms of the brane separation L and the charge density q.

Then we have

$$q_2 = q_3 = \bar{Q} - q_4 \ , \qquad q_1 = Q - q_2 = Q - \bar{Q} + q_4$$

The free energy of this solution as a function of the parameter q_4 is given by the plot in fig. 5.16 for $Q = 0.15$ and $\bar{Q} = 0.1$.

From fig. 5.16 it is clear that the lowest free energy is achieved when $q_4 = 0$ which corresponds to the fact that one anti-D5 brane is represented by a Minkowski embedding.

(*ii*) Then we can consider the configuration in which all the branes are disconnected. In this case

$$q_1 = Q - q_2 \ , \qquad q_3 = \bar{Q} - q_4$$

In fig. 5.17 we give the free energy of the D5 branes, and of the the anti-D5 brane. It is clear from fig. 5.17 that the lowest free energy configuration is when both branes on the same layer have the same charge. The free energy of the complete configuration will be then the sum of the free energy of the D5 and of the anti-D5 layers each with charge evenly distributed over the branes. For the case considered we

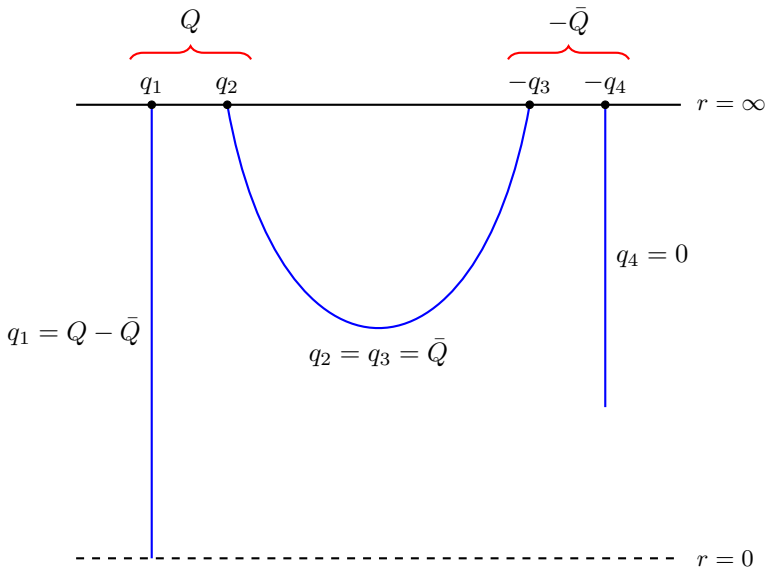

Figure 5.15: Energetically favored solution for unpaired charges when $Q > \bar{Q}$.

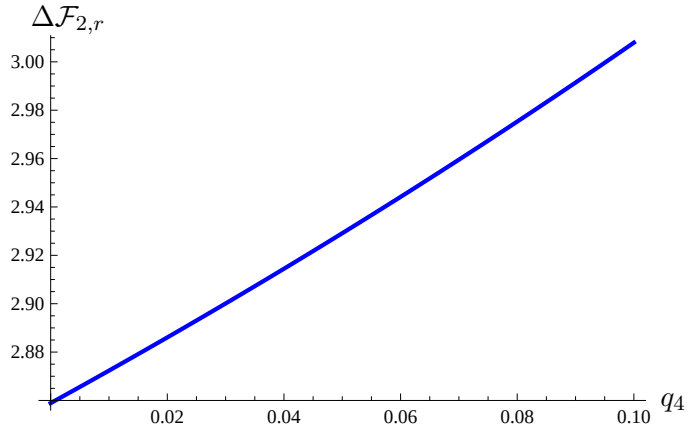

Figure 5.16: Free energy of the solutions when one brane is disconnected and two branes are connected

obtain a free energy $\Delta\mathcal{F}_{2,r} \simeq 3.26$, which however is higher then the free energy of the configuration (i).

In the special case in which Q and $\bar{Q}$ are equal, *e.g.* $Q = \bar{Q} = 0.15$, there are four possible configurations: Either the branes are all disconnected, or

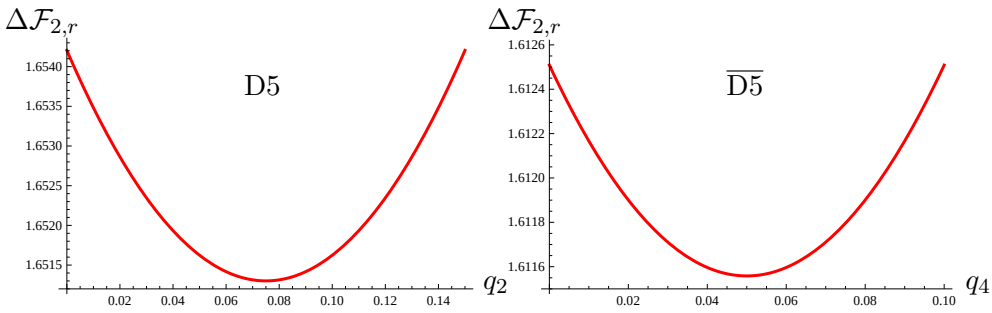

Figure 5.17: Free energy of the solutions when all the branes are disconnected: The energetically favored solution is when they have the same charge.

the two pairs branes are both connected, or a brane and an anti-brane are connected and the other are black hole embeddings, or, finally, a brane and an anti-brane are connected and have all the charges Q and $\bar{Q}$, so the rest are Minkowski embeddings.

When they are all disconnected the physical situation is described in item ii and the energetically favored solution is that with the same charge. When they are all connected the configuration has the following charges.

$$q_1 = Q - q_2 \ , \qquad q_3 = q_1 \ , \qquad q_2 = q_4 \ , \qquad q_3 = \bar{Q} - q_4 = Q - q_2$$

Fig. 5.18 shows the free energy of the system of branes and anti-branes when

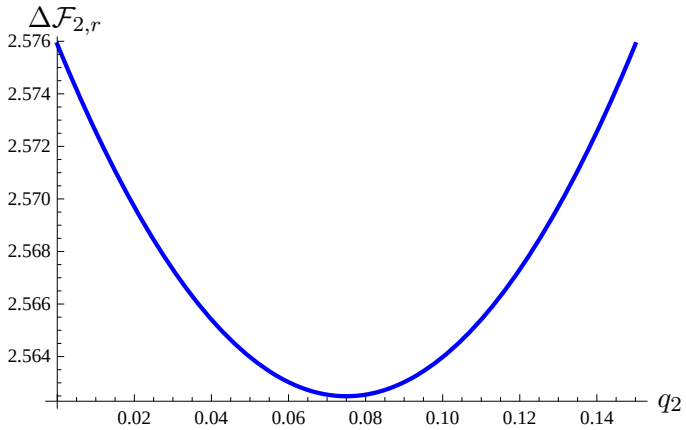

Figure 5.18: Free energy of the solutions when all the branes are connected, the energetically favored solution is when the charge is distributed evenly between the branes and anti-branes.

they are all connected, clearly the energetically most favored solution is that

with the charge distributed evenly. This solution has a lower free energy with respect to the one of all disconnected branes and charges distributed evenly and also with respect to a solution with one brane anti-brane connected system and two black hole embeddings. Since the connected solutions for $L \lesssim 1.357$ and $q = 0$ are always favored with respect to the unconnected ones, also the solution with two Minkowski embeddings and one connected solution has higher free energy with respect to the one with two connected pairs.

Summarizing for $Q = \bar{Q}$ the energetically favored solution is the one with two connected pairs and all the charges are evenly distributed $q_1 = q_2 = q_3 = q_4 = Q/2$.

5.6 Discussion

We have summarized the results of our investigations in section 1. Here, we note that there are many problems that are left for further work. For example, in analogy with the computations in reference [65] which used a non-relativistic Coulomb potential, it would be interesting to study the double monolayer quantum field theory model that we have examined here, but at weak coupling, in perturbation theory. At weak coupling, and in the absence of magnetic field or charge density, an individual monolayer is a defect conformal field theory. The double monolayer which has nested fermi surfaces should have an instability to pairing. It would be interesting to understand this instability better. What we expect to find is an inter-layer condensate which forms in the perfect system at weak coupling and gives the spectrum a charge gap. The condensate would break conformal symmetry and it would be interesting to understand how it behaves under renormalization.

The spontaneous nesting deserves further study. It would be interesting to find a phase diagram for it to, for example, understand how large a charge miss-match can be.

Everything that we have done is at zero temperature. Of course, the temperature dependence of various quantities could be of interest and it would be interesting (and straightforward) to study this aspect of the model.

It would be interesting to check whether the qualitative features which we have described could be used to find a bottom-up holographic model of double monolayers, perhaps on the lines of the one constructed by Sonner [93].

Chapter 6

Holographic D3-probe-D7 Model of a Double Layer Dirac Semimetals

On the rumbling bus, somewhere,
I saw a white notice board on the street.
It is written with clear letters that
You are leaving away the county of Mujin.
Good bye.

I was heavily ashamed.

- Record of a Journey to Mujin by Seung-Ok Kim

The possibility that an inter-layer exciton condensate can form in a double monolayer of two-dimensional electron gases has been of interest for a long time [64]. A double monolayer contains two layers, each containing an electron gas, separated by an insulator so that electrons cannot be transferred between the layers. Electrons and holes in the two layers can still interact via the Coulomb interaction. The exciton which would condense is a bound state of an electron in one layer and a hole in the other layer. This idea has recently seen a revival with some theoretical computations for emergent relativistic systems such as graphene or some topological insulators which suggested that a condensate could form at relatively high temperatures, even at room temperature [15]. A room temperature superfluid would have applications in electronic devices where proposals include ultra-fast switches and dispersionless field-effect transistors [112].

An exciton condensate might be more readily achievable in a double monolayer with relativistic electrons due to particle-hole symmetry and the possibility of engineering nested Fermi surfaces of electrons in one layer and the holes in the other layer. This nesting would enhance the effects of the attractive Coulomb interaction between an electron and a hole. Even at very weak coupling, it can be shown to produce an instability to exciton conden-

sation [65]. However, in spite of this optimism, an inter-layer condensate has yet to be observed in a relativistic material, even in experiments using clean graphene sheets with separations down to the nanometer scale [118]. The difficulty with theoretical computations, where the Coulomb interaction is strong, is the necessity of ad-hoc inclusion of screening, to which the properties of the strongly coupled system have been argued to be sensitive [120].

In this chapter we will study a model of a double monolayer of relativistic two-dimensional electron gases. This model has a known AdS/CFT dual which is easy to study and it can be solved exactly in the strong coupling limit. We shall learn that, in this model. the only condensates which form are excitons, bound states of electrons with holes in the same layer (intra-layer) or bound states of electrons in one layer with holes in the other layer (inter-layer). Moreover, even though at very strong coupling, the idea of a Fermi surface loses its meaning, we find that the tendency to form an inter-layer condensate is indeed greatly enhanced by the charge balance which, at weak coupling, would give nested particle and hole Fermi surfaces. We shall see that, in the strong coupling limit, and when the charges are balanced, an inter-layer condensate can form for any separation of the layers. As well as the inter-layer condensate, such a strong interaction will also form an intra-layer condensate. We find that a mixture of the two condensates is favoured for small charge densities and larger layer separations. For sufficiently large charge densities, on the other hand, the only condensate is the inter-layer condensate. These results for charge balanced layers are summarized in figure 6.1. When the charges are not balanced, so that at weak coupling the Fermi surfaces would not be nested, no inter-layer condensate forms, regardless of the layer separation. This dramatic difference is similar to and even sharper than what is seen at weak coupling [65] where condensation occurs in only a narrow window of densities near nesting.

However, even in the non-nested case, we can find a novel symmetry breaking mechanism where an inter-layer condensate can form. If each electron gas contains more than one species of relativistic electrons (for example, graphene has four species of massless Dirac electrons and some topological insulators have two species), the electric charge can redistribute itself amongst the species to spontaneously nest one or more pairs of Fermi surfaces, with the unbalanced charge taken up by the other electron species. Then the energy is lowered by formation of a condensate of the nested electrons, the others remaining un-condensed. To our knowledge, this possibility has not been studied before. The result is a new kind of symmetry breaking where Fermi surfaces nest spontaneously and break some of the internal

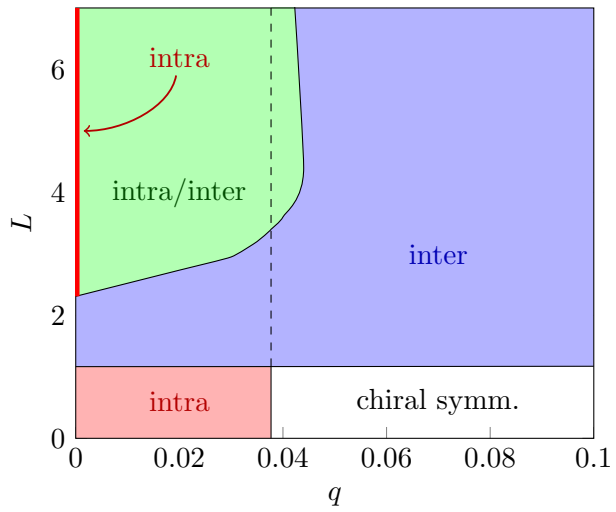

Figure 6.1: (color online) Phase diagram of the charge balanced double monolayer (exactly nested Fermi surfaces). The vertical axis is layer separation L in units of the inverse ultraviolet cutoff, R. The horizontal axis is the charge density q in units of R^{-2}. The green region has both inter- and intra-layer condensates. The blue region has only an inter-layer condensate. The red region has only an intra-layer condensate. The white region has no condensates.

symmetry of the electron gas in each layer. We demonstrate that, for some examples of the charge density, this type of condensate indeed exists as the lowest energy solution.

The model which we shall consider is a defect quantum field theory consisting of a pair of parallel, infinite, planar 2+1-dimensional defects in 3+1-dimensional Minkowski space and separated by a distance L. The defects are each inhabited by N_F species of relativistic massless Dirac Fermions. The Fermions interact by exchanging massless quanta of maximally supersymmetric Yang-Mills theory which inhabits the surrounding 3+1-dimensional bulk. In the absence of the defects, the latter would be a conformal field theory. The interactions which it mediates have a $1/r$ fall-off, similar to the Coulomb interaction and, in the large N planar limit which we will consider, like the Coulomb force, the electron-hole interaction is attractive in all channels.

The field theory action is

$$S = \int d^4x \frac{1}{g^2_{\rm YM}} {\rm Tr}\left[-\frac{1}{2}F_{\mu\nu}F^{\mu\nu} - \sum_{b=1}^{6} D_\mu \Phi^b D^\mu \Phi^b + \ldots\right] + \int d^3x \sum_{a=1}^{2}\sum_{i=1}^{N_F} \bar{\psi}_{ai}\left[i\gamma^\mu \partial_\mu + \gamma^\mu A_\mu + \Phi^6\right]\psi_{ai} \tag{6.1}$$

The first term is the action of $\mathcal{N} = 4$ supersymmetric Yang-Mills theory where A_μ is the Yang-Mills gauge field and Φ^6 is one of the scalar fields and the second term is the action of the defect Fermions. In the second term, the subscript a labels the defects and i the Fermion species. The action includes all of the marginal operators which are compatible with the symmetries. It has a global U(1) symmetry which we associate with electric charge.

The defect field theory (6.1) is already interesting with one layer. It is thought to have a conformally symmetric weak coupling phase for $0 \leq \lambda \leq \lambda_c$. When $\lambda > \lambda_c$, chiral symmetry is broken by an intra-layer exciton condensate [69]. Near the critical point, the order parameter is thought to scale as $\langle \bar{\psi}_{1i}\psi_{1i}\rangle \sim \Lambda^2 \exp\left(-b/\sqrt{\lambda - \lambda_c}\right)$ where Λ is an ultraviolet (UV) cutoff. In the strong coupling phase, the condensate and therefore the charge gap are finite only when the coupling is tuned to be close to its critical value. The holographic construction examines this theory in the strong coupling limit, where $\lambda \gg \lambda_c$. In that limit, it is cutoff dependent and it can only be defined by introducing a systematic UV cutoff. We will find a string-inspired way to do this, tantamount to defining the model (6.1) as a limit of the IIB string theory which is finite and resolves the singularities. It will allow us to study the strong coupling limit using the string theory dual of this system.

When there are two monolayers, the field theory (6.1) can also have an inter-layer exciton condensate with order parameter $\langle \bar{\psi}_{1i}\psi_{2i}\rangle$. The results of reference [65] suggest that, with balanced charge densities and nested Fermi surfaces, the inter-layer condensate occurs even for very weak coupling. Not much is known as to how it would behave at strong coupling. It is the strong coupling limit of this model which we will now solve using its string theory dual.

The string theory dual of the defect field theory is the D3-probe-D7 brane system of IIB string theory[70]. A monolayer is a single stack of N_F D7 coincident branes. A double monolayer has two parallel stacks, one of N_F D7 branes and another of N_F anti-D7 branes separabilityted by a distance L. In both cases, the D7 brane stacks overlap $N >> N_F$ coincident D3 branes. With the appropriate orientation, the lowest energy states of open strings

which connect the D3 to the D7 branes are massless two-component relativistic Fermions that propagate on 2+1-dimensions and are the defect fields in (6.1). In the large N and strong coupling limits, the D3 branes are replaced by the $AdS_5 \times S^5$ background and solving the theory reduces to extremizing the classical Born-Infeld action $S \sim N_F T_{\rm D7} \int d^8\sigma \sqrt{-\det(\gamma + 2\pi\alpha' F)}$ for the D7 brane embedded with world-volume gauge field strength F and metric γ_{ab} in $AdS_5 \times S^5$. However, there is an immediate problem with this setup. Any D7 brane geometry which approaches the appropriate D7 brane boundary conditions at the boundary of AdS^5 is unstable. This is a reflection of the fact that the strong coupling limit of the quantum field theory on a single D7 brane is not conformally symmetric. We shall use a suggestion by Davis et.al. [44] who regulated the D7 brane by embedding it in the extremal black D3 brane geometry, with metric

$$\begin{aligned}\frac{ds^2}{R^2} &= \frac{r^2\left(-dt^2+dx^2+dy^2+dz^2\right)}{\sqrt{1+R^4r^4}} \\ &\quad + \sqrt{1+R^4r^4}\left(\frac{dr^2}{r^2} + d\psi^2 + \sin^2\psi \sum_{i=1}^{5} (d\theta^i)^2\right) \end{aligned} \tag{6.2}$$

where $\sum_{i=1}^{5}(\theta^i)^2 = 1.$ and $R^4 = \lambda\alpha'^2$. The asymptotic, large r limit of this metric is 10-dimensional Minkowski space. It has a horizon at $r = 0$. In the near horizon limit, which produces the IIB string on $AdS_5 \times S^5$, $rR \ll 1$, it approaches the Poincaré patch of $AdS_5 \times S^5$. Since R contains the string scale α', $1/R$ can be regarded as a (UV) cutoff.

The D7 and anti-D7 world-volumes are almost entirely determined by symmetry. They have 2+1-dimensional Poincaré invariance and wrap (t, x, y). The model (6.1) has an $SO(5)$ R-symmetry. The D7's must therefore wrap $(\theta^1, \ldots, \theta^5)$ to form an S^4. For the remaining world-volume coordinate, we use the radius r in (6.2). The dynamical variables are then $\psi(r)$ and the positions $z_1(r)$ and $z_2(r)$ of D7 and anti-D7, which by symmetry can only be functions of r. $\psi = \frac{\pi}{2}$ is a point of higher symmetry, corresponding to parity in the defect field theory with massless Fermions. $\psi(r) = \frac{\pi}{2} + \frac{c}{r^2} + \ldots$ is required to approach $\frac{\pi}{2}$ at $r \to \infty$ and, if it becomes r-dependent at all ($c \neq 0$), parity is broken by an intra-layer condensate. Parity can be restored if pairs of branes have condensates of opposite signs. This would break flavour symmetry when N_F is even, $U(N_F) \to U(N_F/2) \times U(N_F/2)$. Whether this sort of flavour symmetry breaking or parity and time reversal breaking takes place is an interesting dynamical question which will be studied elsewhere. Finally, it will turn out that, either $z_{1,2}(r)$ are constants, or

the D7 and anti-D7 meet and smoothly join together at a minimum radius, r_0. Asymptotically, $z_{1,2}(r) = \pm L/2 \mp R r_0^4/r^4 + \ldots$.

We have performed numerical computations to determine the lowest energy embeddings of the D7 (and anti-D7) branes as a function of the charge density (q) and the brane-anti-brane separation L. In the following we outline the results of these computations. The formalism for studying the embeddings of the probe D branes is already well-known in the literature and we refer the reader there for details. Examples for double monolayers can be found in references [54, 91, 93–96, 100]

When we suspend a single D7 brane in the black D3 brane metric (6.2), we find that the lowest energy solution truncates before it reaches the horizon. This is called a "*Minkowski embedding*". The function $\psi(r)$ moves from $\psi = \frac{\pi}{2}$ at $r \sim \infty$ to $\psi = 0$ or $\psi = \pi$ at the r where the brane pinches off. The S^4 which the world-volume wraps shrinks to a point there and this collapsing cycle is what makes the truncation smooth. This brane geometry is interpreted as a charge-gapped state. The lowest energy charged excitation is a fundamental string which would be suspended between the D7 brane and the horizon. In this case, that string has a minimum length and therefore a mass gap.

We can introduce a charge density q on the single monolayer. When the D7 brane carries a charge density, its world volume must necessarily reach the horizon. This is called a "*black hole embedding*". Charge in the quantum field theory corresponds to D7 brane world-volume electric field $E_r \sim q$. This hedgehog-like electric field points outward from the centre of the brane. The radial lines of flux of the electric field can only end if there are sources. Such sources would be fundamental strings, suspended between the D7 brane and the horizon. However, the strings have a larger tension than the D7 brane and they pull the the D7 brane to the horizon resulting in a gapless state. This is confirmed by numerical solutions of the embedding equation of a single brane and, indeed, we find that the S^4 which is wrapped by the world volume shrinks to a point as it enters the horizon. This state no longer has a charge gap. Even in the absence of a charge gap, we find that, for small charge densities, there is still an intra-layer exciton condensate. Our numerical studies show that it persists up to a quantum phase transition at a critical density $q_{\text{crit.}} \approx 0.0377/R^2$. At densities greater than the critical one, $\psi = \frac{\pi}{2}$, is a constant.

Now, consider the double monolayer with D7 and anti-D7 branes. A D7-anti-D7 pair of branes would tend to annihilate. We prevent this annihilation by requiring that they be separated by a distance L as they approach the boundary at $r \to \infty$. When their world volume enters the bulk, they can

still come together and annihilate – their world volumes fusing together at a minimal radius r_0. This competes with the tendency of a monolayer brane to pinch off at some radius. Indeed, when the charge density is zero, we see both behaviours. When the stacks of branes are near enough, that is, $L < L_c \simeq 2.31R$ is small enough, they join. This state has an inter-layer condensate. When they are farther apart, they remain un-joined. Instead, they pinch off to form Minkowski embedding, corresponding to a state with intra-layer condensates.

When we introduce balanced charges q and $-q$ on the D7 and anti-D7, respectively, there are four modes of behaviour which are summarized in table 6.1. Each of these behaviours occurs in the phase diagram in figure 6.1. Type 1 solutions are maximally symmetric with $\psi = \frac{\pi}{2}$ and $z_{1,2} =$

	$z_2 - z_1 = L$, const.	$z_2(r) - z_1(r) \to 0$ at r_0
$c = 0$	**Type 1** un-joined, $\psi = \frac{\pi}{2}$ BH, no condensate	**Type 2** joined, $\psi = \frac{\pi}{2}$ inter
$c \neq 0$	**Type 3** un-joined, $\psi(r)$ r-dependent Mink ($q = 0$) intra BH ($q \neq 0$) intra	**Type 4** joined, $\psi(r)$ r-dependent intra+inter only when $q \neq 0$

Table 6.1: Types of possible solutions for the balanced charge $(q, -q)$ case, where (Mink,BH) stand for (Minkowski,black-hole) embeddings.

$\pm L/2$. They occur in the white region of figure 6.1. They have no exciton condensates at all. Type 3 solutions occur in the red region. They have $\psi(r)$ a nontrivial function, but $z_{1,2} = \pm L/2$. The branes do not join. They are Minkowski embeddings when $q = 0$ and black hole embeddings when $q \neq 0$. Type 3 has an intra-layer exciton condensate only. There is a quantum phase transition between type 1 and type 3 solutions at $q_c = 0.0377$. Both type 1 and type 3 solutions occur only for very small layer separations, or order the UV cutoff. Type 2 solutions occupy the blue region. They have $\psi = \frac{\pi}{2}$, constant, $z_{1,2}(r)$ are nontrivial functions. The D7 and anti-D7 branes join at a radius, $r_0 \neq 0$. The intra-layer condensate vanishes and there is a non-zero inter-layer condensate. In type 4 solutions, both $\psi(r)$ and $z_{1,2}(r)$ have nontrivial profiles. The D7 and anti-D7 branes join and $\psi(r)$ also varies

with radius. This phase has both and inter- and intra-layer condensate. This solution exists only when q is nonzero and, then, only for small values of q. For $r_0 \simeq 0$ we have $q < 0.0377$, when r_0 grows, the allowed values of q decrease.

Consider a double monolayer with un-balanced charges, $Q > 0$ on the D7 and $-\bar{Q} < 0$ on the anti-D7 brane. The same argument as to why a single charged D7 brane must have a Minkowski embedding applies and, on the face of it, it is impossible for the branes to join before they reach the horizon. There is, however, another possibility which arises when there are more than one species of Fermions on each brane, that is, $N_F > 1$. In that case, one or more of the Fermion species can nest spontaneously, with the deficit of charge residing in the other species. This would break internal symmetry. For example, if $Q > \bar{Q} > 0$, k branes take up charge $\bar{Q}$ and the remaining $N_F - k$ take up the remainder $Q - \bar{Q}$, this would break $U(N_F) \times U(N_F) \to U(N_F - k) \times U(k) \times U(N_F - k) \times U(k)$. Then the branes with matched charges ($\bar{Q}$) would join, further breaking the symmetry $U(N_F - k) \times U(k) \times U(N_F - k) \times U(k) \to U(N_F - k) \times U(k) \times U(N_F - k)$. Then, $N_F - k$ charged D7 branes and $N_F - k$ uncharged anti-D7 branes either break parity or some of the remaining $U(N_F - k) \times U(N_F - k)$ symmetry. The uncharged branes must take up a Minkowski embedding. We have computed the energies of some of these symmetry breaking states for the case where $N_F = 2$. We find a range of charge densities where spontaneous nesting is energetically preferred. The implications of this idea for double monolayer physics is clear. The Fermion and hole densities of individual monolayers would not necessarily have to be fine tuned in order to nest the Fermi surfaces. It could happen spontaneously.

The intra-layer and inter-layer condensates discussed here have not been seen in graphene to date (with a possible exception [97]), presumably because the coupling is not strong enough. Our results show that the inter-layer condensation is extremely sensitive to Fermi surface nesting, even in the strong coupling limit. It would be interesting to better explore spontaneous nesting, since creating favourable conditions for it could be a way forward with graphene.

Chapter 7

Conclusion

P.S. please if you get a chanse put some flowers
on Algernons grave in the bak yard

- Flowers for Algernon by Daniel Keyes

In this thesis, we introduced why we need to study AdS/CFT correspondence and the key idea of the conjecture. We also showed how to apply the holographic duality to the concerned dual field theory, and presented the motivation of our project during the PhD program. I will summarize the previous chapters by exhibiting the research procedures and how and what we achieved as follows.

The first candidate we considered for dual model of double monolayer graphene is D3-probe-D7 model based on [37]. Because supersymmetry and conformal symmetry are completely broken for this model, the embedding is not stable. We turn on the internal fluxes to stabilize the model, and turn on an external magnetic field as well. I led the research to seeking a condition of stability of the double layer model and simulating and analyzing behaviors of the model. We finally analyzed *magnetic catalysis and inverse magnetic catalysis* for double monolayers [54]. This is presented in the chapter 3

This set-up in [54, 91] itself is very interesting, and recently it inverse magnetic catalysis research in QCD is active. However, there is a critical weak point that the model cannot contain intra-layer EC at all for our semimetal perspective. Thus, we leave the research for the future work. Instead, we employ an extremal black D3-brane geometry instead of AdS to imbed D7-branes [101]. It is presented in the chapter 6 and the appendix B.

We also introduce an external magnetic field[28] on the D3-probe-D5-branes to break supersymmetry and conformal symmetry and make fermion defects probe branes. D3 and probe D5-branes are no more in the BPS

[28]The dual field theory does not contain an external magnetic field. We could regard it as two form B gauge field in the supergravity background. They are equivalent in DBI action of the probe branes.

states, they act repulsive forces each other. The strength grows toward the Poincaré Killing horizon, D5-branes pinch off somewhere (Minkowski embedding). This has a mass gap. This is the gravity dual of the mass generation that accompanies intra-layer EC in a single monolayer. In the Fig. 1.15, the electric external gates would change the effective charge density. It is also known that a doped bilayer graphene also has a band gap. In a single monolayer to have a nonzero charge density, there must be a density of fundamental strings suspended between the D5-brane and the Poincaré horizon. However, the fundamental string tension is always greater than the D5-brane tension and such strings would therefore pull the D5-brane to the horizon(BH embedding). The result is a gapless state. For an infinite distance L between the layers in the phase diagram, we recover exactly the behavior of a single layer [102] where at $\mu \sim 2.9$(Asymptotic dotted line in the Fig. 1.15) the system undergoes a BKT transition between the intra-layer BH embedding phase to the chiral symmetric one. Note that the other dotted line is where the 1st order phase transition occurs. It is presented in the chapter 5.

We had studied how to introduce the charge density in the single monolayer model [102] and we present it in the appendix C. We showed the effect of internal fluxes are interestingly similar to that of charge density. It is presented in the chapter 2. It was essential to study the content in the chapter 5.

In the chapter 4 and the appendixB, we considered a holographic model of dynamical symmetry breaking in 2+1-dimenisons, where a parallel D7-anti-D7 brane pair fuse into a single object, corresponding to the $U(1) \times U(1) \to U(1)$ symmetry breaking pattern. We show that the current-current correlation functions can be computed analytically and exhibit the low momentum structure that is expected when global symmetries are spontaneously broken. We also find that these correlation functions have poles attributable to infinite towers of vector mesons with equally spaced masses.

Bibliography

[1] M. E. Peskin and D. V. Schroeder, "An introduction to quantum field theory," Perseus Books, 1995.

[2] A. Zee, "Quantum Field Theory in a Nutshell," Princeton University Press, 2003.

[3] M. B. Green, J. H. Schwarz, and E. Witten, Superstring Theory. Vols. 1 and 2, . Cambridge, Uk: Univ. Pr. (1987) (Cambridge Monographs On Mathematical Physics).

[4] J. Polchinski, String theory. Vols. 1 and 2, . Cambridge, UK: Univ. Pr. (1998).

[5] K. Becker, M. Becker, and J. H. Schwarz, String theory and M-theory: A modern introduction, Cambridge, UK: Cambridge Univ. Pr. (2007)

[6] We retrieved the following websites in 2010-10-01. Joseph Polchinski's homepage :
http://www.kitp.ucsb.edu/joep/,
John McGreevy's home page :
http://physics.ucsd.edu/∼mcgreevy/,
David Tong's lecture notes :
http://www.damtp.cam.ac.uk/user/tong/teaching.html,
Gordon Semenoff's string theory lecture:
http://www.phas.ubc.ca/*sim*gordonws/529/

[7] H. Georgi, Lie Algebras In Particle Physics: from Isospin To Unified Theories, Westview Press; 2nd ed. (1999)

[8] E. D'Hoker, D. Z. Freedman, "Supersymmetric gauge theories and the AdS / CFT correspondence," [hep-th/0201253].

[9] E. Witten, "Anti-de Sitter space and holography, " Adv. Theor. Math. Phys. **2** (1998) 253,hep-th/9802150

[10] E. Witten, "Anti-de Sitter space, thermal phase transition, and confinement in gauge theories," Adv. Theor. Math. Phys. 2, **505** (1998) [arXiv:hep-th/9803131].

[11] H. Nastase, "Introduction to AdS-CFT," (2007) [arXiv:0712.0689 [hep-th]].

[12] J. M. Maldacena, "The Large N limit of superconformal field theories and supergravity," Adv. Theor. Math. Phys. **2**, 231-252 (1998). [hep-th/9711200].

[13] J. Polchinski, Phys. Rev. Lett. **75**, 4724 (1995) [hep-th/9510017].

[14] O. Aharony, S. S. Gubser, J. M. Maldacena, H. Ooguri, Y. Oz, so called **MAGOO** "Large N field theories, string theory and gravity," Phys. Rept. **323**, 183-386 (2000). [hep-th/9905111].

[15] A. K. Geim, K. S. Novoselov, Nat. Mater. **6** 183 (2007); K. Novoselov, Nature Materials **6** 720 - 721 (2007); M. I. Katsnelson, Materials Today **10** 20 (2007).

[16] A. H. Castro Neto, F. Guinea, N. M. R. Peres, K. S. Novoselov, A. K. Geim, Rev. Mod. Phys. **81**, 109 (2009); A. H. Castro Neto, "Selected Topics in Graphene physics", [arXiv:1004.3682[cond-mat]

[17] Edward McCann, Mikito Koshino, "The electronic properties of bilayer graphene", Rep. Prog. Rep. Prog. Phys. **76**, 056503 (2013)

[18] We retrieved the information included in `http://mafija.fmf.uni-lj.si/seminar/files/2010_2011/zala_lenarcic.pdf` in 2011-07-01.

[19] S. A. Hartnoll, "Lectures on holographic methods for condensed matter physics," Class. Quant. Grav. **26**, 224002 (2009). [arXiv:0903.3246 [hep-th]].

[20] D. T. Son and A. O. Starinets, Ann. Rev. Nucl. Part. Sci. **57**, 95 (2007) [arXiv:0704.0240 [hep-th]].

[21] J. McGreevy, "Holographic duality with a view toward many-body physics," Adv. High Energy Phys. **2010**, 723105 (2010). [arXiv:0909.0518 [hep-th]].

[22] G. T. Horowitz and J. E. Santos, JHEP **1306**, 087 (2013) [arXiv:1302.6586 [hep-th]].

[23] E. Witten, "Bound States of Strings and p-Branes," Nucl. Phys. **B460** (1996) 335-350, hep-th/9510135.

[24] We retrieved the information included in `http://youtu.be/9pQwemGQ_gE` in 2015-10-01.

[25] We retrieved the information included in `http://spectrum.ieee.org/semiconductors/materials/graphene-makes-transistors-tunable` in 2015-10-01, and it is imaged by Emily Cooper.

[26] A. Karch, E. Katz, "Adding flavor to AdS / CFT," JHEP **0206**, 043 (2002). [arXiv:hep-th/0205236 [hep-th]].

[27] T. Sakai, S. Sugimoto, "Low energy hadron physics in holographic QCD," Prog. Theor. Phys. **113**, 843-882 (2005). [arXiv:hep-th/0412141 [hep-th]].

[28] T. Sakai, S. Sugimoto, "More on a holographic dual of QCD," Prog. Theor. Phys. **114**, 1083-1118 (2005). [hep-th/0507073].

[29] C. V. Johnson and A. Kundu, "External Fields and Chiral Symmetry Breaking in the Sakai-Sugimoto Model," JHEP **0812**, 053 (2008) [arXiv:0803.0038 [hep-th]].

[30] E. Antonyan, J. A. Harvey, S. Jensen, D. Kutasov, "NJL and QCD from string theory," [hep-th/0604017].

[31] E. Antonyan, J. A. Harvey, D. Kutasov, "Chiral symmetry breaking from intersecting D-branes," Nucl. Phys. **B784**, 1-21 (2007). [hep-th/0608177].

[32] A. Parnachev, D. A. Sahakyan, "Photoemission with Chemical Potential from QCD Gravity Dual," Nucl. Phys. **B768**, 177-192 (2007). [hep-th/0610247].

[33] J. L. Davis, M. Gutperle, P. Kraus, I. Sachs, "Stringy NJL and Gross-Neveu models at finite density and temperature," JHEP **0710**, 049 (2007). [arXiv:0708.0589 [hep-th]].

[34] O. Bergman, G. Lifschytz, M. Lippert, "Response of Holographic QCD to Electric and Magnetic Fields," JHEP **0805**, 007 (2008). [arXiv:0802.3720 [hep-th]].

[35] N. Evans and K. -Y. Kim, "Vacuum alignment and phase structure of holographic bi-layers", arXiv:1311.0149 [hep-th].

[36] R. C. Myers and M. C. Wapler, "Transport Properties of Holographic Defects," JHEP **0812**, 115 (2008) [arXiv:0811.0480 [hep-th]].

[37] O. Bergman, N. Jokela, G. Lifschytz and M. Lippert, "Quantum Hall Effect in a Holographic Model," arXiv:1003.4965 [hep-th].

[38] N. Jokela, G. Lifschytz, M. Lippert, "Magneto-roton excitation in a holographic quantum Hall fluid," JHEP **1102**, 104 (2011). [arXiv:1012.1230 [hep-th]].

[39] J. L. Davis, H. Omid, G. W. Semenoff, "Holographic Fermionic Fixed Points in d=3," [arXiv:1107.4397 [hep-th]].

[40] J. Polchinski, "String theory. Vol. 2: Superstring theory and beyond," Cambridge, UK: Univ. Pr. (1998) 531 p.

[41] J. Polchinski, "Dirichlet branes and Ramond-Ramond charges," Phys. Rev. Lett. 75 (1995) 4724 [arXiv:hep-th/9510017]

[42] P. Breitenlohner, D. Z. Freedman, "Positive Energy in anti-De Sitter Backgrounds and Gauged Extended Supergravity," Phys. Lett. **B115**, 197 (1982).

[43] P. Breitenlohner, D. Z. Freedman, "Stability in Gauged Extended Supergravity," Annals Phys. **144**, 249 (1982).

[44] J. L. Davis, P. Kraus, A. Shah, "Gravity Dual of a Quantum Hall Plateau Transition," JHEP **0811**, 020 (2008). [arXiv:0809.1876 [hep-th]].

[45] M. Kruczenski, D. Mateos, R.C. Myers and D.J. Winters, "Towards a holographic dual of large-Nc QCD," JHEP **0405** (2004) 041 [arXiv:hep-th/0311270].

[46] D. Mateos, R.C. Myers and R.M. Thomson, "Thermodynamics of the brane," JHEP **0705**, (2007) 067 [arXiv:hep-th/0701132].

[47] Y. Suprunenko, V. Cheianov, V. I. Fal'ko, arXiv:1206.5646; R. V. Gorbachev, A. K. Geim, M. I. Katsnelson, K. S. Novoselov, T. Tudorovskiy, I. V. Grigorieva, A. H. MacDonald, K. Watanabe, T. Taniguchi, L. A. Ponomarenko, arXiv:1206.6626.

[48] V. P. Gusynin, V. A. Miransky, I. A. Shovkovy, "Catalysis of dynamical flavor symmetry breaking by a magnetic field in (2+1)-dimensions," Phys. Rev. Lett. **73**, 3499-3502 (1994). [hep-ph/9405262].

[49] S. Nakamura, "Nonequilibrium Phase Transitions and Nonequilibrium Critical Point from AdS/CFT," Phys. Rev. Lett. 109, 120602 (2012) [arXiv:1204.1971 [hep-th]].

[50] S. Nakamura, "Negative Differential Resistivity from Holography," Prog. Theor. Phys. 124, 1105 (2010) [arXiv:1006.4105 [hep-th]]

[51] F. Preis, A. Rebhan, A. Schmitt, "Inverse magnetic catalysis in dense holographic matter," JHEP **1103**, 033 (2011). [arXiv:1012.4785 [hep-th]].

[52] V. G. Filev, C. V. Johnson, J. P. Shock, "Universal Holographic Chiral Dynamics in an External Magnetic Field," JHEP **0908**, 013 (2009). [arXiv:0903.5345 [hep-th]].

[53] V. G. Filev, R. C. Raskov, "Magnetic Catalysis of Chiral Symmetry Breaking. A Holographic Prospective," Adv. High Energy Phys. **2010**, 473206 (2010). [arXiv:1010.0444 [hep-th]].

[54] Joshua L. Davis and Namshik Kim, "Flavor-symmetry Breaking with Charged Probes," JHEP 1206 064 (2012) [arXiv:1109.4952[hep-th]].

[55] J. L. Davis, H. Omid and G. W. Semenoff, "Holographic Fermionic Fixed Points in d=3," JHEP 1109, 124 (2011) [arXiv:1107.4397 [hep-th]].

[56] D. Marolf and S. F. Ross, "Boundary Conditions and New Dualities: Vector Fields in AdS/CFT," JHEP 0611, 085 (2006) [hep-th/0606113].

[57] E. Witten, "Baryons in the 1/n Expansion," Nucl. Phys. B **160**, 57 (1979).

[58] E. Witten, "SL(2,Z) action on three-dimensional conformal field theories with Abelian symmetry," [hep-th/0307041].

[59] Jean-Loic Kneur, Marcus Benghi Pinto, Rudnei O. Ramos, "Phase diagram of the magnetized planar Gross-Neveu model beyond the large-N approximation," Phys.Rev.D88:045005, 2013 [arXiv:1306.2933 [hep-ph]].

[60] E. S. Fraga, B. W. Mintz, J. Schaffner-Bielich, "A search for inverse magnetic catalysis in thermal quark-meson models", [arXiv:1311.3964[hep-ph]].

[61] Falk Bruckmann, Gergely Endrodi, Tamas G. Kovacs, "Inverse magnetic catalysis in QCD", [arXiv:1311.3178[hep-lat]]

[62] E. M. Ilgenfritz, M. Muller-Preussker, B. Petersson, A. Schreiber, "Magnetic catalysis (and inverse catalysis) at finite temperature in two-color lattice QCD",[arXiv:1310.7876[hep-lat]]

[63] C. H. Zhang and Y.N. Joglekar, "Excitonic condensation of massless fermions in graphene bilayers", Phys. Rev. **B 77**, 233405 (2008).

[64] Yu. E. Lozovik, A. A. Sokolik, "Electron-hole pair condensation in graphene bilayer", Pis'ma v Zh. Eksper. Teoret. Fiz., **87**, 61 (2008).

[65] B. Seradjeh, H. Weber and M. Franz, "Vortices, zero modes and fractionalization in bilayer-graphene exciton condensate", Phys. Rev. Lett. **101**, 246404 (2008).

[66] H. Min, R. Bistritzer, J.-J. Su, A.H. MacDonald, "Room-temperature superfluidity in graphene bilayers", Phys. Rev. **B 78**, 121401 (2008).

[67] B. Seradjeh, J. E. Moore, M. Franz, "Exciton condensation and charge fractionalization in a topological insulator film", Phys. Rev. Lett. **103**, 066402 (2009).

[68] U. Lombardo and H. J. Schulze, Lect. Notes Phys. **578**, 30 (2001) [astro-ph/0012209].

[69] D. Kutasov, J. Lin and A. Parnachev, Nucl. Phys. B **858**, 155 (2012) [arXiv:1107.2324 [hep-th]].

[70] The probe D7 brane was first used as a model of graphene in: S.-J.Rey, Prog.Theor.Physics [Suppl.] **177** 128 (2009).

[71] K.G. Klimenko, "Three-dimensional Gross-Neveu model in an external magnetic field", Theor. Math. Phys. **89**, 1161 (1992).

[72] V.P. Gusynin, V.A. Miransky, I.A. Shovkovy, "Catalysis of dynamical flavor symmetry breaking by a magnetic field in (2+1)-dimensions", Phys. Rev. Lett. **73** (1994) 3499 [hep-ph/9405262]

[73] V.P. Gusynin, V.A. Miransky, I.A. Shovkovy, "Dynamical flavor symmetry breaking by a magnetic field in (2 + 1)-dimensions", Phys. Rev. **D 52** (1995) 4718 [hep-th/9407168]

[74] G. W. Semenoff, I. A. Shovkovy and L. C. R. Wijewardhana, "Phase transition induced by a magnetic field," Mod. Phys. Lett. A **13**, 1143 (1998) [arXiv:hep-ph/9803371].

[75] G. W. Semenoff, I. A. Shovkovy and L. C. R. Wijewardhana, "Universality and the magnetic catalysis of chiral symmetry breaking," Phys. Rev. D **60**, 105024 (1999) [arXiv:hep-th/9905116].

[76] V. G. Filev, C. V. Johnson and J. P. Shock, "Universal Holographic Chiral Dynamics in an External Magnetic Field," JHEP **0908**, 013 (2009) [arXiv:0903.5345 [hep-th]].

[77] G. W. Semenoff and F. Zhou, "Magnetic Catalysis and Quantum Hall Ferromagnetism in Weakly Coupled Graphene," JHEP **1107**, 037 (2011) [arXiv:1104.4714 [hep-th]].

[78] S. Bolognesi and D. Tong, "Magnetic Catalysis in AdS4," Class. Quant. Grav. **29**, 194003 (2012) [arXiv:1110.5902 [hep-th]].

[79] J. Erdmenger, V. G. Filev and D. Zoakos, "Magnetic catalysis with massive dynamical flavours," arXiv:1112.4807 [hep-th].

[80] S. Bolognesi, J. N. Laia, D. Tong and K. Wong, "A Gapless Hard Wall: Magnetic Catalysis in Bulk and Boundary," JHEP **1207**, 162 (2012) [arXiv:1204.6029 [hep-th]].

[81] I. A. Shovkovy, "Magnetic Catalysis: A Review," arXiv:1207.5081 [hep-ph].

[82] M. Blake, S. Bolognesi, D. Tong and K. Wong, "Holographic Dual of the Lowest Landau Level," JHEP **1212**, 039 (2012) [arXiv:1208.5771 [hep-th]].

[83] V. G. Filev and M. Ihl, "Flavoured Large N Gauge Theory on a Compact Space with an External Magnetic Field," arXiv:1211.1164 [hep-th].

[84] C. Kristjansen and G. W. Semenoff, "Giant D5 Brane Holographic Hall State", JHEP **1306**, 048 (2013) [arXiv:1212.5609 [hep-th]].

[85] C. Kristjansen, R. Pourhasan and G. W. Semenoff, "A Holographic Quantum Hall Ferromagnet", arXiv:1311.6999 [hep-th].

[86] Kentaro Nomura and Allan H. MacDonald, "Quantum Hall Ferromagnetism in Graphene", Phys. Rev. Lett. **96**, 256602

[87] A. Karch and L. Randall, "Open and closed string interpretation of SUSY CFT's on branes with boundaries," JHEP **0106**, 063 (2001) [arXiv:hep-th/0105132].

[88] A. Karch and L. Randall, "Locally localized gravity," JHEP **0105**, 008 (2001) [arXiv:hep-th/0011156].

[89] O. DeWolfe, D. Z. Freedman and H. Ooguri, Phys. Rev. D **66**, 025009 (2002) [hep-th/0111135].

[90] J. Erdmenger, Z. Guralnik and I. Kirsch, Phys. Rev. D **66**, 025020 (2002) [hep-th/0203020].

[91] Grignani Grignani, Namshik Kim and Gordon W. Semenoff, "D7-anti-D7 bilayer: holographic dynamical symmetry breaking," Phys. Lett. B **722**, 360 (2013) [arXiv:1208.0867 [hep-th]].

[92] Grignani Grignani, Namshik Kim and Gordon W. Semenoff, "D3-D5 Holography with Flux," Phys. Lett. B **715**, 225 (2012) [arXiv:1203.6162 [hep-th]].

[93] J. Sonner, "On universality of charge transport in AdS/CFT," JHEP **1307**, 145 (2013) [arXiv:1304.7774 [hep-th]].

[94] N. Evans and K. Y. Kim, "Vacuum alignment and phase structure of holographic bi-layers," Phys. Lett. B **728**, 658 (2014) [arXiv:1311.0149 [hep-th]].

[95] V.G. Filev, "A Quantum Critical Point from Flavours on a Compact Space," JHEP **1408**, 105 (2014) [arXiv:1406.5498 [hep-th]].

[96] V.G. Filev, M. Ihl and D. Zoakos, "Holographic Bilayer/Monolayer Phase Transitions," JHEP **1407**, 043 (2014) [arXiv:1404.3159 [hep-th]]; JHEP **1312**, 072 (2013) [arXiv:1310.1222 [hep-th]].

[97] F. Amet, J. R. Williams, K. Watanabe, T. Taniguchi, and D. Goldhaber-Gordon Phys. Rev. Lett. **110**, 216601 (2013).

[98] G. W. Semenoff, "Condensed Matter Simulation Of A Three-Dimensional Anomaly," Phys. Rev. Lett. **53**, 2449 (1984).

[99] N. Evans, A. Gebauer, K. -Y. Kim and M. Magou, "Phase diagram of the D3/D5 system in a magnetic field and a BKT transition," Phys. Lett. B **698**, 91 (2011) [arXiv:1003.2694 [hep-th]].

[100] G. Grignani, N. Kim, A. Marini and G. W. Semenoff, "Holographic D3-probe-D5 Model of a Double Layer Dirac Semimetal," JHEP **1412**, 091 (2014) [arXiv:1410.4911 [hep-th]].

[101] G. Grignani, A. Marini, N. Kim and G. W. Semenoff, "Exciton Condensation in a Holographic Double Monolayer Semimetal," arXiv:1410.3093 [hep-th].

[102] K. Jensen, A. Karch, D. T. Son and E. G. Thompson, "Holographic Berezinskii-Kosterlitz-Thouless Transitions," Phys. Rev. Lett. **105**, 041601 (2010) [arXiv:1002.3159 [hep-th]].

[103] S. S. Pal, Phys. Rev. D **82**, 086013 (2010) [arXiv:1006.2444 [hep-th]].

[104] S. Kobayashi, D. Mateos, S. Matsuura, R. C. Myers and R. M. Thomson, "Holographic phase transitions at finite baryon density," JHEP **0702**, 016 (2007) [hep-th/0611099].

[105] D. S. L. Abergel, M. Rodriguez-Vega, Enrico Rossi, S. Das Sarma, "inter-layer excitonic superfluidity in graphene", Phys. Rev. **B 88**, 235402 (2013), arXiv:1305:4936 [cond-mat] (2013).

[106] A. Gamucci, D. Spirito, M. Carrega, B. Karmakar, A. Lombardo, M. Bruna, A. C. Ferrari, L. N. Pfeiffer, K. W. West, Marco Polini, V. Pellegrini, "Electron-hole pairing in graphene-GaAs heterostructures", arXiv:1401.0902 [cond-mat.mes-hall].

[107] A. A. High, J. R. Leonard, A. T. Hammack, M. M. Fogler, L. V. Butov, A. V. Kavokin, K. L. Campman, A. C. Gossard, "Spontaneous Coherence in a Cold Exciton Gas", Nature **483**, 584-588 (2012), arXiv:1109.0253.

[108] A. A. High, J. R. Leonard, M. Remeika, L. V. Butov, M. Hanson, A. C. Gossard, "Spontaneous coherence of indirect excitons in a trap", Nano Lett., **2012**, 12 (5), pp 2605-2609, arXiv:1110.1337 (2011).

[109] S. Utsunomiya, L. Tian, Roumpos, C. W. Lai, N. Kumada, T. Fujisawa, M. Kuwata-Gonokami, A. Loefler, S. Hoeling, A. Forchel and Y. Yamamoto, "Observation of Bogoliubov excitations in exciton-polariton condensates", Nature Physics **4**, 700 (2008).

[110] K. G. Lagoudakis, M. Wouters, M. Richard, A. Baas, I. Carusotto, R. Andre, L. S. Dang, B. Deveaud-Pledran, "Quantized vortices in an exciton-polariton condensate", Nature Physics, **4**,(9), 706-710.

[111] D. Nandi, A. D. K. Finck, J. P. Eisenstein, L. N. Pfeiffer, K. W. West, "Exciton condensation and perfect Coulomb drag", Nature **488**, 481-484 (2012).

[112] S. Banerjee, L. Register, E. Tutuc, D. Reddy, A. MacDonald, "Bilayer Pseudospin Field-effect Transistor (BiSFET), a proposed new logic device", Electron Device Letters, IEEE **30**, 158 (2009).

[113] A. A. High, E. E. Novitskaya, L. V. Butov and A. C. Gossard, "Control of exciton fluxes in an excitonic integrated circuit." Science **321**, 229-231 (2008).

[114] Y. Y. Kuznetsova, M. Remeika, A. A. High, A. T. Hammack, L. V. Butov, M. Hanson, M and A. C. Gossard, "All- optical excitonic transistor", Optics Lett. **35**, 1587-1589 (2010).

[115] D. Ballarini, M. De Giorgi, E. Cancellieri, R. Houdré, E. Giacobino, R. Cingolani, A. Bramati, G. Gigli, G. and D. Sanvitto, "All-optical polariton transistor", Nature Comm. **4**, 1778 (2013).

[116] F. Dolcini, D. Rainis, F. Taddei, M. Polini,R. Fazio and A. H. MacDonald, "Blockade and counterflow supercurrent in exciton-condensate Josephson junctions", Phys. Rev. Lett. **104**, 027004 (2010).

[117] S. Peotta, M. Gibertini, F. Dolcini, F. Taddei, M. Polini, L. B. Ioffe, R. Fazio and A. H. MacDonald, "Joseph- son current in a four-terminal superconductor/exciton- condensate/superconductor system", Phys. Rev. **B 84**, 184528 (2011).

[118] R.V. Gorbachev, A.K. Geim, M.I. Katsnelson, K.S. Novoselov, T. Tudorovskiy, I.V. Grigorieva, A.H. MacDonald, S.V. Morozov, K. Watanabe, T. Taniguchi, L.A. Ponomarenko, "Strong Coulomb drag and broken symmetry in double-layer graphene", Nat. Phys. **8**, 896 (2012).

[119] S. Kim, I. Jo, J. Nah, Z. Yao, S. K. Banerjee and E. Tutuc, "Coulomb drag of massless fermions in graphene", Phys. Rev. **B 83**, 161401 (2011).

[120] D. Neilson, A. Perali, A. R. Hamilton, "Excitonic superfluidity and screening in electron-hole bilayer systems", Phys. Rev. **B 89**, 060502 (2014)

[121] Z.F. Ezawa, K. Hasebe, "Inter-layer exchange interactions, SU(4) soft waves, and skyrmions in bilayer quantum Hall ferromagnets," Phys. Rev. **B65**, 075311 (2002).

[122] S.Q. Murphy, J.P. Eisenstein, G.S. Boebinger, L.W. Pfeiffer, K.W. West, "Many-body integer quantum Hall effect: Evidence for new phase transitions," Phys. Rev. Lett. **72**, 728 (1994).

[123] K. Moon, H. Mori, K. Yang, S. M. Girvin, A .H .MacDonald, I. Zheng, D. Yoshioka, S.-C. Zhang, 'Spontaneous inter-layer coherence in double-layer quantum Hall systems: Charged vortices and Kosterlitz-Thouless phase transitions'', Phys. Rev. **B 51**, 5143 (1995).

[124] Y. Zhang, Z. Jiang, J. P. Small, M. S. Purewal, Y. W. Tan, M. Fazlollahi, J. D. Chudow, J. A. Jaszczak, H. L. Stormer, P. Kim, " Landau-level splitting in graphene in high magnetic fields", Phys. Rev. Lett. **96**, 136806 (2006).

[125] A. F. Young, C. R. Dean, L. Wang, H. Ren, P. Cadden-Zimansky, K. Watanabe, T. Taniguchi, J. Hone, K. L. Shepard, P. Kim, "Spin and valley quantum Hall ferromagnetism in graphene", Nature Physics, **8**, 553-556 (2012).

[126] D. A. Abanin, K. S. Novoselov , U. Zeitler, P. A.Lee, A. K. Geim, L. S. Levitov, "Dissipative Quantum Hall Effect in Graphene near the Dirac Point", Phys. Rev. Lett. **98**, 196806 (2007)

[127] J. G. Checkelsky, L. Li, N. P. Ong, "The zero-energy state in graphene in a high magnetic field", Phys. Rev. Lett. **100**, 206801 (2008).

[128] J. G. Checkelsky, L. Li, N. P. Ong, "Divergent resistance at the Dirac point in graphene: Evidence for a transition in a high magnetic field", Phys. Rev. **B79**, 115434 (2009).

[129] H.A. Fertig, "Energy spectrum of a layered system in a strong magnetic field," Phys. Rev. **B40**, 1087(1989).

[130] T. Jungwirth and A.H. MacDonald, "Pseudospin anisotropy classification of quantum Hall ferromagnets," Phys. Rev. **B63**, 035305 (2000).

[131] D. V. Khveshchenko, "Magnetic field-induced insulating behaviour in highly oriented pyrolitic graphite", Phys. Rev. Lett. **87**. 206401 (2001), [arXiv:cond-mat/0106261].

[132] K. Nomura, A. H. MacDonald, "Quantum Hall ferromagnetism in graphene", Phys. Rev. Lett. **96**, 256602 (2006).

[133] M. O. Goerbig, "Electronic properties of graphene in a strong magnetic field", Rev. Mod. Phys. **83**, 1193"1243 (2011).

[134] Y. Barlas, K. Yang, A. Macdonald, "Quantum Hall effects in graphene-based two-dimensional electron systems", Nanotechnology **12**, 052001 (2012).

Appendix A

Some Calculations for Chapter 4.

The Lagrangian we are intrested in is

$$\mathcal{L} = (1+f^2)r^2\sqrt{1+r^4\dot{z}(r)^2} \mp f^2.r^4\dot{z}(r) \tag{A.1}$$

$z(r)$ is a cyclic variable, and the equation of the motion is

$$\frac{d}{dr}\left[\frac{(1+f^2)r^6\dot{z}}{\sqrt{1+r^4\dot{z}(r)^2}} \mp f^2r^4\right] . = 0 \tag{A.2}$$

The solution for the equationA.2 is

$$z_\pm(r) = \pm\frac{L}{2} \mp \int_r^\infty dr\dot{z}_+(r).$$

This $z_\pm$ is the position of the brane to the right (+) or left (-) of $z = 0$, and $\dot{z}_\pm$ is

$$\dot{z}_\pm(r) = \pm\frac{f^2r^4+P}{r^2\sqrt{(r^4-P)((1+2f^2)r^4+P)}}.$$

P is an integration constant proportional to the pressure needed to hold the branes with their asymptotic separation L.

$$\frac{(1+f^2)r^6\dot{z}}{\sqrt{1+r^4\dot{z}(r)^2}} \mp f^2r^4 = \pm P \tag{A.3}$$

When they are not joined, they do not interact, at least in this classical limit, and P must be zero. When they are joined, P must be nonzero and they are joined at a minimum radius $r_0 = P^{\frac{1}{4}}$ and L and P are related by

$$\begin{aligned} LP^{\frac{1}{4}} &= 2\int_1^\infty dr\frac{f^2r^4+1}{r^2\sqrt{(r^4-1)((1+2f^2)r^4+1)}} \\ &= \frac{\pi^{3/2}\left(3f^2\,{}_2F_1\left(\frac{1}{4},\frac{1}{2};\frac{3}{4};\frac{1}{-2f^2-1}\right) + {}_2F_1\left(\frac{1}{2},\frac{5}{4};\frac{7}{4};\frac{1}{-2f^2-1}\right)\right)}{4\sqrt{2+4f^2}\Gamma\left(\frac{3}{4}\right)\Gamma\left(\frac{7}{4}\right)} \end{aligned} \tag{A.4}$$

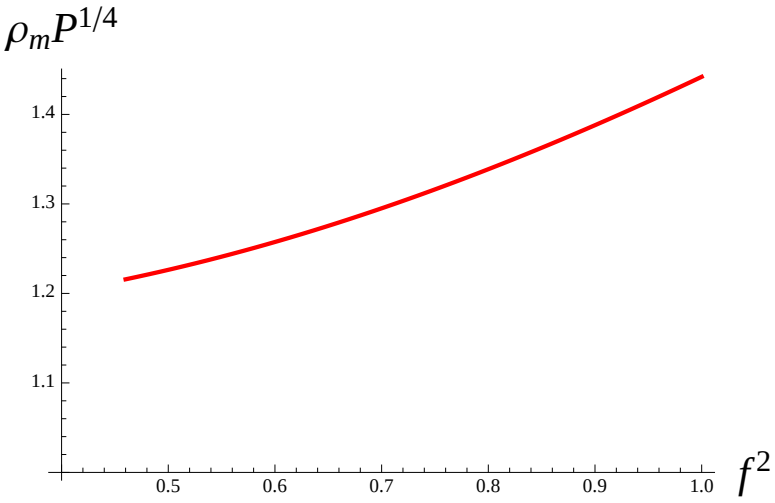

Figure A.1: ρ_m as a function of f^2.

We have redefined the radial coordinate as

$$\rho = \int_r^\infty \frac{dr}{r^2}\sqrt{1+r^4\dot{z}^2}$$

To analyze the joined configuration, we note that in that case ρ reaches a maximum

$$\rho_m = \frac{(1+f^2)}{r_0}\int_0^1 \frac{dx}{\sqrt{(1-x^4)((1+2f^2)-x^4)}} \tag{A.5}$$

$$= \frac{\sqrt{\pi}\left(f^2+1\right)\Gamma\left(\frac{5}{4}\right)\,{}_2F_1\left(\frac{1}{4},\frac{1}{2};\frac{3}{4};\frac{1}{-2f^2-1}\right)}{r_0\sqrt{2f^2+1}\Gamma\left(\frac{3}{4}\right)} \tag{A.6}$$

$$= \frac{L}{2}\frac{\int_0^1 \frac{dx(1+f^2)}{\sqrt{(1-x^4)((1+2f^2)-x^4)}}}{\int_0^1 \frac{dx(f^2+x^4)}{\sqrt{(1-x^4)((1+2f^2)-x^4)}}} \tag{A.7}$$

$$= \frac{3L\left(f^2+1\right)}{2\left(\frac{{}_2F_1\left(\frac{1}{2},\frac{5}{4},\frac{7}{4};\frac{1}{-2f^2-1}\right)}{{}_2F_1\left(\frac{1}{4},\frac{1}{2},\frac{3}{4};\frac{1}{-2f^2-1}\right)}+3f^2\right)} \tag{A.8}$$

A plot of eq.(A.6) is given in Fig.A.5.

The regularized energy can be computed as the difference between the on-shell actions of the joined solution and that of the disjoined one. It is

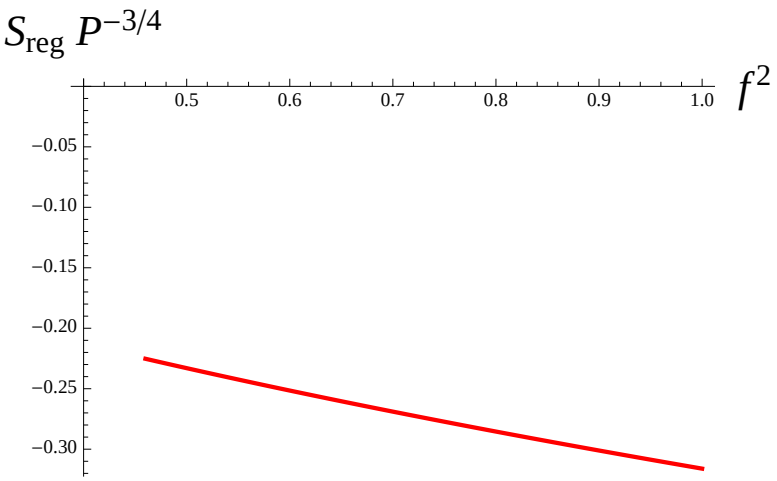

Figure A.2: Regularized energy, it is always negative, the joined solution has always lower energy.

given by

$$S_{\text{reg}} = \int_{r_0}^{\infty} dr \left(\frac{\left(2f^2+1\right) r^6 - f^2 r^2 r_0^4}{\sqrt{\left(r^4 - r_0^4\right)\left(\left(2f^2+1\right) r^4 + r_0^4\right)}} - \sqrt{2f^2+1} r^2 \right) - \int_0^{r_0} dr \sqrt{2f^2+1} r^2$$

This can be computed exactly

$$S_{\text{reg}} = -\frac{\pi^{3/2} r_0^3 \left(3f^2\, {}_2F_1\left(\frac{1}{4}, \frac{1}{2}; \frac{3}{4}; \frac{1}{-2f^2-1}\right) + {}_2F_1\left(\frac{1}{2}, \frac{5}{4}; \frac{7}{4}; \frac{1}{-2f^2-1}\right)\right)}{18\sqrt{4f^2+2}\,\Gamma\left(\frac{3}{4}\right)^2}$$

and from its plot in Fig.A.2 it seems smooth and always negative for $23/50 < f^2 < 1$.

From these results it is simple to compute the energy as a function of L, which is simply given by the confining potential

$$S_{\text{reg}} = -\frac{P}{6} L \tag{A.9}$$

Appendix B

The Phase Diagram of D3-probe-D7 System

We present the detail numerical procedure to obtain the phase diagram 6.1 in the chapter 6.

B.1 Geometry of branes

We consider a pair of probe branes, a D7 brane and an anti-D7 suspended in the asymptotically flat D3-brane solution. We use coordinates where the metric background is

$$ds^2 = \left(1+\frac{R^4}{r^4}\right)^{-1/2}\left(-dt^2+dx^2+dy^2+dz^2\right)+\left(1+\frac{R^4}{r^4}\right)^{1/2}\left(dr^2+r^2d^2\Omega_5\right) \tag{B.1}$$

and

$$d^2\Omega_5 = d\psi^2+\sin^2\psi d^2\Omega_4 \tag{B.2}$$

where we have written the geometry to display the directions the D3 lie in (t,x,y,z). We then introduce the coordinates

$$\rho = r\sin\psi\ , \qquad l = r\cos\psi$$

so that the metric (6.2) becomes

$$\begin{aligned} ds^2 = &\left(1+\frac{R^4}{(\rho^2+l^2)^2}\right)^{-1/2}\left(-dt^2+dx^2+dy^2+dz^2\right) \\ &+\left(1+\frac{R^4}{(\rho^2+l^2)^2}\right)^{1/2}\left(d\rho^2+dl^2+\rho^2d^2\Omega_4\right) \end{aligned} \tag{B.3}$$

We make an ansatz for the D7 brane and anti-D7 brane geometries where they both fill the directions x,y,t,ρ and wrap the $S^4\subset S^5$ according to

	t	x	y	z	ρ	l	θ_1	θ_2	θ_3	θ_4
D3	$\times$	$\times$	$\times$	$\times$						
D7/$\overline{\text{D7}}$	$\times$	$\times$	$\times$	$z(\rho)$	$\times$	$l(\rho)$	$\times$	$\times$	$\times$	$\times$

(B.4)

They sit at points in the remainder of the directions z, l and the points $z(\rho), l(\rho)$ generally depend on ρ. The wrapped S^4 has an $SO(5)$ symmetry. The geometry of the D7 brane and anti-D7 brane are both given by the ansatz

$$\begin{aligned} ds^2 = &\left(1+\frac{R^4}{(\rho^2+l^2)^2}\right)^{-1/2}\left(-dt^2+dx^2+dy^2\right) \\ &+\left(1+\frac{R^4}{(\rho^2+l^2)^2}\right)^{1/2}\left(d\rho^2\left(1+l'(\rho)^2+\frac{z'(\rho)^2}{1+\frac{R^4}{(\rho^2+l^2)^2}}\right)+\rho^2 d^2\Omega_4\right) \end{aligned} \tag{B.5}$$

The introduction of a charge density requires D7 world-volume gauge fields. In the $a_\rho = 0$ gauge, the field strength 2-form F is given by

$$2\pi l_s^2 F = a_0'(\rho) d\rho \wedge dt \tag{B.6}$$

In this expression, $a_0(\rho)$ will result in the world volume electric field which is needed in order to have a nonzero $U(1)$ charge density in the quantum field theory. The temporal gauge field A_0 are defined in terms of it as

$$a_0 = 2\pi l_s^2 A_0 \tag{B.7}$$

In this Section, we will use the field strength (B.6) for both the D7 brane and the anti-D7 brane.

The asymptotic behavior at $\rho \to \infty$ for the embedding functions in (B.5) is

$$l(\rho) \to m + \frac{c}{\rho^3} + \dots \tag{B.8}$$

and the D7 brane and anti-D7 brane are separated by a distance L,

$$z(\rho) \to \frac{L}{2} - \frac{\rho_0^4}{\rho^4} + \dots \tag{B.9}$$

for the D7 brane and

$$z(\rho) \to -\frac{L}{2} + \frac{\rho_0^4}{\rho^4} + \dots \tag{B.10}$$

for the anti-D7 brane. The asymptotic behavior of the gauge field (B.6) is

$$a_0(\rho) = \mu - \frac{q}{\rho^4} + \dots \tag{B.11}$$

with μ and q related to the chemical potential and the charge density, respectively.

There are two constants which specify the asymptotic behavior in each of the above equations. In all cases, we are free to choose one of the two constants as a boundary condition, for example we could choose m, q, ρ_0. Then, the other constants, c, μ, L, are fixed by requiring that the solution is non-singular.

We will only consider solutions where the boundary condition is $m = 0$. This is the chiral symmetric boundary condition. Its equivalent in the dual gauge theory is obtained by specifying that the hypermultiplet is massless and the theory has chiral symmetry. Then, when we solve the equation of motion for $l(\rho)$, there are two possibilities. First $c = 0$ and $l(\rho) = 0$, a constant for all values of ρ. This is the chirally symmetric phase. Secondly, $c \neq 0$ and l is a non-constant function of ρ. This describes the phase with spontaneously broken chiral symmetry. The constant c is proportional to the intra-layer chiral condensate $\langle \bar{\psi}_1 \psi_1 \rangle$ for the D7 brane and $\langle \bar{\psi}_2 \psi_2 \rangle$ for the anti-D7 brane.

To be more general, we will consider consider a stack of N_f D5-branes and N_f anti-D7 branes. The Born Infeld action for either the stack of D7 or anti-D7 branes is given by

$$S = \mathcal{N}_7 \int d\rho \rho^4 \sqrt{\left(1 + \frac{R^4}{(l^2 + \rho^2)^2}\right)(1 - a_0{}'^2 + l'^2) + z'^2} \tag{B.12}$$

where

$$\mathcal{N}_7 = \frac{N_f}{48\pi^5 l_s^8 g_s} V_{2+1}$$

with V_{2+1} the volume of the 2+1-dimensional space-time, l_s the string length, g_s the string coupling and N_F the number of D7 branes. The Wess-Zumino terms that occur in the D brane action will not play a role in the D7 brane problem.

The variational problem of extremizing the Born-Infeld action (B.12) involves two cyclic variables, $a_0(\rho)$ and $z(\rho)$. Being cyclic, their canonical

momenta must be constants,

$$Q = -\frac{\delta S}{\delta a_0'} \equiv 2\pi l_s^2 \mathcal{N}_7 q \ , \qquad q = \frac{\rho^4 {a_0}' \left(2\rho^2 l^2 + l^4 + \rho^4 + R^4\right)}{\left(l^2+\rho^2\right)^2 \sqrt{\frac{(2\rho^2 l^2 + l^4 + \rho^4 + R^4)(1 - {a_0}'^2 + l'^2)}{\left(l^2+\rho^2\right)^2} + z'^2}} \tag{B.13}$$

$$\Pi_z = \frac{\delta S}{\delta z'} \equiv \mathcal{N}_7 \rho_0^4 \ , \qquad \rho_0^4 = \frac{\rho^4 z'}{\sqrt{\frac{(2\rho^2 l^2 + l^4 + \rho^4 + R^4)(1 - {a_0}'^2 + l'^2)}{\left(l^2+\rho^2\right)^2} + z'^2}} \ , \tag{B.14}$$

Solving (B.13) and (B.14) for $a_0'(\rho)$ and $z'(\rho)$ in terms of q and ρ_0 we get

$$a_0' = -\frac{q\left(l^2+\rho^2\right)\sqrt{1+l'^2}}{\sqrt{l^2\left(l^2+2\rho^2\right)\left(\rho^8+q^2-\rho_0^8\right)+q^2\rho^4+\left(\rho^8-\rho_0^8\right)\left(\rho^4+R^4\right)}} \tag{B.15}$$

$$z' = \frac{\rho_0^4\left(l^4+2l^2\rho^2+\rho^4+R^4\right)\sqrt{1+l'^2}}{\left(l^2+\rho^2\right)\sqrt{l^2\left(l^2+2\rho^2\right)\left(\rho^8+q^2-\rho_0^8\right)+q^2\rho^4+\left(\rho^8-\rho_0^8\right)\left(\rho^4+R^4\right)}} \tag{B.16}$$

We can now use the Legendre transformed action to find $l(\rho)$ for fixed ρ_0 and fixed charge q, eliminating $a_0'(\rho)$ and $z'(\rho)$ using equations (B.15) and (B.16).

After scaling out the parameter R, $(\rho, l, z, a_0) \to R(\rho, l, z, a_0)$, such a Routhian reads

$$\begin{aligned}\mathcal{R} &= \frac{S}{\mathcal{N}_7} - \rho_0^4 \int d\rho z'(\rho) - q \int d\rho a_0'(\rho) \\ &= \int d\rho \frac{\sqrt{\left(1+l'^2\right)\left(l^4\left(\rho^8+q^2-\rho_0^8\right)+2l^2\rho^2\left(\rho^8+q^2-\rho_0^8\right)+q^2\rho^4+\left(\rho^4+1\right)\left(\rho^8-\rho_0^8\right)\right)}}{l^2+\rho^2}\end{aligned} \tag{B.17}$$

The Euler-Lagrange equation for $l(\rho)$ can be derived by varying the Routhian (B.17) and reads

$$\begin{aligned}&\left(l^2+\rho^2\right) l''\left(l^2\left(l^2+2\rho^2\right)\left(\rho^8+q^2-\rho_0^8\right)+q^2\rho^4+\left(\rho^4+1\right)\left(\rho^8-\rho_0^8\right)\right) \\ &+2\left(1+l'^2\right)\left(\rho l'\left(2l^2\rho^6\left(l^4+3l^2\rho^2+3\rho^4+1\right)+2\rho^{12}+\rho^8+\rho_0^8\right)+l\left(\rho^8-\rho_0^8\right)\right)=0\end{aligned} \tag{B.18}$$

This equation must be solved with the boundary conditions in equation (B.8)-(B.11) (recalling that we can choose only one of the integration constants, the other being fixed by regularity of the solution) in order to find the function $l(\rho)$. Once we know that function, we can integrate equations (B.15) and (B.16) to find $a_0(\rho)$ and $z(\rho)$.

Clearly, $l = 0$, a null constant, for all values of ρ, is always a solution of equation (B.18), even when ρ_0 and the charge density are nonzero. However, for some range of the parameters, it will not be the most stable solution.

Using the asymptotic behavior (B.8) with $m = 0$ and $c = c$, the solution, up to the order 23 in the $\frac{1}{\rho}$ expansion, has the form

$$\begin{aligned}l(\rho) &= \frac{c}{\rho^3} - \frac{2c}{7\rho^7} + \frac{c\left(189c^2-21q^2+21\rho_0^8+22\right)}{154\rho^{11}} - \frac{c\left(807c^2-86q^2+31\rho_0^8+44\right)}{495\rho^{15}} \\ &+\frac{c\left(2525985c^4+c^2\left(-561330q^2+561330\rho_0^8+930444\right)+31185q^4-2q^2\left(31185\rho_0^8+48241\right)+31185\rho_0^{16}+20032\rho_0^8+32648\right)}{526680\rho^{19}} \\ &-\frac{c\left(2476927215c^4-174c^2\left(3057600q^2-2010225\rho_0^8-2193536\right)+7\left(4086075q^4-2q^2\left(2508030\rho_0^8+2776603\right)+929985\rho_0^{16}+798676\rho_0^8+1403864\right)\right)}{211988700\rho^{23}}+O\left(\left(\frac{1}{\rho}\right)^{27}\right)\end{aligned}$$

in terms of the modulus c.

B.2 Double monolayers without charge density

The equation of motion for l in this case is

$$\begin{aligned}&\left(l^2+\rho^2\right) l''\left(l^2\left(l^2+2\rho^2\right)\left(\rho^8-\rho_0^8\right)+\left(\rho^4+1\right)\left(\rho^8-\rho_0^8\right)\right)\\&+2\left(1+l'^2\right)\left(\rho l'\left(2l^2\rho^6\left(l^4+3l^2\rho^2+3\rho^4+1\right)+2\rho^{12}+\rho^8+\rho_0^8\right)+l\left(\rho^8-\rho_0^8\right)\right)=0\end{aligned} \tag{B.19}$$

There are in principle four type of solutions for which $m = 0$ in (B.8):

1. Unconnected, constant $l = 0$ solution that reaches the Poincaré horizon, $l = 0$ *and* $\rho = 0$, *i.e.* a black-hole (BH) embedding.
2. A connected constant $l = 0$ solution.
3. A ρ-dependent unconnected solution with $\rho_0 = 0$, where the brane pinches off ($\rho = 0$) before reaching the Poincaré horizon, *i.e.* a Minkowski embedding.
4. A connected ρ-dependent solution.

These solutions are summarized in the following table. We look for solution with $m = 0$ in (B.8). We can distinguish four types of solutions according to the classification of table B.1.

	$\rho_0 = 0$	$\rho_0 \neq 0$
$c = 0$	**Type 1** unconnected, $l = 0$ BH, chiral symm.	**Type 2** connected, $l = 0$ Mink, inter
$c \neq 0$	**Type 3** unconnected, ρ-dependent l Mink, intra	**Type 4** connected, ρ-dependent l Mink, intra/inter

Table B.1: Types of possible solutions, where Mink stands for Minkowski embeddings and BH for black-hole embeddings.

Type 1 solutions are trivial both in l and z (they are both constants). They correspond to two parallel black hole (BH) embeddings for the D7 and the anti-D7. This configuration is the chiral symmetric one. However,

by studying the fluctuations around this solution we will show in the next section that it is unstable,

In type 2 solutions the chiral symmetry is broken by the inter-layer condensate ($\rho_0 \neq 0$). In this case the branes have non flat profiles in the z direction. Solutions of type 3 and 4 are the really non-trivial ones to find. Type 3 solutions have non-zero expectation value of the intra-layer condensate and there are only Minkowski (Mink) embeddings. Type 4 solutions break chiral symmetry in both the inter- and intra-layer channel. For type 2 and 4 solutions the D7 and the anti-D7 world-volumes have to join smoothly at a finite $\rho = \rho_0$. These are indeed connected solutions and of course they are Minkowski embeddings.

Let's consider the solutions of the type 3, types 1 and 2 are just $l = 0$.

The equation for l (B.19) with $\rho_0 = 0$ simplifies further to

$$l'' + 2\left(l'^2 + 1\right)\frac{\left(2l^2\left(l^4 + 3l^2\rho^2 + 3\rho^4 + 1\right) + 2\rho^6 + \rho^2\right)l' + l\rho}{\rho\left(l^2 + \rho^2\right)\left(l^4 + 2l^2\rho^2 + \rho^4 + 1\right)} = 0 \quad \text{(B.20)}$$

In this case it is obvious from (B.16) that $z(\rho)$ is a constant. Solutions of type 3 are those for which $l(\rho)$ goes to a constant, l_0, at $\rho = 0$ so that the four-sphere in the world-volume of the D7-brane shrinks to zero.

A solution to (B.20) of this type can be obtained by a shooting technique. The differential equation can be solved from either direction: from $\rho = 0$ or from the boundary at $\rho = \infty$. In either case, there is a one-parameter family of solutions, from $\rho = 0$ the parameter is l_0, from infinity it is the value of the modulus c in (B.19), which can be used to impose the boundary conditions at $\rho \to \infty$ with $c = 0$.

To find the solution fix some $\bar{\rho}$ in the middle (say $\bar{\rho} = 2$). Start with shooting from the origin. For constant values of l at the origin $\rho = 0$, integrate the solution outwards to $\bar{\rho}$ and compute l and its derivative at $\bar{\rho}$. For each solution, put a point on a plot of $l'(\bar{\rho})$ vs. $l(\bar{\rho})$ (the red curve in Figure B.1). Then, do the same thing starting from the boundary at $\rho = \infty$, and varying the coefficient c of the expansion around infinity. This is given by the blue curve in Figure B.1.

To find a condition on the derivative at $\rho = 0$ we found an asymptotic expansion of the solution around the origin, the first few terms read

$$l(\rho) = l_0 - \frac{\rho^2}{5l_0\left(l_0^4 + 1\right)} + \frac{\left(375l_0^8 + 325l_0^4 + 46\right)\rho^4}{1750l_0^3\left(l_0^4 + 1\right)^3} + O\left(\rho^6\right) \quad \text{(B.21)}$$

When the two solutions, coming from $\rho = 0$ and from $\rho = \infty$ meet at the intermediate point, then there is a solution. The only value of l_0 at which

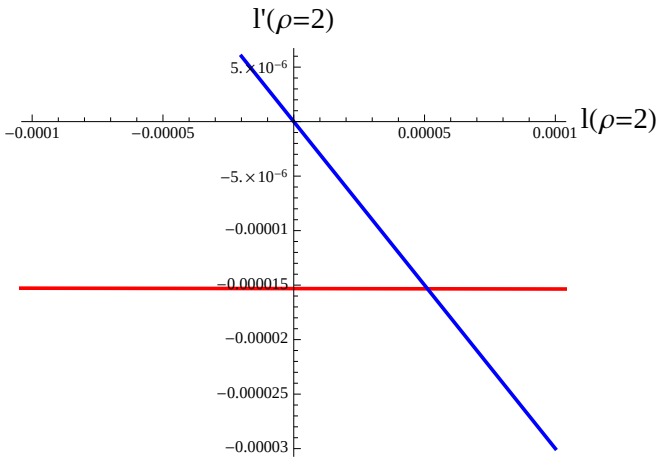

Figure B.1: Unconnected solution for $\rho_0 = 0$, there is a unique solution when the blue and red curves cross.

this happens is $l_0 \simeq 0.254$ and for the parameter c we get $c \simeq 0.051$. With these values $l(\bar{\rho} = 2) = 0.00628566$, $l'(\bar{\rho} = 2) = -0.00921382$. The precision of these numbers could easily be improved by scanning the region around the point where the two curves meet. The solution is plotted in Figure B.2.

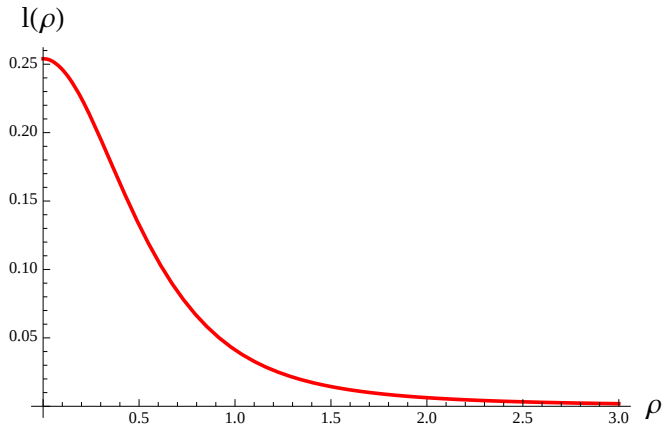

Figure B.2: Unconnected solution for $\rho_0 = 0$ and $q = 0$.

Consider now the solution of equation (B.19) of type 4. In this case we look for a D7 that joins at some given ρ_0 the corresponding anti-D7. At ρ_0, $z'(\rho_0) \to \infty$. At $\rho = \rho_0$ we choose $l'(\rho_0) = 0$ and $l(\rho_0) = l_0$ and we use l_0 for the shooting technique at the turning point ρ_0. At infinity we use

the expansion (B.19) with $q = 0$ to define the boundary conditions. The shooting technique provides a unique solution for each value of ρ_0.

B.2.1 Fluctuations

Consider first the constant disconnected solution, the fluctuation around it can be easily found by writing $l(\rho) = \epsilon\delta l(\rho)$ and expanding eq.(B.20) at the first order in ϵ. We get

$$\rho\left(\rho\left(\rho^4+1\right)\delta l'' + \left(4\rho^4+2\right)\delta l'\right) + 2\delta l = 0$$

whose general solution reads

$$\begin{aligned}\delta l = a_1\rho^{\frac{1}{2}i\left(\sqrt{7}+i\right)}\,{}_2F_1\left(-\frac{1}{8}+\frac{i\sqrt{7}}{8},\frac{5}{8}+\frac{i\sqrt{7}}{8};1+\frac{i\sqrt{7}}{4};-\rho^4\right)\\ +a_2\rho^{-\frac{1}{2}i\left(\sqrt{7}-i\right)}\,{}_2F_1\left(-\frac{1}{8}-\frac{i\sqrt{7}}{8},\frac{5}{8}-\frac{i\sqrt{7}}{8};1-\frac{i\sqrt{7}}{4};-\rho^4\right)\end{aligned} \tag{B.22}$$

for small ρ this solution goes like

$$\delta l \sim a_1\rho^{-\frac{1}{2}+\frac{i\sqrt{7}}{2}} + a_2\rho^{-\frac{1}{2}-\frac{i\sqrt{7}}{2}}$$

the complex exponents is a sign of the instability of the solution $l = 0$ for $q = \rho_0 = 0$.

When ρ_0 is non zero instead, we can show, with a similar argument, that the constant connected solution is actually stable. The equation for the fluctuation now is

$$2\delta l\left(\rho_0^8-\rho^8\right) - \rho\left(\left(\rho^5+\rho\right)\delta l''\left(\rho^8-\rho_0^8\right) + 2\delta l'\left(2\rho^{12}+\rho^8+\rho_0^8\right)\right) = 0$$

which expanded around ρ_0 becomes

$$4\left(\rho-\rho_0\right)\delta l + \rho_0^2\left(1+\rho_0^4\right)\left(\delta l' + 2\left(\rho-\rho_0\right)\delta l''\right) = 0$$

The general solution of this equation is

$$\begin{aligned}\delta l = a_1\sqrt[4]{4\rho-4\rho_0}J_{\frac{1}{4}}\left(\frac{\sqrt{2}\rho}{\sqrt{\rho_0^2\left(\rho_0^4+1\right)}}-\frac{\sqrt{2}\rho_0}{\sqrt{\rho_0^2\left(\rho_0^4+1\right)}}\right)\\ +a_2\sqrt[4]{4\rho-4\rho_0}Y_{\frac{1}{4}}\left(\frac{\sqrt{2}\rho}{\sqrt{\rho_0^2\left(\rho_0^4+1\right)}}-\frac{\sqrt{2}\rho_0}{\sqrt{\rho_0^2\left(\rho_0^4+1\right)}}\right)\end{aligned} \tag{B.23}$$

whose expansion around ρ_0 gives

$$\delta l \sim a_1 \left[\text{const}\sqrt{\rho-\rho_0} + O\left((\rho-\rho_0)^5/2\right)\right] + a_2 \left[\text{const} + \text{const}\sqrt{\rho-\rho_0} + O\left((\rho-\rho_0)^2\right)\right]$$

thus it is always possible to take a linear combination of these solutions that has a derivative with a correct behavior, *i.e* the solution with integer powers of $\rho - \rho_0$. Thus when $\rho_0 \neq 0$ the solution $l = 0$ is stable.

There are then three types of solutions of the equation of motion (B.19) representing bi-layers. Solutions of type 2, 3 and 4.

B.2.2 Free energy

We want now to compare the energies of these solutions for fixed separations of the layers. By setting the asymptotic behavior of $z(\rho)$ (B.9) and (B.10) we implicitly defined the layer separation for a connected solution as

$$L = 2\int_{\rho_0}^{\infty} d\rho z' = 2\int_{\rho_0}^{\infty} d\rho \frac{\rho_0^4\sqrt{l^4+2l^2\rho^2+\rho^4+1}\sqrt{1+l'^2}}{\left(l^2+\rho^2\right)\sqrt{\rho^8-\rho_0^8}} \tag{B.24}$$

for zero charge density. This separation is plotted in Fig.B.3 for the constant connected and the ρ-dependent connected solutions. The first has two branches and a minimum at $\rho_0 \simeq 0.84$ where $L \simeq 1.166$, the latter does not exist for $\rho_0 > 0.265$, but joins with the constant connected at that point.

The energy of the solutions at fixed separation L is given by the on shell action (B.12), $S/\mathcal{N}_7$ where we plug in the three possible solutions we found.

$$E(l;\rho_0) = \int_{\rho_0}^{\infty} d\rho\rho^8 \sqrt{1+\frac{1}{\left(l^2+\rho^2\right)^2}}\sqrt{\frac{1+l'^2}{\rho^8-\rho_0^8}} \tag{B.25}$$

This energy is divergent since in the large ρ limit the argument of the integral goes as $\sim \rho^4$. However, in order to find the energetically favored configuration, we are only interested in the difference between the energy of two solutions, which is always finite. We then choose the energy of the unconnected ($\rho_0 = 0$) constant $l = 0$ solution, type 1, as the reference energy (zero energy level), so that any other (finite) energy density can be defined as $\Delta E(l;\rho_0) = E(l;\rho_0) - E(l=0;\rho_0=0)$. The solution of type 1 always has a higher energy with respect to solutions 2, 3 and 4 and indeed it is always unstable.

By means of numerical computations we obtain for the energy density ΔE of the solutions 2, 3 and 4, the behaviors depicted in Figure B.4. At

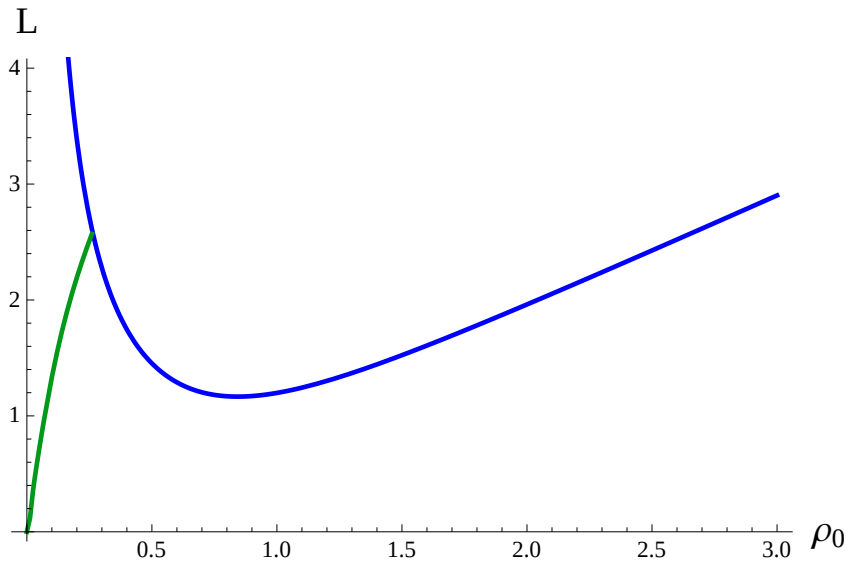

Figure B.3: Brane separation L as a function of ρ_0, which in this case represents the distance from the Poincarè horizon reached by the brane. The blue line corresponds to the connected solution (type 2) and the green line to the connected non constant solution (type 4).

small separation, at variance with the D5-$\bar{\text{D}}$5 case, the configuration which is energetically favored is the Minkowski embedding disconnected solution. At $L = 1.1674$ the constant connected becomes energetically favored with a jump in energy. Then, up to $L = 2.31$ the constant connected solution with an inter-layer condensate is preferred. For larger separation $L > 2.31$ the disconnected configuration is preferred and the condensation is in the intra-layer channel.

The green lines in the figures show the value of the energy and separation for the connected solution with non zero $z(\rho)$ and $l(\rho)$. These configurations have both intra and inter layer condensates. As can be seen from Fig.5.8 they are never energetically favored.

B.3 Double monolayers with charge density

Now we consider the configurations with a charge density different from zero. The equation of motion in this case is given by the most general equation (B.18).

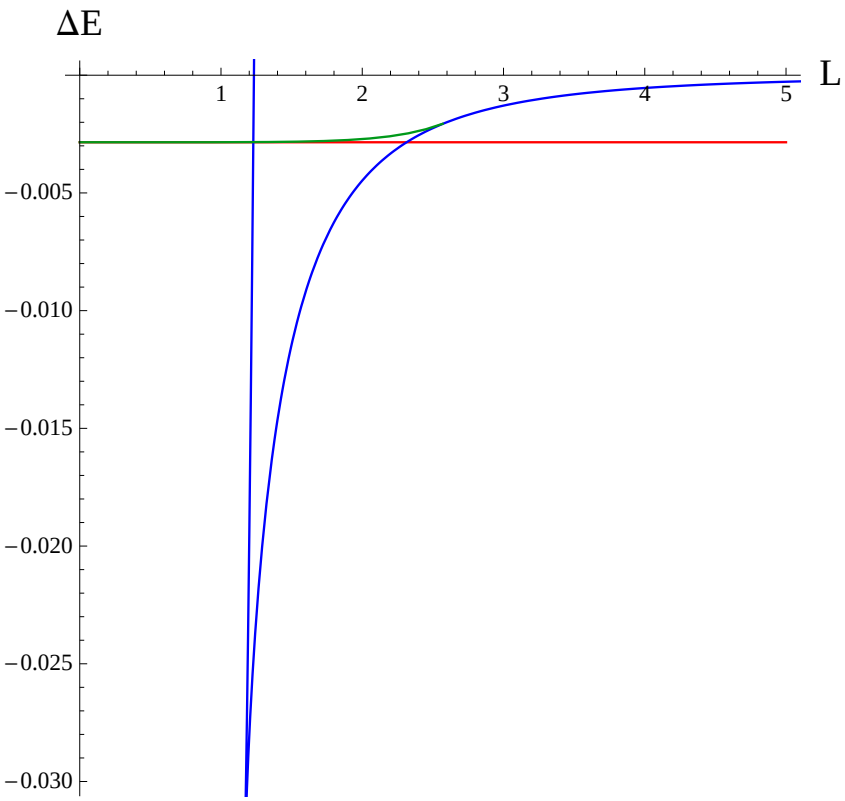

Figure B.4: Regularized energy density ΔE as a function of the brane separation L. The blue line corresponds to the connected solution (type 2), the red line to the unconnected one (type 3) and the green line to the connected non constant solution (type 4). All the solutions are regulated with respect to the constant unconnected solution of type 1.

We look for solution with $m = 0$ in (B.8). We can distinguish four types of solutions according to the classification of table B.2.

Type 1 solutions are trivial both in l and z (they are both constants). They correspond to two parallel black hole (BH) embeddings for the D7 and the anti-D7. This configuration is the chiral symmetric one. In type 2 solutions the chiral symmetry is broken by the inter-layer condensate ($\rho_0 \neq 0$): In this case the branes have non flat profiles in the z direction. Solutions of type 3 and 4 are the really non-trivial ones to find. Type 3 solutions have non-zero expectation value of the intra-layer condensate and they can be only black hole embeddings, this is the true difference with the zero charge case, where this type of solutions were Minkowski embeddings, when the charge

	$\rho_0 = 0$	$\rho_0 \neq 0$
$c = 0$	**Type 1** unconnected, $l = 0$ BH, chiral symm.	**Type 2** connected, $l = 0$ Mink, inter
$c \neq 0$	**Type 3** unconnected, ρ-dependent l BH, intra	**Type 4** connected, ρ-dependent l Mink, intra/inter

Table B.2: Types of possible solutions, where Mink stands for Minkowski embeddings and BH for black-hole embeddings.

density is non-zero only BH embeddings are allowed. A charge density on the D7 world-volume is indeed provided by fundamental strings stretched between the D7 and the Poincaré horizon. These strings have a tension that is always greater than the D7-brane tension and thus they pull the D7 down to the Poincaré horizon. For this reason when $q \neq 0$ the only disconnected solutions we will look for are BH embedding.

Type 4 solutions break chiral symmetry in both the inter- and intra-layer channel. For type 2 and 4 solutions the D7 and the anti-D7 world-volumes have to join smoothly at a finite turning point $\rho = \rho_t$. These are indeed connected solutions and of course they are Minkowski embeddings.

We now state what we have found, we will then provide support to our statements.

1. The constant $l = 0$ disconnected solution $\rho_0 = 0$, when a charge is present, is stable, this can be shown by an analysis of the fluctuations about it.

2. The constant $l = 0$ connected solution with $\rho_0 \neq 0$ joins at the point ρ_t where $z'(\rho)$ in (B.16) diverges. This is given by the real solution of

$$q^2\rho^4 + \left(\rho^8 - \rho_0^8\right)\left(\rho^4 + 1\right) = 0 \tag{B.26}$$

which is

$$\rho_t = \left[\frac{1}{6}\left(\frac{2\sqrt[3]{2}\left(-3q^2+3\rho_0^8+1\right)}{\sqrt[3]{\sqrt{4\left(3q^2-3\rho_0^8-1\right)^3+\left(9q^2+18\rho_0^8-2\right)^2}+9q^2+18\rho_0^8-2}}\right.\right.$$
$$\left.\left.+2^{2/3}\sqrt[3]{\sqrt{4\left(3q^2-3\rho_0^8-1\right)^3+\left(9q^2+18\rho_0^8-2\right)^2}+9q^2+18\rho_0^8-2}-2\right)\right]^{1/4} \tag{B.27}$$

as can be checked numerically for any value of q and ρ_0.

For this solution the brane separation L, as a function of ρ_0, has a minimum and two branches, as for the blue line in the $q = 0$ case of Fig.B.3, a branch where it decreases for increasing ρ_0 and a branch where it increases for increasing ρ_0. Consequently the energy, measured with respect to the constant disconnected solution, has a form similar to the one of the energy for $q = 0$, *i.e.* the blue line in Fig.B.4.

3. The BH-embedding solution, which is non-constant and has $\rho_0 = 0$, exists only for $q < 0.038$, as can be show by means of the shooting technique described in the previous section.

4. The connected non-constant solution joins at the point ρ_t where $z'(\rho)$ in (B.16) diverges. This is given by the real solution of

$$l^2\left(l^2+2\rho^2\right)\left(\rho^8+q^2-\rho_0^8\right)+q^2\rho^4+\left(\rho^8-\rho_0^8\right)\left(\rho^4+1\right)=0 \tag{B.28}$$

which in turn depends on the solution l itself.

This solution exists only for small values of q. For $\rho_0 \simeq 0$ we have $q < 0.038$, when ρ_0 grows, the allowed values of q decrease.

B.3.1 Fluctuations

The equation of motion for disconnected solutions with charge density is given by (B.18) with $\rho_0 = 0$, namely

$$\left(l^2+\rho^2\right)\left(l^2\left(l^2+2\rho^2\right)\left(\rho^8+q^2\right)+\rho^{12}+\rho^8+q^2\rho^4\right)l''$$
$$+\left(\left(2l^2\left(3\rho^2l^2+l^4+3\rho^4+1\right)+2\rho^6+\rho^2\right)l'+\rho l\right)\left(l'^2+1\right)=0 \tag{B.29}$$

Clearly $l = 0$ is a solution and fluctuations around it can be easily found by writing $l(\rho) = \epsilon\delta l(\rho)$ and expanding at the first order in ϵ. The equation for $\delta l(\rho)$ reads

$$2\rho^3\delta l' + 2\rho^2\delta l + q^2\delta l'' = 0$$

whose general solution is

$$\delta l = a_1\,{}_1F_1\left(\frac{1}{4};\frac{3}{4};-\frac{\rho^4}{2q^2}\right) + a_2\rho\,{}_1F_1\left(\frac{1}{2};\frac{5}{4};-\frac{\rho^4}{2q^2}\right)$$

For small ρ this goes like

$$\delta l \simeq a_1 - a_1\frac{\rho^4}{6q^2} + a_2\rho + O\left(\rho^5\right)$$

Being all the power of ρ non negative integers, we only have normalizable modes and this shows that the $l = 0$ solution becomes stable when there is a charge density.

When ρ_0 is non vanishing, *i.e.* when considering connected solutions with a non trivial profile in the z direction, the equation for the fluctuations around the $l = 0$ solution reads

$$-2\delta l\left(\rho^8-\rho_0^8\right)-\rho\left(2\left(2\rho^{12}+\rho^8+\rho_0^8\right)\delta l'+\rho\delta l''\left(q^2\rho^4+\left(\rho^4+1\right)\left(\rho^8-\rho_0^8\right)\right)\right)=0$$

Expanded around ρ_0 it becomes

$$4\left(\rho_0^4+1\right)\rho_0^4\left(2(\rho-\rho_0)\delta l''+\delta l'\right)+16\rho_0^2\delta l(\rho-\rho_0)-q^2\rho_0\delta l''=0$$

and this has a solution for $\rho \simeq \rho_0$ of the form

$$\delta l = a_1+a_2(\rho-\rho_0)+\frac{2a_2\rho_0^3\left(\rho_0^4+1\right)(\rho-\rho_0)^2}{q^2}+\frac{8\rho_0(\rho-\rho_0)^3\left(a_1q^2+3a_2\left(\rho_0^4+1\right)^2\rho_0^5\right)}{3q^4}+O\left((\rho-\rho_0)^4\right)$$

in terms of integer powers of $\rho-\rho_0$ and two moduli. The $l = 0$ connected solution therefore is stable.

B.3.2 Black Hole embedding ρ dependent solution

The black hole embedding ρ-dependent profile is a solution of Eq.(B.29) and it can be found by means of the usual shooting technique. The boundary conditions that can be imposed for $\rho \to \infty$ are defined by the expansion in (B.19) where the modulus c can be varied to match the solution coming from $\rho = 0$. The latter can be obtained imposing boundary conditions derived

by expanding the solution around $\rho \sim 0$ and demanding that $l(\rho) \to 0$ for $\rho \to 0$. The first terms of this expansion up to ρ^{17} are

$$\begin{aligned} l(\rho) =& \alpha\rho - \frac{\alpha\rho^5}{5\left(\alpha^2+1\right)q^2} + \frac{\rho^9\left(-5\alpha^9q^2 - 20\alpha^7q^2 - 30\alpha^5q^2 - 20\alpha^3q^2 + 11\alpha^3 - 5\alpha q^2 + 8\alpha\right)}{90\left(\alpha^2+1\right)^3q^4} \\ &+ \frac{\rho^{13}\left(385\alpha^9q^2 + 1450\alpha^7q^2 + 2040\alpha^5q^2 + 1270\alpha^3q^2 - 343\alpha^3 + 295\alpha q^2 - 184\alpha\right)}{3510\left(\alpha^2+1\right)^4q^6} \\ &+ \frac{\rho^{17}\alpha}{5967000\left(\alpha^2+1\right)^7q^8}\left(131625\alpha^{18}q^4 + 1184625\alpha^{16}q^4 + 4738500\alpha^{14}q^4\right. \\ &+50\alpha^{12}q^2\left(221130q^2 - 20173\right) + 50\alpha^{10}q^2\left(331695q^2 - 111499\right) \\ &+50\alpha^8q^2\left(331695q^2 - 255263\right) + 25\alpha^6\left(442260q^4 - 619044q^2 + 21209\right) \\ &+25\alpha^4\left(189540q^4 - 418766q^2 + 50213\right) + \alpha^2\left(1184625q^4 - 3739750q^2 + 931552\right) \\ &\left.+25\left(5265q^4 - 21994q^2 + 8464\right)\right) + O\left(\rho^{21}\right) \end{aligned} \tag{B.30}$$

The expansion is written in terms of the modulus α which is the parameter that can be varied to adjust the shooting technique.

A typical solution is presented in Fig.B.5, where it is clear that it reaches the Poincarè horizon at $l = \rho = 0$ Some examples of the results of the

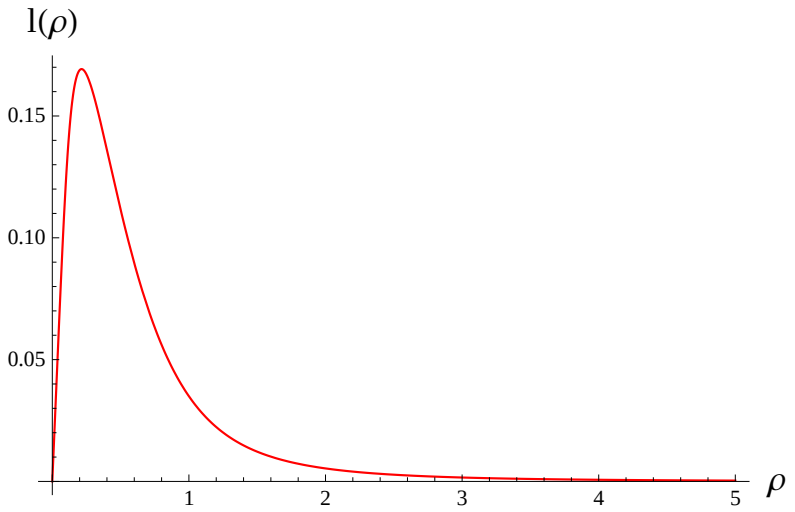

Figure B.5: Black hole embedding solution for $q = 1/100$, it clearly reaches the Poincarè horizon.

shooting technique are given in Figs.B.6, B.7, B.8 B.9.

It is quite clear from these graphs that the solution tends to disappear increasing the charge q, we checked that for $q > 0.0377$ the curves coming

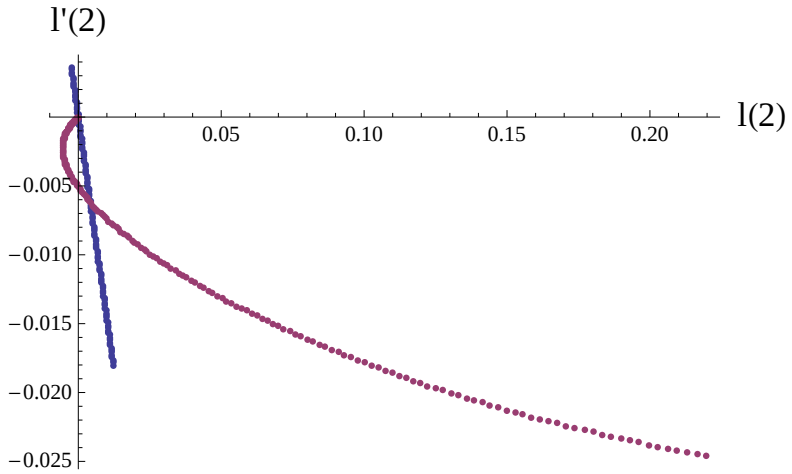

Figure B.6: Shooting technique for $q = 1/50$

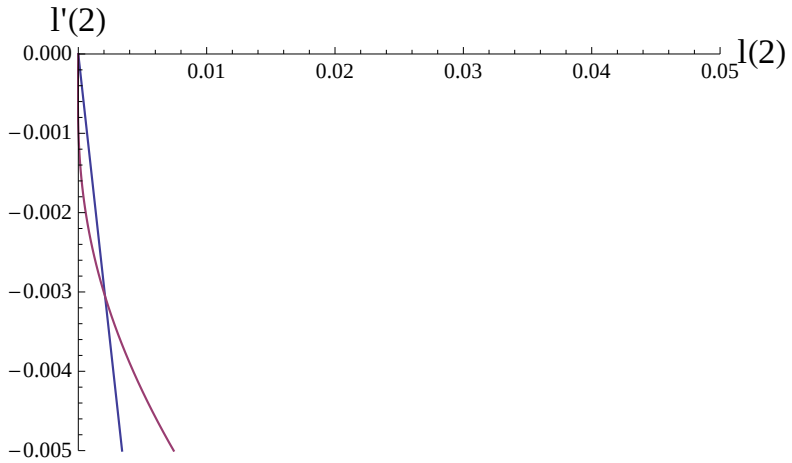

Figure B.7: Shooting technique for $q = 1/30$

from infinity and from zero meet only at $l(2) = l'(2) = 0$, which corresponds to the trivial chirally symmetric solution.

Energy of the ρ-dependent black hole embedding solution

We can now compute the energy of the ρ-dependent black hole embedding solutions that we have found by varying the value of the charge. This is given by the Routhian in (B.17) with $\rho_0 = 0$, computed on the solutions

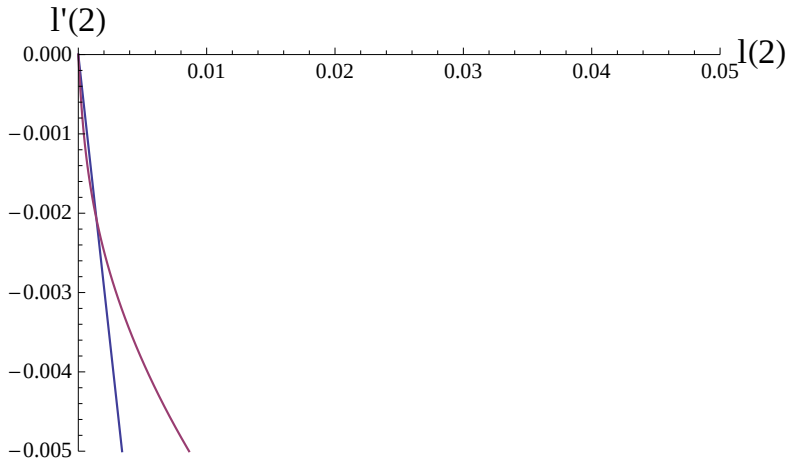

Figure B.8: Shooting technique for $q = 1/28$

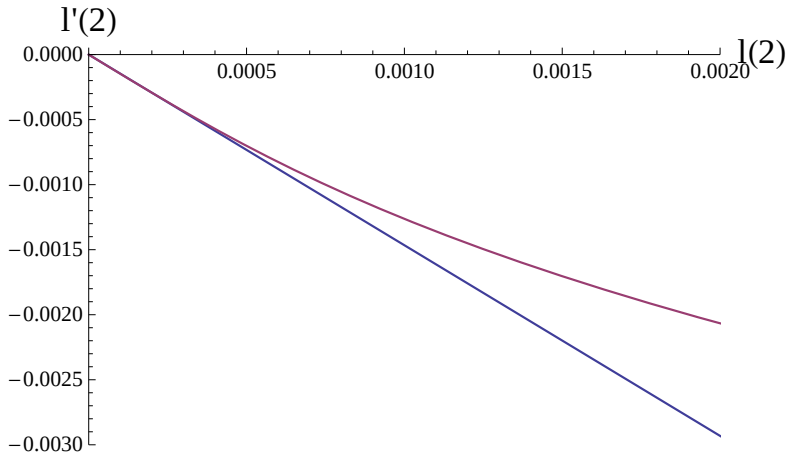

Figure B.9: Shooting technique for $q = 2/53 \simeq 0.0377$

found numerically.

$$\begin{aligned}\mathcal{R} &= \frac{S}{\mathcal{N}_7} - q\int d\rho a_0'(\rho) \\ &= \int d\rho \frac{\sqrt{(1+l'^2)\left(l^4\left(\rho^8+q^2\right)+2l^2\rho^2\left(\rho^8+q^2\right)+q^2\rho^4+\left(\rho^4+1\right)\rho^8\right)}}{l^2+\rho^2}\end{aligned} \tag{B.31}$$

Again this energy is divergent and has to be regulated by subtracting to it the energy of the constant $l = 0$ disconnected solution with the same charge, namely

$$\Delta E = \int_0^\infty d\rho \left(\frac{\sqrt{(1+l'^2)\left(l^4\left(\rho^8+q^2\right)+2l^2\rho^2\left(\rho^8+q^2\right)+q^2\rho^4+\left(\rho^4+1\right)\rho^8\right)}}{l^2+\rho^2} - \sqrt{q^2+\left(\rho^4+1\right)\rho^4} \right) \tag{B.32}$$

This quantity is plotted in Fig.B.10 as a function of the charge q. It is clear from this plot that the energy of the ρ-dependent black-hole embedding solution is always lower then its ρ-independent counterpart. For $q \simeq 0.0377$ the two solutions actually merge, so that for higher values of the charge the only existing solution is the chirally symmetric one.

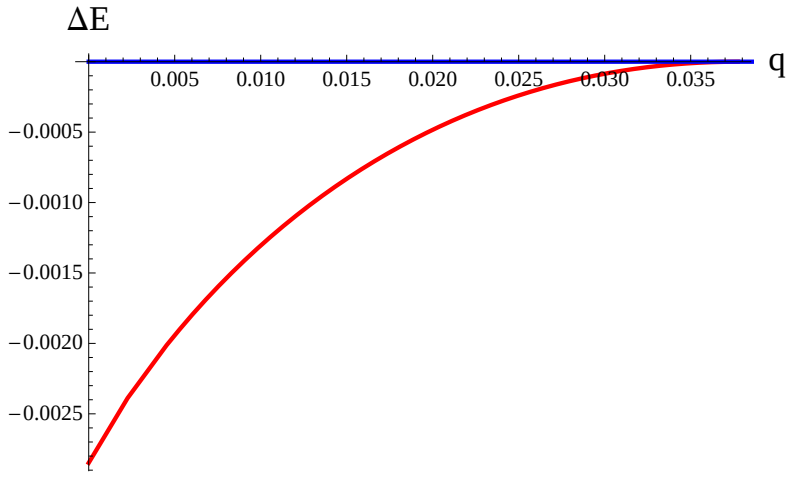

Figure B.10: Energy of the ρ-dependent black-hole embedding solution, red line, measured with respect to the energy of the constant chirally symmetric solution, blue line.

B.4 Connected solutions

When ρ_0 in (5.13) is non zero there is a non trivial profile in the z direction and it is possible to construct connected solutions even when there is a charge density. In this case the inter-layer condensate is stable only when the layers have charge densities of equal magnitude and opposite sign, so that the total system is charge neutral.

According to the classification shown in table B.2 we can distinguish two types of connected solutions, *i.e.* type 2 and type 4. Let us consider first

the type 2 solutions. These have a flat profile in the l direction, $l = 0$, and thus for such solutions we can easily write the brane separation as

$$L = 2\int_{\rho_t}^{\infty} d\rho \frac{\rho_0^4\left(\rho^4+1\right)}{\rho^2\sqrt{q^2\rho^4+\left(\rho^8-\rho_0^8\right)\left(\rho^4+1\right)}} \tag{B.33}$$

where ρ_t is given in (B.27).

Since we want the energy of the solution as a function of the layer separation L and the charge q we need to perform a Legendre transform of the action S only with respect to the charge, namely

$$\mathcal{R}_q = \frac{S}{\mathcal{N}_7} - q\int d\rho a_0'(\rho) = \int d\rho \frac{\left(l^2\left(l^2+2\rho^2\right)\left(\rho^8+q^2\right)+\rho^4\left(\rho^8+\rho^4+q^2\right)\right)}{l^2+\rho^2} \sqrt{\frac{l'^2+1}{l^2\left(l^2+2\rho^2\right)\left(\rho^8+q^2-\rho_0^8\right)+q^2\rho^4+\left(\rho^4+1\right)\left(\rho^8-\rho_0^8\right)}} \tag{B.34}$$

This needs to be regularized and we do it with respect to the constant disconnected solution with the same charge. For the $l = 0$ solution then we get

$$\Delta E = \int_{\rho_t}^{\infty} d\rho \left(\frac{\rho^2\left(\rho^8+\rho^4+q^2\right)}{\sqrt{q^2\rho^4+\left(\rho^4+1\right)\left(\rho^8-\rho_0^8\right)}} - \sqrt{\rho^8+\rho^4+q^2}\right) - \int_0^{\rho_t} d\rho\sqrt{\rho^8+\rho^4+q^2} \tag{B.35}$$

There exist also a ρ-dependent connected solution that corresponds to the existence of both intra-layers and inter-layers condensates. These are non trivial solutions of the most general equation of motion (B.18) with the additional condition that there must be a point ρ_t that solves the equation (B.28) where $z'(\rho)$ in (B.16) diverges. Thus to find this solution we impose the boundary condition that l is at ρ_t a solution of (B.28), namely it is given by

$$l(\rho_t) = \sqrt{\sqrt{\frac{\rho_0^8-\rho_t^8}{q^2-\rho_0^8+\rho_t^8}} - \rho_t^2} \tag{B.36}$$

ρ_t has a maximum value that is given by (B.27), namely it is reached when $l = 0$, *i.e.* for the constant connected solution. Then we can get the boundary condition on the first derivative of l, l', computing the equation of motion at ρ_t and using (B.36) to get the value of l at ρ_t. This reads

$$l'(\rho_t) = \frac{\left(\rho_t^8-\rho_0^8\right)\sqrt{\sqrt{\frac{q^2}{q^2-\rho_0^8+\rho_t^8}-1}-\rho_t^2}}{\frac{2q^2\rho_t^7\sqrt{\rho_0^8-\rho_t^8}}{\left(q^2-\rho_0^8+\rho_t^8\right)^{3/2}}+\rho_0^8\rho_t-\rho_t^9} \tag{B.37}$$

Then these boundary conditions can be used to apply the shooting technique by varying the parameter ρ_t in order to match the solution coming from infinity, where the value of the chiral condensate (c in (B.19)) is the modulus that must be varied to obtain the matching.

Solutions of this type exist only for small charges $q < 0.0377$ exactly the same value we found as a threshold for the existence of the black-hole embedding solution. When the charge decrease the range of values of ρ_0 for which the solution exists, increases.

The brane separation L for this solution is defined by twice the integral of z' in (B.16)

$$L = 2\int_{\rho_t}^{\infty} d\rho \frac{\rho_0^4\left(l^4+2l^2\rho^2+\rho^4+1\right)\sqrt{1+l'^2}}{\left(l^2+\rho^2\right)\sqrt{l^2\left(l^2+2\rho^2\right)\left(\rho^8+q^2-\rho_0^8\right)+q^2\rho^4+\left(\rho^8-\rho_0^8\right)\left(\rho^4+1\right)}} \tag{B.38}$$

The energy is given by (B.34) computed on the solution and again we regularize it by subtracting the contribution of the constant disconnected solution with the same charge.

Figure B.11 shows the behavior of the brane separation as a function of the parameter ρ_0 for both type 2 and type 4 solutions when the charge is fixed to $q = 0.001$. The solution of type 2 has two branches as in the zero charge case. The solution of type 4 instead as a different behavior compared to the neutral case. Analogous figures can be obtained for different values of the charge, provided $q < 0.0377$, increasing the charge the growing branch in the green solution becomes smaller and the range of allowed ρ_0 for this solution decreases.

The energy of the connected solutions can be compared to that of the corresponding black-hole solution with the same charge. The $q = 0.001$ case is represented in Fig.B.12 and B.13 where the region around the transition point is enhanced.

From Fig.B.13 it is clear that for $L < 1.16$ the lowest energy solution is the black-hole embedding one with only an inter-layer condensate, at $L = 1.16$ there is a jump in energy to the constant connected which has only an inter-layer condensate and for $L > 2.2$ the energetically favored solution becomes the connected ρ-dependent with both inter and intra layer condensates.

We finally have performed this analysis also for other charges and this has allowed us to finally draw the the phase diagram in chapter 6.

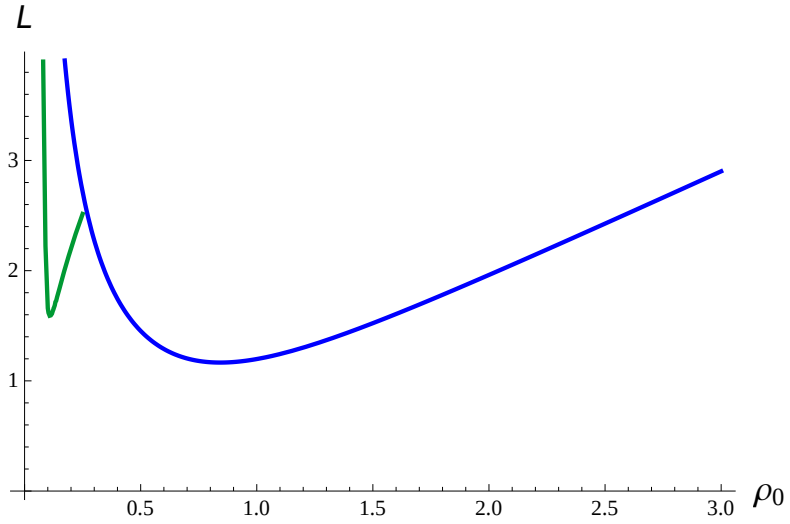

Figure B.11: Brane separation as a function of ρ_0. The blue line is obtained from the constant solution, the green line from the ρ-dependent one.

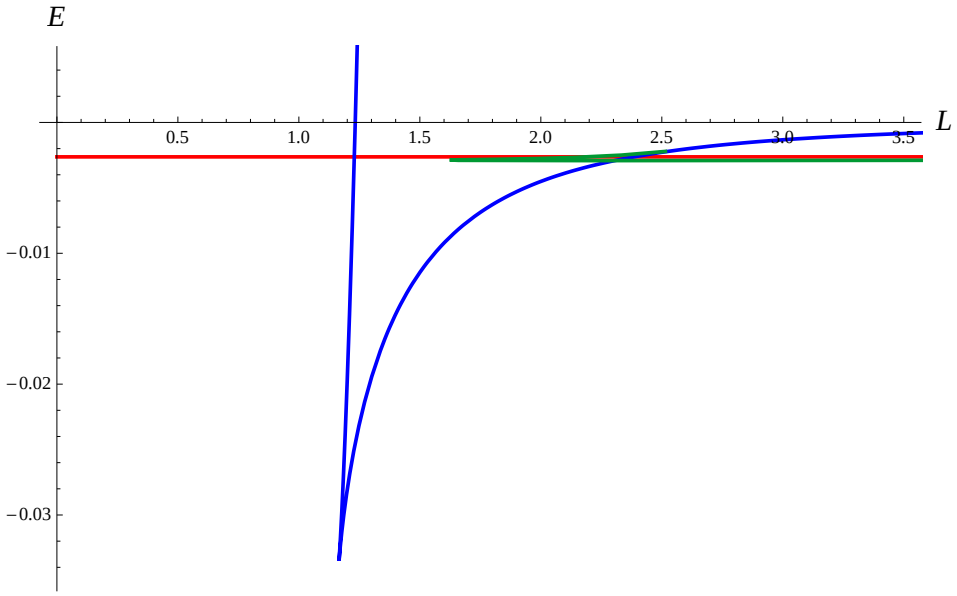

Figure B.12: Energy as a function of L. The blue line is obtained from the constant solution, the green line from the ρ-dependent one and the red line the black hole embedding solution with the same charge $q = 0.001$.

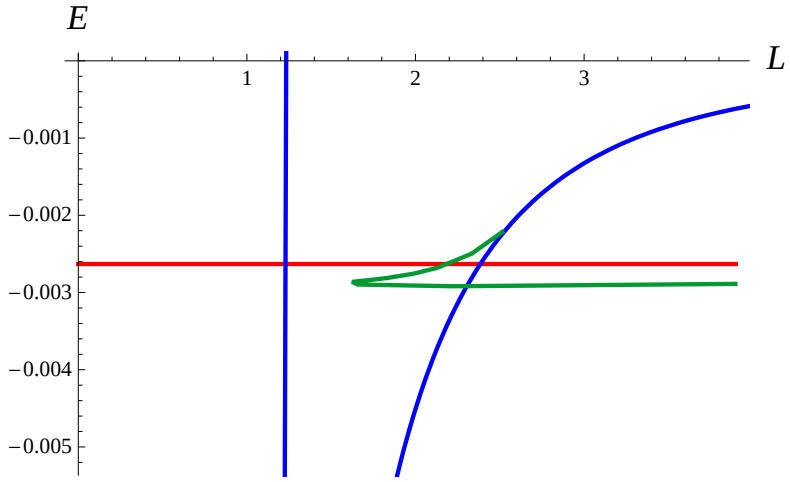

Figure B.13: Close around the transition point in Fig. B.12

Appendix C

BKT Quantum Phase Transition

This chapter is the review of the part of the paper [102] about BKT transition. We will start from the Lagrangian, the equation (2.10).

$$\tilde{L} \sim L - \frac{\partial L}{\partial a_0'} a_0' - \frac{\partial L}{\partial z'} z', \tag{C.1}$$

where $' = \frac{d}{dr}$.

$$u \equiv \sqrt{r^2 + l(r)^2}$$

The equation of motion with respect to $z(r)$ is :

$$\frac{\partial \tilde{L}}{\partial z'} = \frac{\sqrt{(r^4 + f^2 u^4)(1 + \frac{H^2}{u^4}) + d^2}}{\sqrt{1 + l'^2 + u^4 z'^2}} u^4 z' + f u^4 \tag{C.2}$$

$$= \left(\frac{\sqrt{(r^4 + f^2 u^4)(1 + \frac{H^2}{u^4}) + d^2}}{\sqrt{1 + l'^2 + u^4 z'^2}} z' + f \right) u^4 = const. \equiv C \tag{C.3}$$

$$z'^2 = \frac{(1 + l'^2)(C - f u^4)^2}{u^4 \left(u^4 ((r^4 + f^2 u^4)(1 + \frac{H^2}{u^4}) + d^2) - (C - f u^4)^2 \right)} \tag{C.4}$$

$$z' = \frac{(C - f u^4)\sqrt{1 + l'^2}}{u^2 \sqrt{u^4 ((r^4 + f^2 u^4)(1 + \frac{H^2}{u^4}) + d^2) - (C - f u^4)^2}} \tag{C.5}$$

$$\tilde{L} = \sqrt{1 + l'^2} \sqrt{(r^4 + f^2 u^4)(1 + \frac{H^2}{u^4}) + d^2 - \frac{(C - f u^4)^2}{u^4}} \tag{C.6}$$

C should be zero, because of regularity at $r = 0$ and $r = \infty$. Then,

$$\tilde{L} = \sqrt{1 + l'^2} \sqrt{r^4 (1 + \frac{H^2}{u^4}) + f^2 H^2 + d^2} \tag{C.7}$$

Without Wess-Zumino (WZ) term, the Lagrangian was:

$$\tilde{L}' = \sqrt{1+l'^2}\sqrt{(r^4+f^2u^4)(1+\frac{H^2}{u^4})+d^2} \tag{C.8}$$

As the result of [103] , it gives

$$m^2 = -\frac{2H^2}{d^2+H^2+H^2f^2} \tag{C.9}$$

at at IR, $r \ll 1$, and BF bound is violated as

$$\frac{d^2}{H^2}+f^2 < 7 \tag{C.10}$$

By this result, even for $d=0$, violation condition is provided. We compare this with our Rauthian with the WZ term. The Lagrangian up to quadratic order of $l(r)$,

$$L \sim -\sqrt{r^4+d^2+H^2(1+f^2)}\frac{l'^2}{2} + \frac{H^2}{\sqrt{r^4+d^2+H^2(1+f^2)}}\frac{l^2}{r^2}. \tag{C.11}$$

The equation of motion is:

$$0 = \partial_r(\sqrt{r^4+d^2+H^2(1+f^2)}l') + \frac{H^2}{\sqrt{r^4+d^2+H^2(1+f^2)}}\frac{2l}{r^2}$$

$$= \sqrt{r^4+d^2+H^2(1+f^2)}l'' + \frac{2r^3l'}{\sqrt{r^4+d^2+H^2(1+f^2)}} + \frac{H^2}{\sqrt{r^4+d^2+H^2(1+f^2)}}\frac{2l}{r^2}$$

We are interested in IR, $r \ll 1$. Then the equation of motion is:

$$\sqrt{d^2+H^2(1+f^2)}l'' + \frac{H^2}{\sqrt{d^2+H^2(1+f^2)}}\frac{2l}{r^2} = 0 \tag{C.12}$$

$$l'' + \frac{2H^2}{d^2+H^2(1+f^2)}\frac{l}{r^2} = 0 \tag{C.13}$$

This equation of motion gives the result of [103] without WZ term. For the deeper understanding, let us confirm the result without WZ term.

$$L \sim -\sqrt{1+l'^2}\sqrt{(r^4+f^2u^4)(1+\frac{H^2}{u^4})+d^2} \tag{C.14}$$

Expand up to quadratic order of $l(r)$,

$$L \sim -(1+\frac{l'^2}{2})\bigg((1+f^2)(r^4+H^2)+d^2+2l^2(f^2r^2-\frac{H^2}{r^2})\bigg)^{1/2} \tag{C.15}$$

$$L \sim -\sqrt{(1+f^2)(r^4+H^2)+d^2}\,\frac{l'^2}{2} - \frac{(f^2r^2-H^2/r^2)l^2}{\sqrt{(1+f^2)(r^4+H^2)+d^2}}. \tag{C.16}$$

Let us check it carefully with the equation of motion. The equation of motion is:

$$0 = \partial_r(\sqrt{(1+f^2)(r^4+H^2)+d^2}l') - \frac{2(f^2r^2-H^2/r^2)l}{\sqrt{(1+f^2)(r^4+H^2)+d^2}}$$

$$= \sqrt{(1+f^2)(r^4+H^2)+d^2}l'' + \frac{2(1+f^2)r^3l'}{\sqrt{(1+f^2)(r^4+H^2)+d^2}} - \frac{2(f^2r^2-H^2/r^2)l}{\sqrt{(1+f^2)(r^4+H^2)+d^2}}$$

The same result as above is obtained at IR.

$$\sqrt{d^2+H^2(1+f^2)}l'' + \frac{H^2}{\sqrt{d^2+H^2(1+f^2)}}\frac{2l}{r^2} = 0 \tag{C.17}$$

On the other hand, UV limited case presents different results between with or without WZ term. Without WZ, if $r \gg 1$, the equation of motion is:

$$\sqrt{1+f^2}r^2l'' + 2\sqrt{1+f^2}rl' - \frac{2f^2l}{\sqrt{1+f^2}} = 0 \tag{C.18}$$

$$\sqrt{1+f^2}rl'' + 2\sqrt{1+f^2}l' - \frac{2f^2}{\sqrt{1+f^2}}\frac{l}{r} = 0 \tag{C.19}$$

$$(\Box_{AdS_{p+2}} - m^2)\frac{l}{r} = \frac{1}{\sqrt{-g}}\partial_\mu g^{\mu\nu}\sqrt{-g}\partial_\nu\frac{l}{r} - m^2\frac{l}{r} = \frac{1}{r^p}\partial_r r^{p+2}\partial_r(\frac{l}{r}) - m^2\frac{l}{r}$$

$$= rl'' + pl' - \frac{p}{r}l - m^2\frac{l}{r} = 0 \tag{C.20}$$

29

[29] We will explain in more detail in the later section

Thus, for $p = 2$, The mass of this scalar particle, l/r on AdS_4 is:

$$m^2 = -2 + \frac{2f^2}{1+f^2} = \frac{-2}{1+f^2} \geq -2 \tag{C.21}$$

The mass varies by changing S^2 flux, but is larger than -2, which never violates the Breitenlohner-Freedman (BF) bound. With WZ, it is simpler and $m^2 = -2$ as $f = 0$.

To check $C = 0$ case, consider the blackhole embedding at finite temperature.

$$ds^2_{D5} = \frac{w^2}{L^2}(-g_t dt^2 + g_x dx^2 + g_x dy^2) + \frac{L^2}{w^2}(d\rho^2 + \rho^2 d\Omega_2^2 + dl^2 + l^2\rho^2 d\tilde{\Omega}_2^2)$$

where

$$g_t := \frac{(w^4 - w_0^4)^2}{2w^4(w^4 + w_0^4)}, \quad g_x := \frac{w^4 + w_0^4}{2w^4}, \tag{C.22}$$

We required this modified metric to keep $SO(3) \times SO(3)$ isometry. With profiling ansatz, $l := l(r)$, $z := z(r)$ and $d\tilde{\Omega} = 0$,

$$ds^2_{D5} = \frac{w^2}{L^2}(-g_t dt^2 + g_x dx^2 + g_x dy^2) + (\frac{L^2}{w^2} + \frac{L^2 l'(\rho)^2}{w^2} + \frac{w^2}{L^2} z'(\rho)^2)d\rho^2 + \frac{L^2\rho^2}{w^2} d\Omega_2^2$$

$$w^2 = \rho^2 + l^2,$$

$L = L_{WZ} + L_{DBI}$

$$\sim -f(\frac{w^4 + w_0^4}{w^2})^2 z' - (1 - \frac{w_0^4}{w^4})\sqrt{1 + l'^2 + (w^4 + w_0^4)z'^2}\sqrt{(\rho^4 + f^2 w^4)(\frac{1}{w^4 + w_0^4} + \frac{w^4 + w_0^4}{w^4}) + \frac{w^4}{w^4 + w_0^4} d^2}$$

The equation of motion with respect to cyclic z, $\partial_{z'} L = const.$

$$-f(\frac{w^4 + w_0^4}{w^2})^2 - (1 - \frac{w_0^4}{w^4})\sqrt{(\rho^4 + f^2 w^4)(\frac{1}{w^4 + w_0^4} + \frac{w^4 + w_0^4}{w^4}) + \frac{w^4}{w^4 + w_0^4} d^2}\frac{(w^4 + w_0^4)z'}{\sqrt{1 + l'^2 + (w^4 + w_0^4)z'^2}}$$

$$= const. = -4w_0^4 f$$

The consistent constant at the horizon is $-4w_0^4 f$, thus

$$z' = -f(\frac{w^4 - w_0^4}{w^2})^2 \sqrt{\frac{1 + l'^2}{(1 - \frac{w_0^4}{w^4})b(w^4 + w_0^4)^2 - f^2(w^4 + w_0^4)(\frac{w^4 - w_0^4}{w^2})^4}}$$

$$b := (\rho^4 + f^2 w^4)(\frac{1}{w^4 + w_0^4} + \frac{w^4 + w_0^4}{w^4}) + \frac{w^4}{w^4 + w_0^4} d^2$$

Now take $w_0 = 0$, then above constant $C = 0$, and z' is the same as above zero temperature case.

Consider $f \neq 0 (f > 0)$, $H \neq 0$. The Lagrangian is:

$$L \sim -\sqrt{1+\frac{H^2}{u^4}}\sqrt{r^4+f^2u^4}\sqrt{1+l'^2+u^4z'^2} - fu^4z' \tag{C.23}$$

The equation of motion with respect to $l(r)$, $\partial_r(\frac{\partial L}{\partial l'}) = \frac{\partial L}{\partial l}$ is following. We plugged z' by using the equation for $C = 0$ into the equation of motion of $l(r)$.

$$\partial_r(\sqrt{r^4+f^2u^4}\sqrt{1+\frac{H^2}{u^4}}\frac{l'}{\sqrt{1+l'^2+u^4z'^2}}) = 2u^2l\Bigg((r^4+f^2u^4)(-\frac{H^2}{u^8})\sqrt{\frac{1+l'^2}{r^4+H^2(f^2+\frac{r^4}{u^4})}}$$

$$+\sqrt{\frac{1+l'^2}{r^4+H^2(f^2+\frac{r^4}{u^4})}}f^2(1+\frac{H^2}{u^4}) + \sqrt{\frac{r^4+H^2(f^2+\frac{r^4}{u^4})}{1+l'^2}}f^2(\frac{1+l'^2}{r^4+H^2(f^2+\frac{r^4}{u^4})})$$

$$-2f^2\sqrt{\frac{1+l'^2}{r^4+H^2(f^2+\frac{r^4}{u^4})}} = -\frac{2r^4l}{u^6}H^2\sqrt{\frac{1+l'^2}{r^4+H^2(f^2+\frac{r^4}{u^4})}} < 0$$

WZ term is generic if we consider S^2 flux, and it cancels the attractive effect from DBI term. If $H = 0$, the Chern-Simons (CS) term cancels all nonzero forces by flux term. For $H \neq 0$, it also vanishes all attraction by flux.

Let us start with $d \neq 0$, $H \neq 0$ and $l = l(r)$. Then the rescaled and Legendre transformed Lagrangian is:

$$L \sim -\sqrt{1+l'^2}\sqrt{r^4(1+\frac{1}{(r^2+l^2)^2})+d^2}, \tag{C.24}$$

and it can be expanded up to the quadratic order as

$$L \sim \frac{1}{2}\sqrt{1+r^4+d^2}l'^2 - \frac{l^2}{r^2\sqrt{1+r^4+d^2}} \tag{C.25}$$

The equation of motion is:

$$\partial_r(\sqrt{1+r^4+d^2}l') + \frac{2l}{r^2\sqrt{1+r^4+d^2}} = 0 \tag{C.26}$$

$$\sqrt{1+r^4+d^2}l'' + \frac{2r^3 l'}{\sqrt{1+r^4+d^2}} + \frac{2l}{r^2\sqrt{1+r^4+d^2}} = 0 \tag{C.27}$$

For AdS metric, the mass opeartor with scalar field is defined as:

$$\Box_{AdS_{p+2}}\phi = \frac{1}{\sqrt{-g}}\partial_\mu g^{\mu\nu}\sqrt{-g}\partial_\nu\phi = r^2\partial_r^2 + (p+2)r\partial_r\phi + \dots \tag{C.28}$$

At $r \gg 1$, the equation of motion (45) is:

$$r^2 l'' + 2rl' + \frac{2l}{r^4} = r^2 l'' + 2rl' + O(\frac{1}{r^4}) = 0, \tag{C.29}$$

and it is the same as the equation of motion of the AdS_4 scalar field $\frac{l}{r}$.

$$(\Box_{AdS_{p+2}} - m^2)\frac{l}{r} = \frac{1}{\sqrt{-g}}\partial_\mu g^{\mu\nu}\sqrt{-g}\partial_\nu\frac{l}{r} - m^2\frac{l}{r} = \frac{1}{r^p}\partial_r r^{p+2}\partial_r(\frac{l}{r}) - m^2\frac{l}{r}$$

$$= rl'' + pl' - \frac{p}{r}l - m^2\frac{l}{r} = 0$$

For $p = 2$, and $m^2 = -2$ both equations correspond. At $r \ll 1$, the equation of motion is:

$$l'' + \frac{2r^3 l'}{1+d^2} + \frac{2}{1+d^2}\frac{l}{r^2} = 0, \tag{C.30}$$

and it corresponds to the equation of motion for $p = 0$, and $m^2 = -\frac{2}{1+d^2}$.

To see the critical phenomena, let us see the solution of the equation of motion with CS term.

$$l(r) \sim c_+ g_+ + c_- g_- \tag{C.31}$$

$$\nu = \frac{d}{H\sqrt{1+f^2}}; \quad d^2 + H^2(1+f^2) = H^2(1+f^2)(1+\nu^2)$$

$$g_\pm = (H^2(1+f^2)(1+\nu^2))^{-\frac{1}{8}(1\mp\sqrt{\frac{-7+\nu^2+f^2(1+\nu^2)}{(1+f^2)(1+\nu^2)}})} r^{\frac{1}{2}(1\mp\sqrt{\frac{-7+\nu^2+f^2(1+\nu^2)}{(1+f^2)(1+\nu^2)}})} {}_2F_1[x_\pm, y_\pm, z_\pm, w]$$

$$x_\pm = \frac{1}{8}(1 \mp \sqrt{\frac{-7+\nu^2+f^2(1+\nu^2)}{(1+f^2)(1+\nu^2)}})$$

$$y_\pm = \frac{1}{8}(3 \mp \sqrt{\frac{-7+\nu^2+f^2(1+\nu^2)}{(1+f^2)(1+\nu^2)}})$$

$$z_{\pm} = 1 \mp \frac{1}{4}\sqrt{\frac{-7+\nu^2+f^2(1+\nu^2)}{(1+f^2)(1+\nu^2)}}$$

$$w = -\frac{r^4}{H^2(1+f^2)(1+\nu^2)}$$

It seems more appropriate than the Rauthian without CS in [103].

$$\alpha = \sqrt{\frac{d_c^2 - d^2}{H^2(1+f^2)(1+\nu^2)}}; \quad d_c = H\sqrt{7-f^2}; \quad \delta = (\frac{1}{H^2(1+f^2)(1+\nu^2)})^{1/4}; \quad u = \delta r$$

Using the convention of [103], our $g_{\pm}$ is:

$$g_{\pm} = u^{\frac{1\pm\alpha}{2}}\, {}_2F_1[\frac{1\pm i\alpha}{8}, \frac{3\pm i\alpha}{8}, 1\pm\frac{i\alpha}{4}, -u^4] \tag{C.32}$$